LATE QUATERNARY MORPHOTECTONIC EVOLUTION OF THE SONE MEGAFAN, MIDDLE GANGA PLAIN, INDIA

Ph.D. THESIS

by

ADITYA KUMAR VERMA

DEPARTMENT OF EARTH SCIENCES
INDIAN INSTITUTE OF TECHNOLOGY ROORKEE
ROORKEE – 247 667 (INDIA)
JULY, 2018

LATE QUATERNARY MORPHOTECTONIC EVOLUTION OF THE SONE MEGAFAN, MIDDLE GANGA PLAIN, INDIA

A THESIS

Submitted in partial fulfilment of the requirements for the award of the degree

of

DOCTOR OF PHILOSOPHY

in

EARTH SCIENCES

by

ADITYA KUMAR VERMA

DEPARTMENT OF EARTH SCIENCES
INDIAN INSTITUTE OF TECHNOLOGY ROORKEE
ROORKEE – 247 667 (INDIA)
JULY, 2018

INDIAN INSTITUTE OF TECHNOLOGY ROORKEE
ROORKEE

CANDIDATE'S DECLARATION

I hereby certify that the work which is being presented in the thesis entitled "**LATE QUATERNARY MORPHOTECTONIC EVOLUTION OF THE SONE MEGAFAN, MIDDLE GANGA PLAIN, INDIA**" in partial fulfilment of the requirements for the award of the Degree of Doctor of Philosophy and submitted in the Department of Earth Sciences of the Indian Institute of Technology Roorkee, Roorkee is an authentic record of my own work carried out during a period from January, 2013 to July, 2018 under the supervision of Dr. Pitambar Pati, Assistant Professor, Department of Earth Sciences, Indian Institute of Technology Roorkee, Roorkee.

The matter presented in this thesis has not been submitted by me for the award of any other degree of this or any other institution.

(ADITYA KUMAR VERMA)

This is to certify that the above statement made by the candidate is correct to the best of my knowledge.

(Pitambar Pati)
Supervisor

Date:

ABSTRACT

The middle Ganga plain is tectonically most active part of the Indo-Gangetic foreland basin. Though extensive study of neotectonics, geomorphology and sedimentology of the Ganga plain has been carried out in last decades, most of those are confined to the north of the Ganga River. However, the region south of the Ganga River has relatively gained lesser attention in the context of geomorphic and tectonic evolution. The southern middle Ganga plain is mainly drained by the Sone River and its distributaries, forming a megafan and ultimately meeting the axial river Ganga. Fluvial geomorphology of the megafan is mainly dominated by the Sone River by different phases of channel migration triggered by block tilting. Tectonically, the Sone megafan rests over two major subsurface basement faults, namely, West Patna Fault (WPF) and East Patna Fault (EPF). In the present work, morphotectonic evolution of the Sone megafan during the Late Quaternary period has been studied, and the tectono-geomorphic characteristics of the bounding faults have been worked out using an integrated approach such as remote sensing and GIS, Optically Stimulated Luminescence (OSL) dating, shallow subsurface stratigraphy and Ground Penetrating Radar (GPR).

Reconnaissance of the study area was carried out by remote sensing and GIS techniques using Landsat ETM+ images to identify the different geomorphic domains of the megafan. Old alluvial plains, flood plains, active and paleochannels, and spatial drainage anomalies were marked on the image. Based on spatial drainage anomaly, such as convergent drainage, offsetting streams, generation of new streams, change in channel sinuosity etc. possible fault zones of the EPF and WPF were demarcated. Preferred orientation of the ponds revealed some recently abandoned channels. Comparative distribution and morphology of these abandoned ponds indicate that the western part of the megafan is relatively older than the eastern part. Most of the ponds in the eastern part show elongated morphology and their orientation reveals paleochannel pattern. Given the evidence of channel avulsion of Sone River, it is highly likely that these large ponds have resulted from the quick abandonment of some earlier course of either the Sone or its distributary in

recent past. Whereas numerous ponds on the western part of the megafan surface indicate a similar hydrological condition but their shrunken size and almost circular shape associates them with relatively old channel-abandonment events.

Different geomorphic units identified from remote sensing and GIS study were examined and verified in the fieldwork. The vertical sections exposed in pits were investigated for studying the degree of soil development and samples for optically stimulated luminescence (OSL) dating were collected. Different horizons and sub-horizons of the soil profiles were noted, and sedimentary logs of the sections were prepared. Soils in the western part of the megafan are well-developed with 0.5 to 3 m variation of solum thickness as compared to the eastern part where the solum thickness varies from 0.3 to 1.5 m, which is too supported by the micromorphological studies. The surface of the soil profile is blanketed with a silt and clay layer which is characteristic of flooding.

OSL dating of different geomorphic units were carried out to decipher the chronological evolution of the megafan. Based on the OSL ages, the Sone megafan has been divided into Oldest Sone plain (OdSP, age varies from 22 ± 1.84 Ka to 14.25 ± 0.78 Ka) in the west, Old Sone plain (OSP, age varies from 8.0 ± 0.7 Ka to 7.31 ± 0.55 Ka) in the east and Young Sone plain (YSP, age varies from 0.89 ± 0.02 Ka to 0.57 ± 0.1 Ka) in the middle of the megafan surface. The distal part of the megafan shows recent overlap of sediments of the Ganga River (1.3 ± 0.16 and 2.4 ± 0.14 Ka).

To decipher the geomorphic variation, spot heights and contours from the Survey of India toposheets on a scale of 1:50000 were used to create digital elevation model (DEM) of the megafan surface. A 3-D view of the DEM shows the regional topographic architecture of the Sone megafan. The profiles extracted from DEM across the fault zone indicated the fault trace of the EPF and WPF. However, surficial signatures of West Patna Fault are comparatively low due to erosion, extreme settlement and agricultural activities.

Ground Penetrating Radar (GPR) study was carried out across the demarcated fault zone of WPF and EPF. Displacement in the GPR profile

confirms the effect of these faults in the cover sediments in their respective fault zones. The WPF and EPF are normal faults which dip towards the west and east directions, respectively, forming a horst below the megafan.

Soft sediment deformation structures identified as seismites in the present study area were reported for the first time from the south of Ganga River in the middle Ganga plain. Their proximity to the EPF indicates moderate-size earthquakes (or aftershock triggered by major earthquakes) on the fault in the past or mega earthquake in the nearby Himalaya.

The integrated approach adopted for the present study shows that the Late Quaternary evolution of the Sone megafan occurred largely under the tectonic controls exhibited by probable uplift along the peripheral bulge region. As the megafan rests on the tectonic block bounded by the EPF and WPF, compression from SW and the Himalaya promotes block tilting which in turn influences the fluvial geomorphology of the megafan in space and time. Similar block tilting and megafan growth has been reported in the northern part of the present area i.e. in the Gandak megafan. By analyzing the present result, it is quite evident that similar geological processes are too acting in the present area of study. The Sone River initially flowing in the western part of the megafan responded to first event of tectonic uplift along northwestern part of the tectonic block formed between the WPF and EPF by eastward shifting of the channel. This is supported by the OSL ages from the western part of the megafan. The river continued to shift eastward until the second event of tectonic tilt uplifted the southwestern part of the block causing the river to reverse the direction of shifting. The river was shifting westward until it attained a rather stable course which is the present course of the river. The river may have attained this stability in the past also, allowing only the downstream part of the river to undergo avulsions in east-west directions as many paleochannels appear in the downstream as compared to the upstream. Based on the inferences drawn from combined study of geomorphic, and pedological features with OSL dating, the Sone megafan was identified with 4 geomorphic units, namely, OdSP lying to the west of the Sone River, OSP covering the eastern part of the plain, YSP spread in triangular shape near downstream part of the river, and AFP belt of

fresh sediments along present channels of Sone and Ganga rivers. The block tilting and channel migration can be well correlated with the influence of the Himalayan tectonics on the Ganga plain and especially on the fault bounded tectonic blocks. The tectonic blocks tilt and twist due to compression between the peninsula and the Himalaya. Hence the rivers of the alluvial plain shift their course in response to the tectonic tilting which in turn modifies the geomorphology, sedimentology and pedology of the region.

ACKNOWLEDGEMENTS

Since my first day of joining as a research scholar, I have felt at home at IIT Roorkee. These five years of study and research have given me unique opportunities. It has been a period of intense learning for me, not only in the scientific arena, but also on a personal level. This thesis represents not only my work at the keyboard, it presents the results of work done in field and laboratory alike with the help of a number of remarkable individuals who I wish to acknowledge.

First and foremost, I would like to express my sincere gratitude to my advisor **Dr. Pitambar Pati**, for the continuous support of my Ph.D. research, for his patience, motivation, and immense knowledge. His guidance helped me in all the time of research and writing of this thesis. I could not have imagined having a better advisor and mentor for my Ph.D.

Besides my advisor, I would like to thank the rest of my research committee: **Prof. R. Krishnamurthy, Prof. Arun K. Saraf**, **Dr. A. S. Maurya** and **Dr. J. Das**, for their insightful comments and encouragement, which helped my research from various perspectives.

My sincere thanks also go to **Prof. S. Bajpai** (Head of Department), **Prof. D. C. Srivastava** and **Dr. Manoj K. Jaiswal**, Assistant Professor, Department of Earth Sciences, Indian Institute of Science Education and Research (IISER) Kolkata, who gave access to the laboratory and research facilities. Without their precious support it would not be possible to conduct this research.

I thank my fellow labmates: **Dr. Vijay Sharma**, **Chinmay Dash**, **Ankit Gupta** and **Narendra Patel** and my friends **Dr. Susanta Borgohain Gaurav Singh** and **Rajesh P. Shukla** for the stimulating discussions, for the sleepless nights we were working together before deadlines, and for all the fun we have had in the last five years. Also, I thank my friends **Belligraham Narzary** and **Mahadev** in IISER Kolkata.

Last but not the least, I would like to thank my family: my parents and to my brothers for supporting me spiritually throughout writing this thesis and my life in general.

CONTENTS

ABSTRACT *i*

ACKNOWLEDGEMENTS *v*

CONTENTS *vii*

LIST OF FIGURES *ix*

LIST OF TABLES *xv*

Chapter 1 ***1***

1.1 INTRODUCTION 1

1.2 GENERAL DESCRIPTION OF THE STUDY AREA 2

1.3 ALLUVIAL STRATIGRAPHY OF THE MIDDLE GANGA PLAIN 8

1.4 REVIEW OF PREVIOUS WORK 10

1.5 RESEARCH OBJECTIVES 12

1.6 SCOPE OF THE PRESENT STUDY 13

1.7 ORGANISATION OF THE THESIS 14

Chapter 2 ***17***

2.1 SATELLITE IMAGES AND DIGITAL ELEVATION MODELS 17

2.2 DRAINAGE CHARACTERISTICS 22

2.3 DRAINAGE EVOLUTION 27

Chapter 3 ***31***

3.1 INTRODUCTION 31

3.2 SEISMITES IN THE MIDDLE GANGA PLAIN 32

3.3 METHODOLOGY 34

3.4 DEFORMATION STRUCTURES IDENTIFIED IN THE STUDY AREA 35

3.5 MECHANISM AND IMPLICATIONS OF SEISMITES 40

Chapter 4 ***47***

4.1 INTRODUCTION 47

4.2 EVALUATION OF PALEODOSE 49
4.2 MECHANISM 51
4.3 SAMPLE COLLECTION AND PREPARATION 51
4.4 OSL MEASUREMENT 53
4.5 ANNUAL DOSE-RATE 53
4.6 AGE ESTIMATION 54
4.7 RESULTS 54
Chapter 5 ***57***
5.1 INTRODUCTION 57
5.2 SOIL MICROMORPHOLOGY OF THE STUDY AREA 61
5.3 MICROMORPHOLOGICAL FEATURES 63
5.4 INFERENCES 67
Chapter 6 ***69***
6.1 INTRODUCTION 69
6.2 PRINCIPLES 70
6.3 METHODOLOGY 72
6.4 DATA ACQUISITION 74
6.5 GPR DATA PROCESSING 75
6.6 SHALLOW SUBSURFACE SECONDARY FAULTS 78
Chapter 7 ***81***
7.1 SUMMARY 81
7.2 CONCLUSIONS 87
BIBLIOGRAPHY ***89***

LIST OF FIGURES

Figure 1.1 Middle Ganga plain showing the Gandak and Sone megafan with important faults in the area. The base image is taken from Google Earth. 3

Figure 1.2 River basin map of Middle Ganga Plain (source: Water Resources Department, Government of Bihar). 5

Figure 1.3 Map showing the basement depth, important rivers, epicentres and basement fault in the region (GSI, 2000). 7

Figure 1.4 Indo Indo-Asian collision zone showing the estimated slip potential along the Himalaya. Yellow segments along the bars show the slip potential on a scale of 1 to 10 meters, that is, the potential slip that has accumulated since the last recorded great earthquake, or since 1800. The green portions show possible additional slip permitted by ignorance of the preceding historic record. The bars are not intended to indicate the locus of specific future great earthquakes but are simply spaced at equal intervals. Rupture area of major historical earthquakes along the Himalaya (light yellow boundary). Focal mechanism of major earthquakes (M>5) between 1963 and 1999. Black arrows show slip vectors on north dipping planes. (modified after Avouac et al., 2001 and Bilham et al., 2001).....9

Figure 1.5 Distribution of soil sodicity and salinity across the Sone River in its megafan (source: NBSS and LUP, 2002). 12

Figure 2.1 Satellite image draped over DEM to obtain a perspective view of the southern middle Ganga plain. 19

Figure 2.2 DEM of the Sone megafan created from spot heights in 1:50000 scale SOI toposheets (exaggeration value: 14). 20

Figure 2.3 Digital Elevation Model (DEM) of the study area illustrating surface topography, NE-SW trending East Patna Fault (EPF), and the presence

of its secondary faults on the surface and subsurface in the fault zone. 21

Figure 2.4 Map of the active drainage towards the south of river Ganga in middle Ganga plain. The short-dotted line shows the boundary of the Sone megafan. 22

Figure 2.5 Map of active drainage in parts of Sone megafan affected within the fault-zone of East Patna Fault. 23

Figure 2.6 The ponds digitized from the topographic maps and Landsat image are concentrated between the BKF and the EPF. They show the contrasting difference in alignment and superficial size in comparison to ponds towards the west of BKF. The locations of GPR profiles and seismites near the EPF. The paleochannels of the Sone River (marked by white arrows) are clearly visible in the satellite image of the area. . 25

Figure 2.7 Longitudinal river profile of the Ganga River and Dhowa nadi indicating tectonically active nature of the EPF. The background image is a part of the SRTM DEM of southern Ganga plain with drainage network, general elevation of the area is decreasing from SW towards NE. The x-axis represents profile length in kilometers, and the y-axis shows elevation in meters. The black lines in the graph show best fir curve for the elevation profile by averaging 40 points on x-axis. 26

Figure 2.8 Four geomorphic units identified in the Sone megafan. OdSP- Oldest Sone Plain, OSP- Old Sone Plain, YSP- Young Sone Plain, AFP- Active Floodplain. Base image is obtained from Google Earth. 28

Figure 2.9 Standard FCC of Landsat ETM+ (R:7 G:4 B:2) showing braided network of paleochannels of Sone River. The darker tones show higher moisture towards the east of Sone and ponds appear as dark patches near the river. 28

Figure 3.1 The study area is shown by a translucent rectangle in the southern part of the middle Ganga plain containing major river systems and the

basement structures (EPF: East Patna Fault; MSR: Munger-Saharsa Ridge. 34

Figure 3.2 (a) Listric microfault and associated sagging of the sand beds observed on the bank of river Dardha (shown by yellow arrows), (b) figure redrawn and labelled from the actual photograph.....36

Figure 3.3 (a) Pillar and pocket structure formed by the upward movement of water saturated sediments by intense shaking of the region due to earthquake event (marked by yellow arrows), (b) deformation structures redrawn, marked and labelled by black arrows.....36

Figure 3.4 (a) Water escape structures preserved in the riverine sand bed as liquefaction cusps and disturbed laminae (shown by yellow arrows in actual photograph), (b) structures redrawn from the photograph (marked by black arrows). 37

Figure 3.5 (a) Alternating sand and dark colored fine sediment layers deformed into V-shaped wedges identified as thixotropic wedges observed on the eastern bank of the river Dardha (shown by yellow arrows), (b) prominent features redrawn and labelled from the actual photograph. 37

Figure 3.6 (a) The actual photograph showing fold and associated sagging observed in the overlying sand layers underlain by undeformed inclined sand beds resulting from impact by cyclic shear waves (shown by yellow arrows), (b) structures redrawn and labelled from the photograph.....38

Figure 3.7 (a) The refolding of intensely folded clay layer between sand beds associated with the downsagging of overlying sand beds occurring with other seismites in the same location (marked by yellow arrows in the photograph), (b) features redrawn and labelled from the actual photograph. 38

Figure 3.8 Exposure at Janardanpur showing the deformation by small-scale normal fault causing localized drag fold in clay bed trapped in the sand bed.....39

Figure 3.9 The cross-stratification structures are shown by the sand beds deposition indicating fluvial environment. Topset and foreset dipping 3° and 22° respectively towards NE direction. Location – Janardanpur. . 39

Figure 3.10 Abrupt termination of clay beds against a steep plane. Often during earthquake-induced downsagging of the sediments, the adjacent beds tend to abruptly terminate against the steep walls of the sagging structure thus formed. Exposure at Janardanpur..... 40

Figure 3.11 Sedimentary logs showing some of the best-developed soil profiles indicative of fluvial environment in the study area. 42

Figure 4.1 Types of samples to which different dating techniques can be applied (Aitken, 1998). 48

Figure 4.2 Age range of various methods. Actual limits are dependent on circumstances such as state of sample preservation (Aitken, 1998)... 48

Figure 4.3 The event dated in optical dating is the setting to zero, or near zero, of the latent luminescence acquired at some time in the past (Aitken, 1998). 49

Figure 4.4 Additive method of paleodose evaluation. Each data point is average OSL from a group of aliquots. Laboratory dose is zero for N. P is read off as paleodose (Aitken, 1998). 50

Figure 4.5 The regeneration plot. The aliquots have been bleached and dosed. N is the natural OSL. P is read off as paleodose by regeneration..... 50

Figure 4.6 Sample numbers and their locations in the study area. Base map is a Resourcesat2 satellite image: AWiFS (R: 5 G:4 B:3). 54

Figure 5.1 Relative thickness of different types of soil identified in field observation and their respective locations shown on satellite image. The base image is a standard FCC of Landsat ETM+ image (R:7 G:4 B:2). 59

Figure 5.2 (a) Section from YSP showing sand deposit with no soil development, 2 (b) Section from YSP, gravel and sand beds in paleochannel of Sone River, 22 (c) Section from distal part of Sone megafan, gray sand desposit by Ganga River, 6. Numbers show the section location (refer to figure 5.1).....60

Figure 5.3 (a) Moderately developed soil section from OSP, 5 (b) weakly developed B-horizon of soil section from OSP, 4 (c) Section from OSP, shows thick sand deposition dipping towards the river paleochannel, 3. Numbers show the section location (refer to figure 5.1). 61

Figure 5.4 Some of the sections from OdSP. (a), (b), (c) and (d) show the hard and compact, well-developed loamy soil profiles from OdSP at locations 10, 15, 21 and 17, respectively. (e) a section from the paleochannel of Sone River, 23. Refer to figure 5.1 for locations in the study area. 62

Figure 5.5 (a) Apedal,Fe-Mn impregnated dense ground mass, rootlets filled with silica, YSP (b) Weakly developed sub angular blocky structure, OSP (c) Moderately developed sub angular blocky structure, OSP (d) Stipple-specled b-fabric,cross cutting void, YSP (e) Fractured Quartz grain(QZ) and accumulation of Fe-Mn rich material, YSP (f) Moderately developed reticulate striated b-fabric, OSP. 65

Figure 5.6 (a) Deformed reticulate striated b-fabric, OdSP (b) Muscovite laths and Fe-Mn impregnated dense ground mass, OdSP (c) Strongly developed spheroidal blocky peds, OdSP (d) Very strongly developed spheroidal blocky peds, OdSP (e) Strongly developed peds with altered Biotites, OdSP (f) Moderately developed sub angular blocky peds with Channels filled with secondary materials, OdSP. 66

Figure 6.1 GPR data acquisition and resulting radar reflection profile (a) Data acquisition at a single survey point, showing GPR system components and subsurface reflector configuration (b) radar reflection profile resulting from sequential plotting of individual traces from adjacent survey points. Positions of air wave, ground wave and primary reflections are indicated (Neal. 2004). 71

Figure 6.2 Location of ground penetrating radar (GPR) survey carried out across East Patna Fault (EPF) near Daniawan village in Patna, Bihar. The base image is obtained from Google Earth. 73

Figure 6.3 Location of ground penetrating radar (GPR) survey carried out across East Patna Fault (EPF) in Jehanabad distrct of south Bihar. The base image is obtained from Google Earth..... 73

Figure 6.4 Ground penetrating radar (GPR) setup with survey, shielded antennae, control unit and fibre cables for survey in distance mode... 74

Figure 6.5 GPR profiles across the East Patna Fault show both antithetic and synthetic nature of secondary faults (a) Image of GPR profile obtained (b) Schematic diagram of the profile. 79

Figure 6.6 Ground Penetrating Radar (GPR) profile across West Patna Fault near Bikramganj. Figure on the left is a part of radargram showing the fault signatures. The right figure shows location of GPR survey path as white line (~3 km) across WPF (shown by black solid line). The base image is taken from Google Earth..... 79

Figure 7.1 A 3-D representational model of middle Ganga plain showing major faults and three generations of Sone River channels in the study area. The rose plot of paleochannel direction shows NNE, ENE and NE direction of Sone during I, II and III phases, respectively. I-, II- and III-phase are oldest, older and present course of the river. 82

Figure 7.2 Different tilting direction causing distinct phases of Sone megafan evolution. Phase 1: development of oldest soils while eastward tilting. Phase 2: development of thick clay-sand alternating beds during westward tilting. Phase 3: deposition of coarse sand beds around current course of the Sone River during present stable period..... 83

LIST OF TABLES

Table 4.1 OSL age of the sediments from Sone megafan.....55

Table 5.1 Soil horizon letter designations (source: Encyclopædia Britannica, Inc).....58

Table 6.1 Dielectric values for common materials (Reynolds, 1997) 72

Chapter 1

INTRODUCTION

1.1 INTRODUCTION

The Indo-Gangetic foreland basin is extensively stretching from the Indus basin in NW to Upper Assam in NE and separating the Himalayan thrust fold belt from the Indian craton. Collision of the Indian and Eurasian plates during the Paleocene led to the formation of this largest sedimentary basin of the Indian subcontinent around 60 Ma ago (Beck et al., 1995; Dewey and Bird, 1970; Sinha et al., 2005b). Continuous sedimentation process for filling up the basin since 20 Ma (Parkash et al., 1980) lead to the present geological setting. Terrigenous clastic sediments deposited by the Himalayan rivers dominate the basin. However, the rivers drawing clastic sediments from the southern peripheral bulge have distributed in the southern reaches of the alluvial tract. The Ganga plain has been divided into Upper, Middle and Lower plain from west to east by Srivastava et al. (1994) and Thomas et al. (2002) on the basis of degree of river incision, soil development, subsidence rate and characteristic geomorphic landforms.

Geomorphology, sedimentology, pedology, surface deformations and structural studies of sub-surface faults, along with geochronology and tectonic studies have been carried out in the Ganga plains by several researchers in the last few decades (Bhosle et al., 2008; Mohindra et al., 1992; Singh, 1996; Singh et al., 2006; Sinha et al., 2009; Sinha and Ghosh, 2012). Recent advances in the extraction of surficial and subsurface geological and geophysical data has increased our understanding of tectonic processes and their role in basin evolution (Miall, 1991, 1981, 1978). However, the middle Ganga plain which spans between the Ghaghara and Kosi rivers, separating the Indian shield from the marginal alluvial plain by the peripheral bulge in south and meeting Himalayan Frontal Thrust (HFT) in the north, has only recently gained the focus of detailed study. As the middle Ganga plain is tectonically more active it needs greater attention in terms of neotectonic and geomorphic studies.

The present study focusses on the geomorphology, neotectonic activity and pedology of southern middle Ganga plain during middle to late Holocene. An integrated approach including remote sensing and GIS, field study, geophysical survey, micromorphological study and Optically Stimulated Luminescence (OSL) dating have been utilised to understand the development of alluvial plain towards south of the Ganga River. Landsat Enhanced Thematic Mapper Plus (ETM+) images have been used to identify different geomorphic units in the area. Digital elevation models (DEMs) have been used to demarcate subtle topographical changes in the plain. Micromorphology of soils has been used to understand the pedogenic processes and varying degree of soil development in different parts of the study area. OSL dating has been carried out to establish the chronology prevailing geomorphic processes and recent tectonic events in the region. Shallow sub-surface geophysical survey has been conducted by ground penetrating radar (GPR) to pick up the ground signatures of active tectonics in the region with the help of radargrams across a subsurface fault in the area. While field study was carried out to observe soil profiles and to collect soil samples, soft sediment deformation structures were identified. These are prominent indicators of seismicity and have been reported for the first time in this area.

1.2 GENERAL DESCRIPTION OF THE STUDY AREA

1.2.1 Geographical Extent

The study area is a part of the marginal plain to the north of the Vindhyan highlands limited between latitude 24.75°N to 25.75°N and longitude 83.0°E to 86.0°E. It covers parts of the middle Ganga plain towards south of the Ganga River, which is also known as south Bihar plain because geopolitically it falls in the Bihar state of India. Thus, its northern extent is bounded by the Ganga River and southern by the exposures of Vindhyan sedimentary rocks (Fig. 1.1).

1.2.2 Physiography

According to Singh (1996), the Ganga plain had remained largely unexplored during past decades due to its extreme flatness and geomorphologically monotonous character. However, its association with the

Himalayan orogeny has invited several geologists to undertake detailed investigation of the region in recent years to study the influence of Himalayan tectonics in the plains.

Physiographically, the middle Ganga plain is not different than the rest of the Ganga plain. Though it lacks major surficial structures or landforms in the first observation, recent advances in the technology, such as availability of spatially high resolution digital elevation models and satellite images, has made it possible to investigate the geomorphology of the region up close. Several landforms including megafans, terminal fans, paleochannels, avulsion surfaces, floodplains, river terraces, etc have been identified in the middle Ganga plain (Singh et al., 2015, 2009, Singh and Awasthi, 2011a, 2011b; Singh and Singh, 2005). These features are significant in understanding the geomorphological as well as tectonic evolution of the plain in response to the Himalayan tectonics.

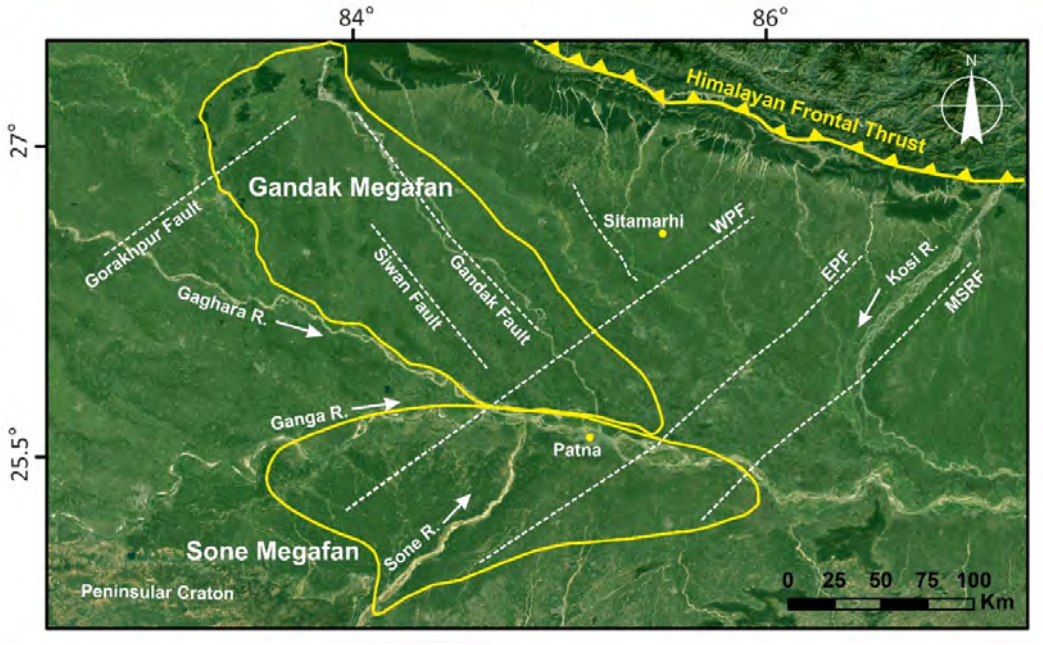

Figure 1.1 Middle Ganga plain showing the Gandak and Sone megafan with important faults in the area. The base image is taken from Google Earth.

The southern middle Ganga plain is mostly flat and devoid of major topographical changes. However, minor relief breaks of few metres in measure, paleochannels, levees, active channels and floodplains, a network of stagnant water bodies are observed. The most prominent alluvial geomorphic feature in the area is the Sone megafan which was formed by the sediments deposited

by the Sone River carried out from the adjacent Indian craton. Thus, it implies that not only the Himalaya, the peninsular shield has also played certain role in development of this vast alluvial tract (Ameen et al., 2007; Bhosle et al., 2008; Khan et al., 2015, 2005). The megafan covers almost entire study area. Average sediment thickness of the megafan increases northward from exposures of Vindhyan rocks (i.e. 0 m) to 500 m near the Ganga River which suddenly increases to 1000–2000 m towards north of the river (Agarwal, 1977; GSI, 2000; Sengupta, 1996). With a variation of 0.03–0.04° slope towards the north, the surface of the southern middle Ganga plain is almost flat. Topographic elevation varies from 50 m in the North to about 120 m in the South, above the mean sea level (Sahu et al., 2010).

1.2.3 Climate

The study area experiences mainly two types of climates: Hot-summer Mediterranean climate (as observed mainly in Patna, Gaya, Munger, Dehri-on-Sone, Jehanabad) and Humid subtropical climate (observed in Kishanganj, Motihari, Jogbani, Araria, Raniganj) (https://en.climate-data.org/region/773). The average temperature in the region varies between 16°–19°C during winters (Dec–Feb), 25°–31°C during summers (Mar–May), 31°–28°C during monsoon (Jun–Sep) and 26°–21°C during post-monsoon (Oct–Dec). So, the year-round average temperature falls around 25°C. The precipitation varies largely in the region from ~100 mm during winter and summer to ~1060 mm during monsoon and ~50 mm during post monsoon season, making it a year-round average of ~1200 mm (https://en.wikipedia.org/wiki/Climate_of_Bihar).

1.2.4 Drainage

The study area is an alluvial plain with varying thickness of unconsolidated sediment-fill. The drainage in such terrain hold an indispensable importance as it not only controls the anthropogenic activities such as agriculture and settlement, but also provides local markers for the neotectonic activity. The drainage on such easily mobilizable sediments often quickly responds to recent tectonic activity by showing channel avulsion, paleochannels and abandoned oriented network of disseminated ponds.

The Sone River is the largest tributary of the Ganga River from southern Ganga plain and is a major contributor of sediments deposited in the area. Migration of the river channels in geological time scales in response to neotectonic activity led to development of the Sone megafan. The Sone River originates from the Amarkantak highlands. It flows almost in east–west direction on the elevated plateau of central India, then suddenly takes a sharp turn to follow northeastward trend near Rohtasgarh plateau and enters into the study area. The other major contributors to the Sone drainage basin are Punpun,

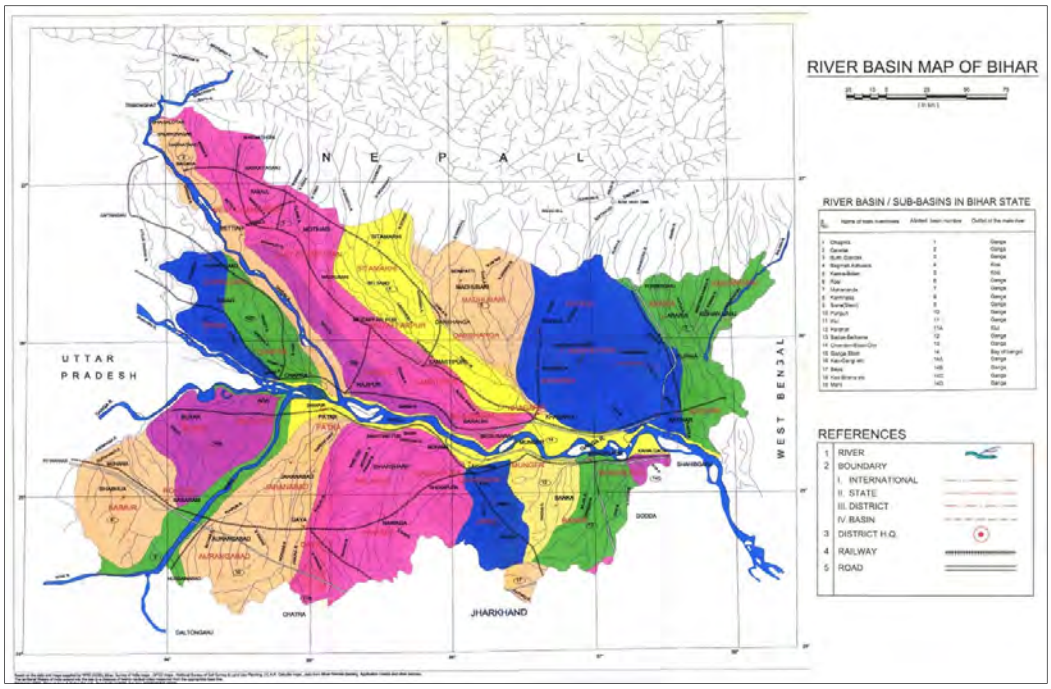

Figure 1.2 River basin map of Middle Ganga Plain (source: Water Resources Department, Government of Bihar).

Phalgu and Dardha rivers. Several ephemeral streams of these rivers locally form a dendritic pattern and rework the surface sediments (Fig. 1.2). Apart from these, the paleodrainage network in the region is represented by numerous abandoned stagnant water bodies characteristic of river migration. Though the overall drainage pattern of the Sone and the Ganga rivers in the alluvial reaches of the Sone-Ganga basin is not controlled by bedrock heterogeneities (Sinha and Friend, 1994), effective structural control over drainage pattern can be observed around the subsurface fault present in the study area. During the Quaternary, tectonics and climate in the region are main controlling factors for

geomorphological and fluvial evolution and sediment remobilization (Sahu and Saha, 2014).

1.2.5 Subsurface features

Subsurface configuration of the foredeep plain is architectured by some major faults, defining horst-graben structures. These faults display northeasterly trends. The West Patna Fault (WPF), East Patna Fault (EPF) and Munger Saharsa Ridge Fault (MSRF) having northeasterly trend form alternate horst and graben from west to east, respectively. These tectonic discontinuities of the foredeep, particularly having a northeasterly trend, are considered to be the locale of post collision strain adjustment along the leading edge of the Indian shield and thus are likely to be of neotectonic (GSI, 2000).

The basement of the Ganga plain spans almost NW-SE adjacent to the Himalayan foothills and is segmented into several tectonic blocks by the NE-SW trending subsurface faults. These NE-SW trending subsurface faults in the Ganga plain were developed due to the NW-SE extension in the Himalayan foreland basin by compression from the southwest direction (Bhosle et al., 2008; Parkash et al., 2000; Pati et al., 2011a, 2011b, Singh et al., 1997, 2006). These active basement faults are buried under thick sediment cover and hence their surface expressions are less pronounced.

The East Patna Fault (EPF) is an NE-SW trending east dipping subsurface normal fault transverse to the trend of the Himalayan Frontal Thrust. It is present in the middle Ganga plain (MGP) buried under the foredeep alluvium cover of varying thickness from 500 m (to the south of the Ganga River, near Patna) to 5000 m at the northern end (near Madhubani) (Fig. 1.3). West Patna Fault is a west dipping subsurface fault while Munger Saharsa Ridge Fault also running parallel to the EPF dips towards east. These subsurface faults correspond to the basement ridges. Based on the subsurface information in the Ganga plain derived from aeromagnetic, gravity, seismic and magnetic surveys carried out by several researchers (Agarwal, 1977; Dasgupta et al., 1987; Karunakaran and Ranga Rao, 1979; Lyon-Caen and Molnar, 1985; Rao, 1973; Sastri et al., 1971; Valdiya, 1976) and deep drillings and the geophysical

surveys conducted by Oil and Natural Gas Corporation (ONGC), presence of the basement ridges in the foredeep has been well established. Subsurface structural confinement of the broad region is represented by the Munger Saharsa Ridge in the east and the Rohtasgarh Ridge in the west. Three important ridges underlying the study area are West Patna Ridge, East Patna Ridge and Munger Saharsa Ridge (Fig. 1.3). North to northeasterly dipping Vindhyan rocks are overlain by the Quaternary alluvium in this ridge-bounded trough (Prakash et al., 1990). In addition, using geophysical signatures such as gravity, aeromagnetic and seismic surveys, Geological Survey of India (GSI, 2000) mapped the subsurface extension of the fault near about 168 km length to the north of the Ganga River (Fig. 1.3). Dasgupta (1993) and Jain and Sinha

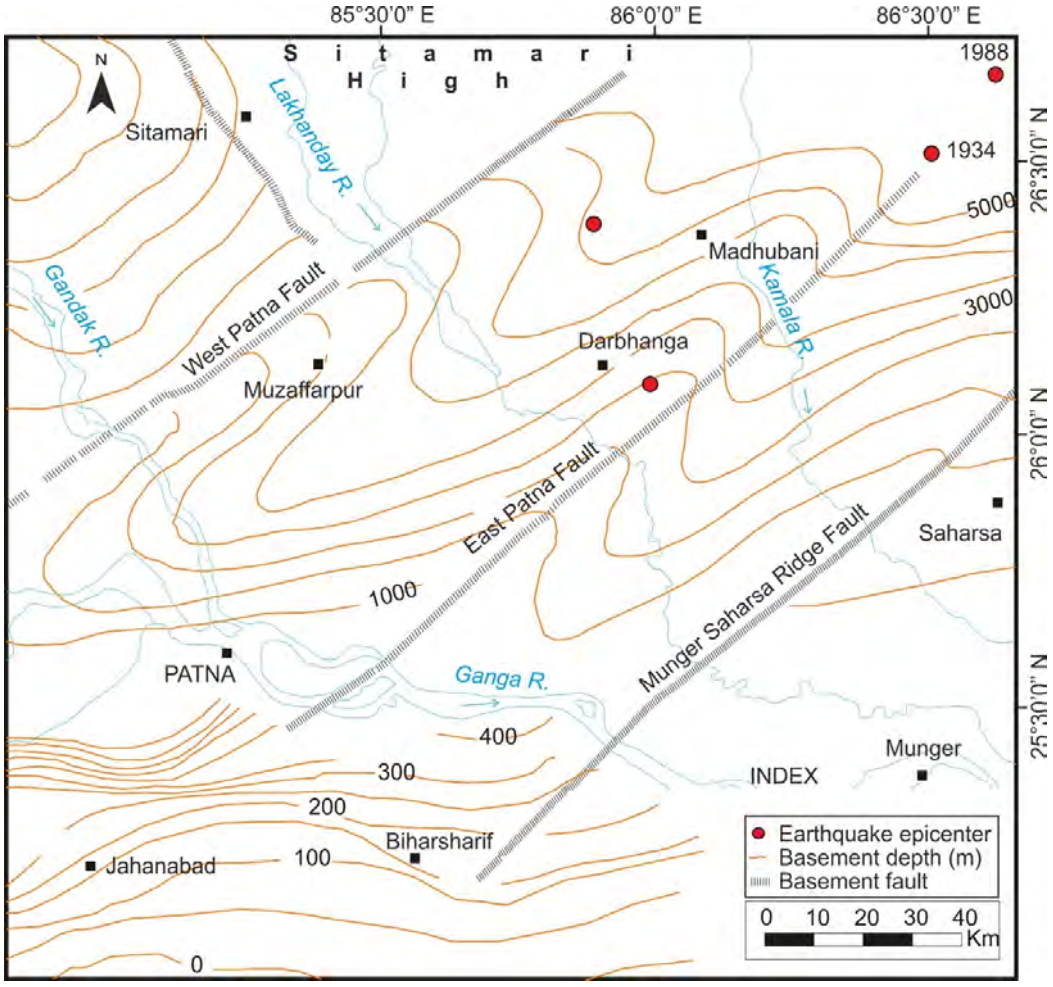

Figure 1.3 Map showing the basement depth, important rivers, epicentres and basement fault in the region (GSI, 2000).

(2005) suggested the active nature of the fault in the northern part of the plain (north of the Ganga River) on the basis of geophysical and geomorphological

evidence, respectively. Though Sinha et al. (2010) and Sahu et al. (2010) suggested the extension of this fault to the south of the Ganga River based on various fluvial anomalies, however, no significant evidence for the continuation was reported.

1.2.6 Earthquake recurrence

The NE–SW trending East Patna Fault lies in the middle of the region and follows the trend of the basement ridges. The fault is oriented transverse to the Himalayan arc, which resides close to its northward extension. As these faults follow the highest horizontal compressive stress direction (NE–SW i.e. transverse to the Himalayan Frontal Thrust), movement along these faults have caused several earthquakes (1833, 1906, 1934 and 1988) in the region (Banghar, 1991). These earthquakes modified the stress regime of the region through the slip along the fault plane and deformation in the source region, thereby releasing the accumulated strain in the region and reducing the slip potential (Fig. 1.4).

1.3 ALLUVIAL STRATIGRAPHY OF THE MIDDLE GANGA PLAIN

The middle Ganga plain is confined between the rivers Rapti and Kosi, occupied largely by the Kosi and Gandak megafans, and Kosi-Gandak interfan area to the north of the Ganga River. Dominant geomorphic feature in the south of the Ganga River is the Sone megafan. Frequent change in river courses in this region leaves abandoned alluvial plains characterized by a different degree of soil development corresponding to the time elapsed since channel abandonment. Shallow sub-surface stratigraphy provided by Singh et al. (1993) shows about 10 m thick surficial unit of sand and mud, identified as “megafan sweep” succession, underlain by more than 60 m thick sand and gravel bed deposited by braided river system in the northern middle Ganga plain (in the Kosi megafan).

Lack of natural exposures has confined the knowledge of the Quaternary alluvial history of the region. Most of the surface in the Ganga plain is covered by newer alluvium (Holocene) which consists of mostly unoxidized sand and silt-clay, indicative of mainly fluvial and fluvio–lacustrine environments. The

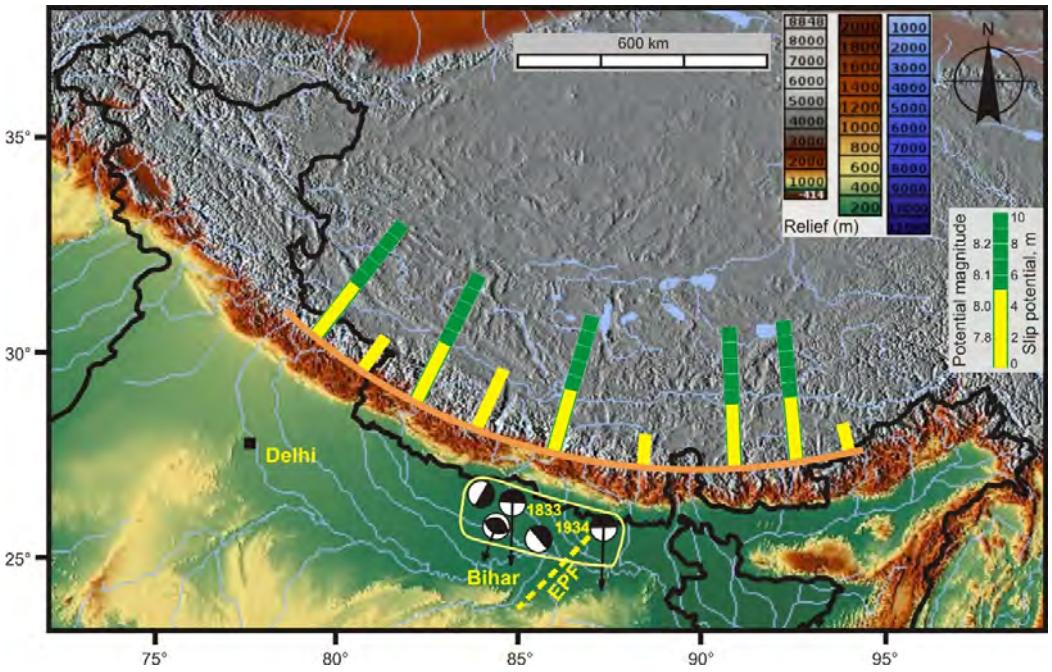

Figure 1.4 Indo Indo-Asian collision zone showing the estimated slip potential along the Himalaya. Yellow segments along the bars show the slip potential on a scale of 1 to 10 meters, that is, the potential slip that has accumulated since the last recorded great earthquake, or since 1800. The green portions show possible additional slip permitted by ignorance of the preceding historic record. The bars are not intended to indicate the locus of specific future great earthquakes but are simply spaced at equal intervals. Rupture area of major historical earthquakes along the Himalaya (light yellow boundary). Focal mechanism of major earthquakes (M>5) between 1963 and 1999. Black arrows show slip vectors on north dipping planes. (modified after Avouac et al., 2001 and Bilham et al., 2001).

channels in this area (i.e. middle Ganga plain) are not incised and the exposed bank sediments are those of the modern, aggrading fluvial system, rather than that of early Holocene or late Pleistocene sediments (Sinha et al., 2005a, 2005b). However, Sahu et al. (2010) reported incision on the southern middle Ganga plain on the proximal part of the Sone megafan, where alluvial deposits of few meters, consisting of sand and clay are exposed.

In the plains south of the Ganga River, Williams and Clarke (1984, 1995) described alluvial sequences in the Belan and Sone valleys ranging in age from Middle Pleistocene to Holocene. The alluvial thickness ranges from 0 m, where the outcrops of the basement (Vindhyan sedimentary rocks) exist near the peninsular region, to 300–400 m near the Ganga River. The Sone megafan

covers an area of about 11,560 km^2. The plain to the east of the Sone River has thick clay deposits with an average thickness of about 1 m underlain by relatively thinner sand beds of an average thickness of 0.3 m. Several locations showing a few centimeters thick alternate sand and clay layers near the base of the exposure imply different quick episodes of floods and standing water conditions in the region. Comparatively, the region to the west of the Sone River shows ~0.4 m thick clay beds capped by the mature soil with the solum thickness varying between 0.3 m and 4 m. The central part the Sone megafan is occupied by recent river deposits composed of coarse-grained sand. Variation in the soil characteristics and other geomorphic signatures show gradual eastward migration of the Sone River over a longer period of time followed by rather quick westward reversal to attain the present stable channel position (Sahu et al., 2010).

1.4 REVIEW OF PREVIOUS WORK

1.4.1 Geomorphology

During the earliest phases of geomorphological study in the Indo-Gangetic plain, two main types of alluvial surfaces were recognised Khadar (newer alluvium) and Bhangar (older alluvium) (Oldham, 1917; Pascoe, 1919). This terminology has still been in use for the alluvial plains of the Ganga plains (Singh, 1996; Singh et al., 2004). Uplands and interfluve overlain by calcareous soils form the older alluvium i.e. Bhangar while the Khadar constitutes the soils of areas close to the rivers which keep receiving fresh sediments from flooding events.

Some systematic geomorphic studies have been carried out in the Ganga plain by Geddes (1960) and Mukerji (1963). Its sediment fill and basement was studied in view of petroleum prospects (Rao, 1973; Sastri et al., 1971). The central part of the Indo-Gangetic plain is occupied by what is known as the Ganga plain which shows a variety of landforms and drainage system. It appears almost flat due to low relief difference over large distances (Singh, 1996). The basin is asymmetric in nature which gently slopes to opposite directions in its northern and southern parts. The Ganga plain has also been

classified into two regions as western Ganga plain (Uttar Pradesh) and eastern Ganga plain (Bihar). The western part is identified with prominent river incisions and rugged terrain while the eastern counterpart is rather flat and devoid of much drainage entrenchment. According to Pathak (1982), the alluvial surface of Ganga plain can be classified into four regions from north to south: *Bhabar belt* (mostly gravel), *Terai belt* (swamps, ponds, small sandy rivers), *Central Alluvial Plain* (major part of the Ganga plain, towards north of the river Ganga and most of the rivers follow southeasterly trend), and *Marginal Alluvial Plain* (located south of the Ganga River, has coarse sandy rivers and sediments are mostly derived from the Peninsular craton). Broadly, the *Bhabar* and *Terai* regions can be combined into single *Piedmont Zone*.

The present study area constitutes this *Marginal Alluvial Plain* in the middle Ganga plain which is marked by coarse sediments derived from the peninsular craton. The region is characterised by high rate of subsidence (Jain and Sinha, 2005; Pati et al., 2011a; Valdiya and Sanwal, 2017). Some of the researchers have recently investigated this part of the Ganga plain by using satellite images, elevation models and bore holes (Sahu et al., 2015, 2010; Verma et al., 2017). The Sone megafan formed in the area due to channel migration of the Sone River in west-east direction. Its distal parts show sand covers on the top which is mostly sourced from the Ganga River. Proximal parts of the megafan show thick accumulation of coarse yellow brownish sand eroded from the adjacent Vindhyan rocks.

1.4.2 Pedology

Srivastava et al. (1994) and Thomas et al. (2002) have divided the Ganga plain into upper, middle and lower plain on the basis of soil developments. The soils of the Ganga plain specially the northern plains have recently been studied in detail by several workers (Kumar et al., 1996; Mohindra et al., 1992; Srivastava, 2001; Srivastava et al., 2017, 2003, 2000, 1994; Thomas et al., 2002). Upper Ganga plain is marked by moderately to well-developed soils. Pedology of the area towards south of the Ganga river has largely remained unexplored. The National Bureau of Soil Survey and Land Use Planning (NBSS and LUP) have published regional soil maps which shows

slight sodicity in most of the study area. Soils towards west of the Sone river however show slight salinity and slight sodicity. Slightly saline soils can also be

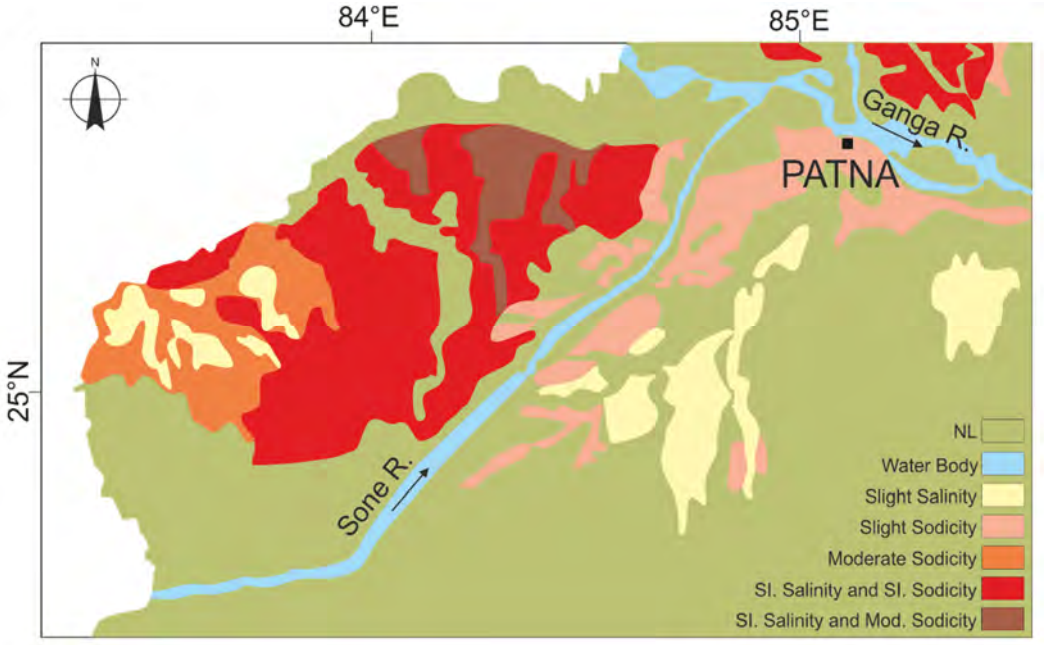

Figure 1.5 Distribution of soil sodicity and salinity across the Sone River in its megafan (source: NBSS and LUP, 2002).

observed on the eastern part (Fig. 1.5). Micromorphological study of the soils from the Sone megafan has not been carried out yet. Thus, the present study has touched upon that factor. More detailed study may prove to be beneficial in working out the paleoclimatic and evolutionary history of this part of the Ganga plain. The present work has also identified the older alluvium at the depth of ~2 to 4 m from surface in proximal parts. Surface of the megafan can be divided into paleochannels, inter-paleochannel area, active channels and floodplains. The inter-paleochannel area shows the older alluvium which is mostly derived from peninsular shield. The extensive deposition of yellowish coarse sand indicates dominant fluvial environment and climatic as well as tectonic control on the megafan evolution.

1.5 RESEARCH OBJECTIVES

Major objectives of the present study can be summarised as follows:

1. To identify the geomorphic processes and related soil developments on the megafan surface.

2. To map the surface and subsurface tectonically adverse features such as faults in the study area.
3. Establishing the relation between tectonics, geomorphology, sedimentology and pedology in the megafan.
4. To carry out ground penetrating radar (GPR) survey to ascertain subsurface nature of fault and record any signature of recent fault activity or development of secondary faults.
5. Establishing the chronological order of tectono-geomorphic adjustments on the megafan surface.

To map the geomorphic units in the area, Landsat Enhanced Thematic Mapper Plus (ETM+) images have been used depending upon the appropriate scene availability. These multi band images have a 30 m spatial resolution and are freely available for download from USGS (https://earthexplorer.usgs.gov). The geomorphic units have been identified on the basis of colour, tonal or textural variations in the images. Digital elevation models have been prepared from the spot heights obtained from toposheets of 1:50,000 scale issued by the Survey of India to identify faults and megafan surface architecture. Shuttle Radar Topography Mission (SRTM) DEM has also been utilised for obtain elevation profiles across fault. In the field, typical profiles representing the soil development have been recorded. Box samples from undisturbed sections for micromorphological study and soil samples have been taken from C horizon for dating. The data obtained from remote sensing was validated in field by geomorphological and pedological studies, and Ground Penetrating Radar (GPR) survey. Geochronology of geomorphic surfaces and faulting events were dated through OSL dating technique. Results from different sources were combined together to work out the tectono-geomorphic evolution of the Sone megafan.

1.6 SCOPE OF THE PRESENT STUDY

Middle to late Holocene evolutionary history of the Sone megafan area is derived from an integrated approach which includes remote sensing and GIS, geomorphic study, geophysical study, fieldwork and soil micromorphology. Neotectonic framework of the area has been established with the help of

present study. The dating of soil samples from different parts of the megafan assisted the establishment of chronological order of major neotectonic events which consequently has implications for identifying the older and younger plains in the region.

1.7 ORGANISATION OF THE THESIS

The work done has been organised in seven chapters covering the introduction about the study area, methodology adopted, findings, discussion and conclusion.

Chapter 1 entitled "**INTRODUCTION**" discusses the reason for selecting this research problem. It also introduces the physiography, drainage network, climate, subsurface features and earthquake occurrences in the study area. The literature review regrading geomorphology and neotectonics of parts of the Ganga plain and objectives of the present study in view of previous studies has also been incorporated into this chapter.

Chapter 2 entitled "**REMOTE SENSING AND GIS STUDY**" deals with the preliminary research about the morphology of the area. It helped with the reconnaissance of the area to demarcate possible locations for carrying out field-based surveying such as sampling spots and GPR survey lines. It includes identification of landforms and geomorphic units in the area.

Chapter 3 entitled "**SOFT SEDIMENT DEFORMATION STRUCTURES**" includes description of deformation structures from the study area identified as seismites. These structures preserved in soft sediments have been explained in terms of their typical formation conditions and relating it to the seismic activity of the area.

Chapter 4 entitled "**OPTICALLY STIMULATED LUMINESCENCE (OSL) DATING OF SEDIMENTS**" briefly explains the procedure followed to collect samples in the field for OSL dating and the protocol of its sample preparation. The dates thus obtained helped in ascertaining the older and younger plains of the southern MGP. It also shows the order of block tilting episodes. A possibility of temporal relationship between Sone megafan and

Gandak megafan has also been discussed based on OSL ages from both parts of the middle Ganga plain.

Chapter 5 entitled "**MICROMORPHOLOGICAL STUDY OF SOIL PROFILES**" discusses degree of soil development in different parts of the Sone megafan with the help of thin sections of soils prepared from typical profiles and its relationship with the tectonic evolution of the area.

Chapter 6 entitled "**GROUND PENETRATING RADAR (GPR) STUDY**" describes the application of GPR in the study area to obtain signatures of recent fault reactivation and their implications in neotectonic history of the Sone megafan. It also includes an overview of basic methods traditionally employed to undertake the GPR survey in field and post processing of the radargrams to deduce structures picked up through survey.

Chapter 7 entitled "**SUMMARY AND CONCLUSION**" summarizes the results obtained through different studies, discusses their role in tectono-geomorphic evolution of the Sone megafan. The conclusions thus obtained from the integrated methodology adopted in present study are summarised in this chapter.

Chapter 2

REMOTE SENSING AND GIS STUDY

Apparent monotony of the surface, easily reworkable nature of unconsolidated alluvium and anthropogenic interactions hinder the employment of traditional field methods to delineate subtle surface deformations. In addition, as the region is filled with ~500 m thick sedimentary cover, direct surface signatures of the subsurface fault are less pronounced. However, the presence of associated secondary faults emanated from a main basement fault is manifested by geomorphic signatures as well as remobilized sediments on the surface. Due to different episodes of fan building events, the geomorphic elements have frequently been reworked and hence a remote sensing based synoptic overview makes the method easy to distinguish these geomorphic elements based on image elements, association and directional continuity. Therefore, a comprehensive approach assimilating interpretation and analysis of soil-geomorphic units in satellite imagery, digital elevation models (DEMs), topographic profiles, geomorphic signatures such as various active and paleo-drainage patterns, together with the association of seismites observed in the field and GPR survey have been used to map the geomorphology and tectonic features on the megafan surface. This approach is imperative to comprehend the processes which resulted into the development of the present alluvial fan.

2.1 SATELLITE IMAGES AND DIGITAL ELEVATION MODELS

The Landsat ETM+ (acquisition date: Oct 13, 2009) image was used (available from http://glovis.usgs.gov) to map the present drainage, ponds, and paleochannels. The bands were layer stacked in ERDAS IMAGINE 14 software. A standard false colour composite (FCC) was prepared from Enhanced Thematic Mapper Plus (ETM+) image using 7-4-2 band combination (the light and bright green colours represent grasslands and healthy vegetation, respectively. Pink areas represent barren soil, oranges and brown represent sparsely vegetated areas. Dry vegetation appears as orange and water as blue. Urban areas appear in shades of magenta). The geomorphic characters such as change in drainage pattern, formation of low-lying swampy and water-logged

areas which are readily found across faults were identified in the image. The toposheets obtained from the Survey of India (SOI) were georeferenced with the satellite imagery in the same geographic coordinate system for the best precision of correlation between features in the image and on the ground. Possible sites for field work and GPR survey were identified from the satellite imagery and topographic maps.

Remote sensing techniques have been widely applied to different problems such as vegetation mapping, hazard zonation, shoreline oscillation mapping, morphodynamics of rivers, etc (Jana et al., 2017, 2016; Lee and Pradhan, 2007; Maiti, 2013; Maiti and Bhattacharya, 2011, 2009, Pradhan, 2013, 2010; Pradhan and Lee, 2010). In geomorphological mapping, the remote sensing is being increasingly used recently as it provides a synoptic overview to see a large area at a stretch (Bhosle et al., 2009; Frodella et al., 2016; Gilvear and Bryant, 2016; Kumar et al., 2018; Pati et al., 2015; Piégay et al., 2015; Sinha and Ghosh, 2012). Geomorphological elements such as flood plain, paleo and active channels, interfluve area, terminal and alluvial fans, river terraces and others are easily seen in satellite image based on their typical geomorphic characteristics. In the present study ETM+ image has been used for mapping the geomorphology and active tectonics on the Sone megafan. Based on tone texture, association; 4 soil geomorphic units have been marked on the megafan surface and based on their OSL ages, these geomorphic units are categorised from older to younger. The Sone megafan has been divided into three distinct plains based on the geomorphic characteristics, OSL ages and soil characteristics. The oldest plain is characterised by NW directed braided paleochannels having maximum channel width vary from 4 to 5 km. Drainage density on this plain is 0.17. The paleochannels are trending in NNE to NE direction. The paleochannels of Sone River on this plain are less wide having maximum channel width varying between 2 to 3 km. There is a striking contrast between the drainage characteristics of older plain and this plain. The drainage density on this plain is 0.4. The active channels in this plain are headed northward initially but change their direction to NE upon closing towards the fault zone of East Patna Fault.

Bhosle et al. (2008, 2009) used remote sensing and GIS techniques to decipher the low-relief neotectonic faults in the Ganga plains. The geomorphologic elements studied in the present study to trace the subsurface faults (East Patna Fault and West Patna Fault) onto the surface include topographic variations, drainage anomalies with water bodies network, as articulated by several workers (Arrowsmith and Zielke, 2009; Azor et al., 2002; Burbank and Anderson, 2001; Keller and Pinter, 1996; Moro et al., 2007).

It has been sometimes asserted that the available SRTM (Shuttle Radar Topography Mission) DEM data has a root mean square error (RMSE) of about ±12 m (Nikolakopoulos et al., 2006; Smith and Sandwell, 2003) which may not be sufficient to demarcate the necessary geomorphic structures (Bhosle et al., 2009; Mukherjee et al., 2013; Pati et al., 2011a). However, the relative accuracy is usually higher to detect subtle features in the flat terrains (Kanoua and Merkel, 2016). Therefore, SRTM DEM was used to obtain river profiles and a DEM was also manually generated from spot heights given in the Survey of India toposheets (absolute error of ±2 m in vertical accuracy, Bhosle et al., 2009) on scale 1:50000. A point density of 4-6 spots/10 km^2 is sufficient to create the DEM for studying regional features (Badura and Przybylski, 2005). In the present study, a point density of 8-10 available spots/10 km^2 was interpolated to prepare the DEM with kriging method, which provides excellent results (as compared to other methods such as IDW and topo to raster) for flat plains like the Indo-Gangetic plain in reproducing artefact morphostructures such as ‘cliffs ‘and ‘significant break in slopes’ which usually form along the faulting activity (Bhosle et al., 2009).

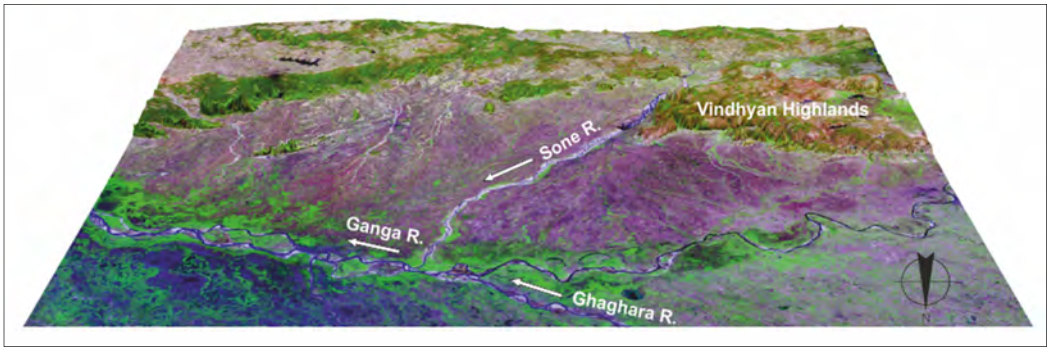

Figure 2.1 Satellite image draped over DEM to obtain a perspective view of the southern middle Ganga plain.

The satellite image (Resourcesat-II AWiFS, 30 m spatial resolution) was draped over the SRTM DEM (30 m spatial resolution) to obtain a perspective view of the study area. It shows that the megafan surface is almost flat with respect to the adjacent Vindhyan Highlands (Fig. 2.1). Another exaggerated DEM (vertical exaggeration value: 14) prepared from height benchmarks was prepared to simulate the megafan under study in a 3D terrain view (Fig. 2.2). A DEM may also be referred to as DTM (digital terrain model) here because it represents the topography of bare ground surface without any building or trees and other such structures. DTMs prepared by using these data have largely been used for mapping active faults in the Ganga plain (Bhosle et al., 2009; Pati et al., 2011a; Singh et al., 2006).

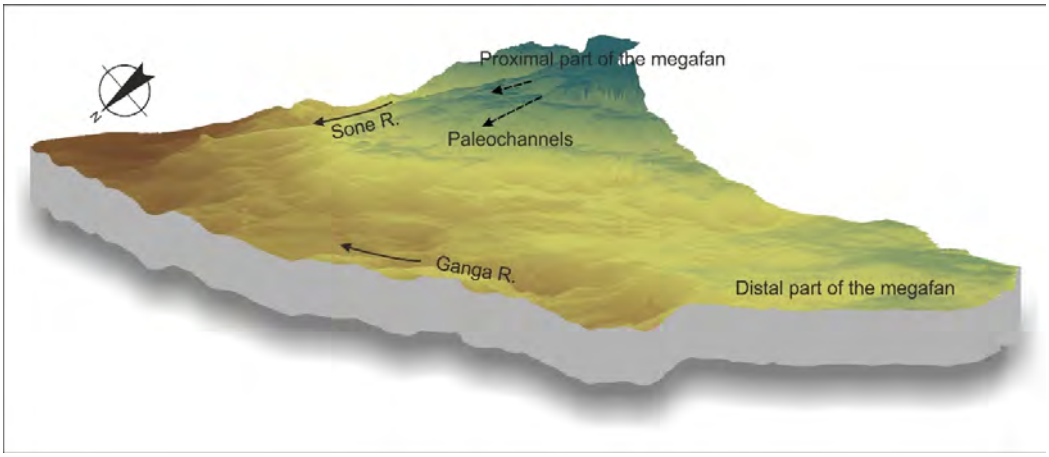

Figure 2.2 DEM of the Sone megafan created from spot heights in 1:50000 scale SOI toposheets (exaggeration value: 14).

Another DEM of the area around the East Patna fault (EPF) was also prepared with Surfer software in orthographic projection. The surface topographic profile extracted from the DEM across the strike of the fault is very effective in determining any surface revelation of tectonic activity of buried faults, which in the present study is a basement fault (EPF). Some topographic profiles were created across the EPF from the DEM and the slope breaks were thus identified at different geographic positions.

The contour height and benchmarks provided in the toposheets were digitised manually in ArcGIS software to create the DEM of surface. The basement contours (values given as depth from the surface) obtained from Seismo-tectonic atlas of India were also digitised similarly. All maps and

digitised files were kept in same geographic reference system (WGS 1984). The digitised points and/or contours were interpolated to create the elevation model of the basement which clearly shows the three ridges (West Patna Ridge, East Patna Ridge and Munger Saharsa Ridge). The surface DEM coupled with the drainage network helped to demarcate a ~30 km wide fault-zone which shows variation of micro relief on the surface and probably represents maximum deformation along the subsurface fault (Fig. 2.3). The surface elevation profiles extracted from the DEM show topographic break across the East Patna Fault which indicates the presence of the fault trace in the southern part of middle Ganga plain. Seismotectonic atlas of India (GSI,

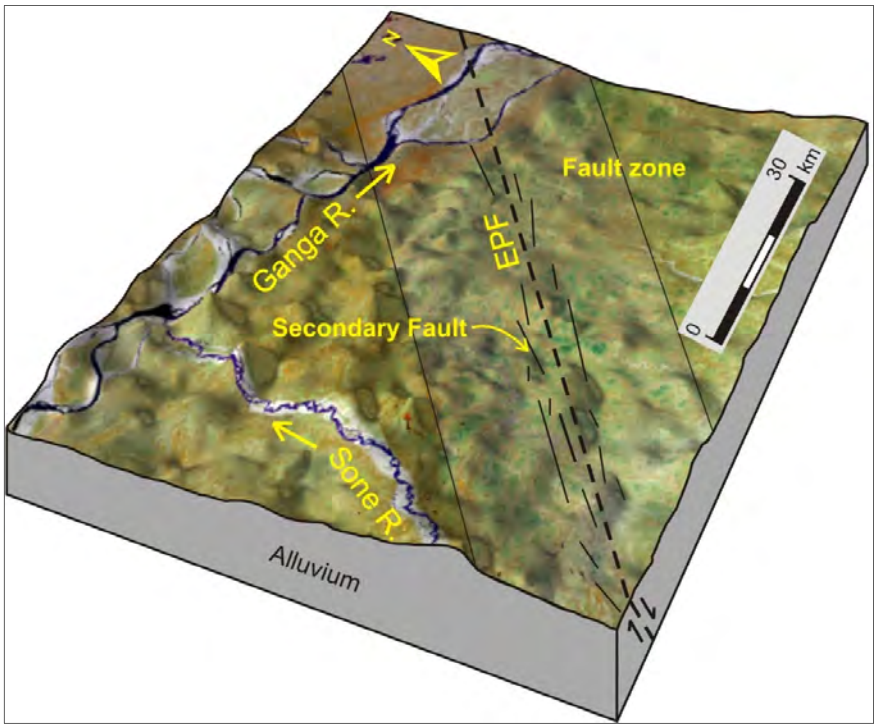

Figure 2.3 Digital Elevation Model (DEM) of the study area illustrating surface topography, NE-SW trending East Patna Fault (EPF), and the presence of its secondary faults on the surface and subsurface in the fault zone.

2000) limits the continuity of the East Patna Fault from the Himalayan Frontal Thrust in north to the Ganga River in south. Some of the recent work considered the fault to be extended up to almost southernmost reaches of the Ganga plain but none have so far accounted evidence for the augmentation of the fault in southern MGP (Sahu et al., 2010; Sinha et al., 2014). Thus, the present study helps to fill the gap by providing direct and indirect evidence of influence of the concealed fault on the surface.

2.2 DRAINAGE CHARACTERISTICS

As observed by (Bhosle et al., 2009; Pati et al., 2011a), drainage patterns in flat terrains are highly sensitive to even weak tectonic movements. Basement reactivation and its related neotectonic activity is evident by river channel migration on the surface (Pati et al., 2008, 2006; Prakash et al., 2017). The drainage pattern in unconsolidated sediment-fill, such as the Ganga plain, is readily modified in accordance with the tectonic activity (Jackson and Leeder, 1994). The drainage map towards south of the Ganga river in middle Ganga plain is shown in fig. 2.4. As the EPF is an active fault (Dasgupta, 1993; Jain and Sinha, 2005; Sahu et al., 2010), change in drainage pattern across the fault has been well observed. Typical drainage morphology indicative of active faults has been identified across the EPF as discussed below.

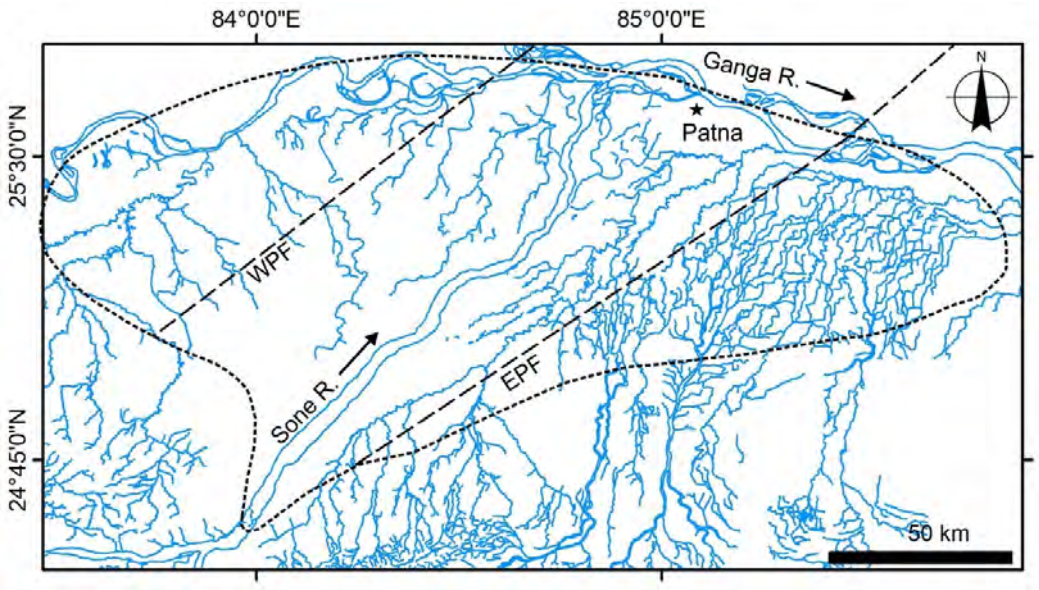

Figure 2.4 Map of the active drainage towards the south of river Ganga in middle Ganga plain. The short-dotted line shows the boundary of the Sone megafan.

2.2.1 Initiation of new streams

Initiation of new streams or bifurcation occurs at down-thrown blocks of normal faults (Bhosle et al., 2009; Pati et al., 2012; Singh et al., 2006). The drainage network digitized from the topographic maps and Landsat image reveals generation of a number of new streams towards the east of the EPF just near the topographic break (Fig. 2.5). Almost all the new streams are

initiating from a particular zone. Generation of new streams were also observed on downthrown block of the West Patna Fault (Fig. 2.4).

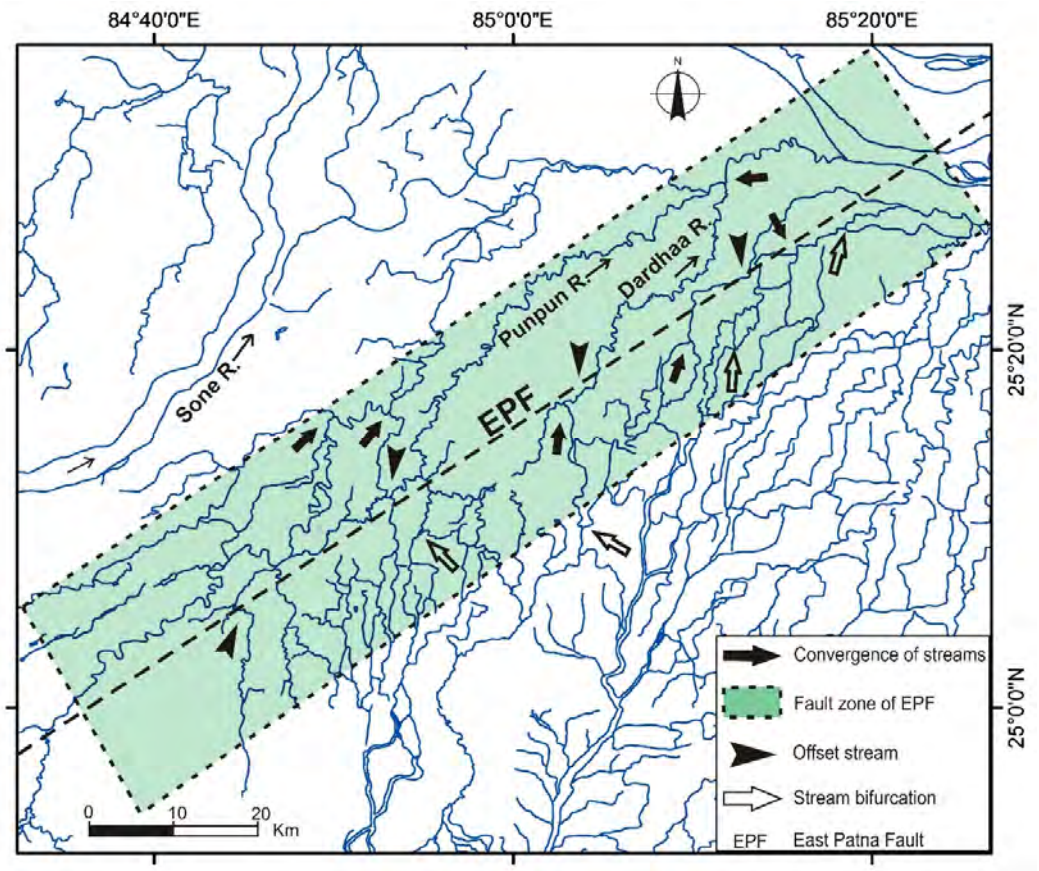

Figure 2.5 Map of active drainage in parts of Sone megafan affected within the fault-zone of East Patna Fault.

2.2.2 Streams offsetting

Channels often shift their course to follow the trend of the faults when they flow across a topographic barrier. If a block is uplifted due to a normal fault running oblique to the regional slope, the stream course deviates to run parallel to the fault for a few kilometres, crosses the fault at a lower elevation and continues along the regional slope (Singh et al., 2006). This leads to offsetting of the stream as observed in the present study. Tilting of a tectonic block in a direction normal to the flow of a stream may also cause offset of the stream course. Normally, offsetting of streams is ascribed to strike slip movement of faults. A veering off as much as 6 km has been recognized in course of the Dardha River in Pipra village of Patna district, Bihar as it flows across the EPF (Fig. 2.5). Other streams offset by 1 to 2 km along the fault. Offsetting of

streams was identified on the upthrown block of the EPF which agrees with the conclusions of Singh et al. (2006), Bhosle et al. (2009) and Pati et al. (2011b).

2.2.3 Convergence of streams

If elevation rise takes place normal to the path of small streams following the regional slopes, then the streams join together forming a convergent drainage pattern. After joining of the streams, larger merged stream may continue along the regional slopes, cutting through higher elevation, if the elevation rise is small. Alternatively, the stream may change direction by about 90°, if the elevation rise is substantial.

In the present study, convergence of several streams is found to the west of EPF (Fig. 2.5). The streams tend to converge in the upthrown block (Gawthorpe and Leeder, 2000; Singh et al., 2006; Bhosle et al., 2009). However, a few convergent streams have also been observed on the downthrown block.

2.2.4 Channel sinuosity

The anomalously high sinuosity is a consequence of movement on active structures as suggested by stream-table experiments (Burnett and Schumm, 1983; Ouchi, 1985; Schumm and Khan, 1972). Increase in stream gradient and decrease in sinuosity are interpreted to indicate long-term uplift. Sinuosity of streams is a characteristic feature on the downthrown block of faults. Due to the lower slope, sinuosity of channels increases on the downthrown block (Bhosle et al., 2009). In the present study increase of sinuosity of Dardha and Punpun rivers after crossing the EPF has been observed (Fig. 2.5).

2.2.5 Water logging

Distribution of natural stagnant water bodies on the megafan surface are clearly visible in the satellite image and can be seen in the toposheets as well. A map of natural ponds with the help of toposheets and ETM+ image has been prepared. The water bodies on either side of the Sone River show a contrasting difference. Western part of the megafan shows numerous small sized, mostly

circular ponds, the eastern counterpart, on the other hand, shows larger ponds, mostly elongated and apparently aligned to a paleochannel network like

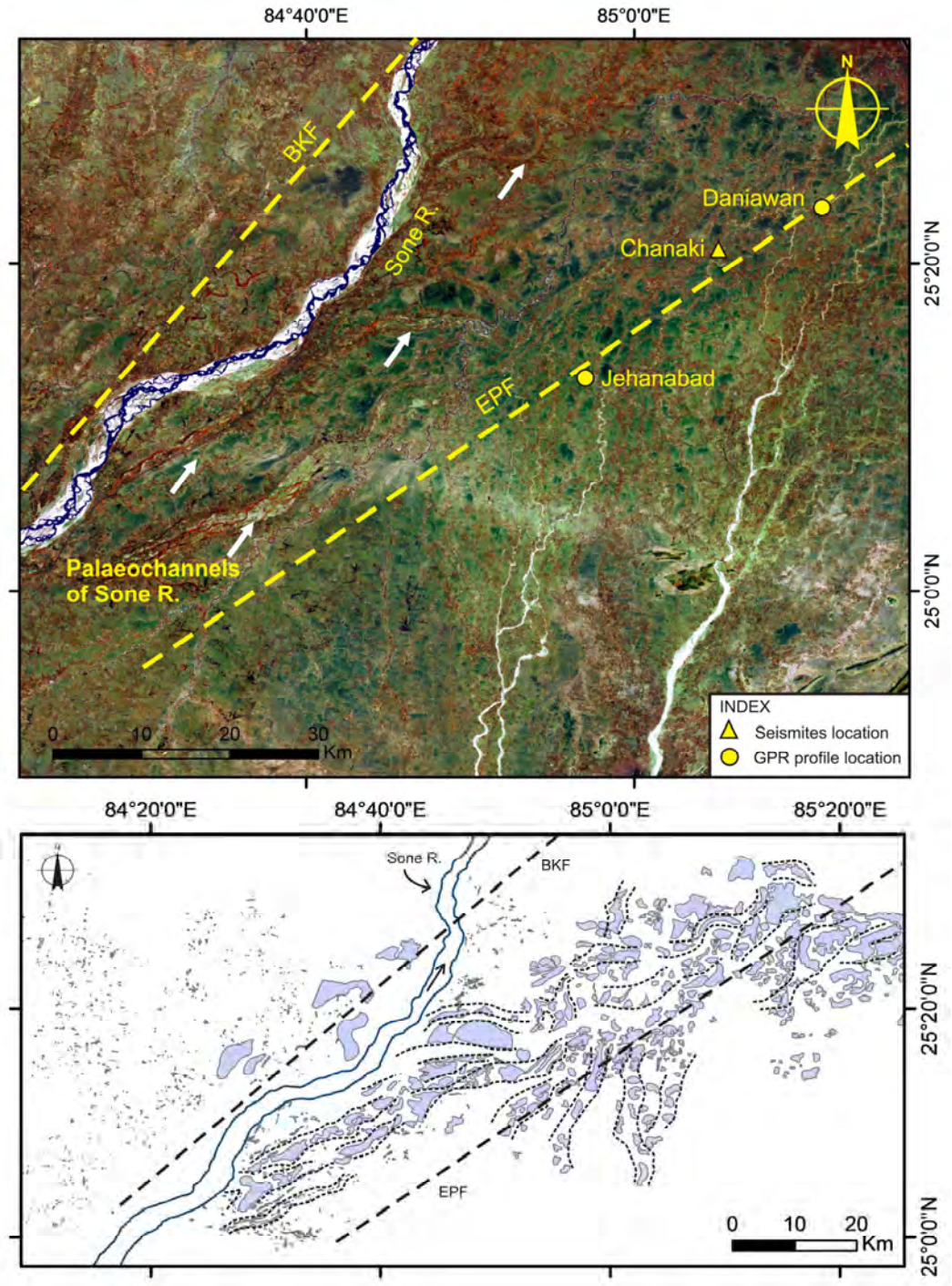

Figure 2.6 The ponds digitized from the topographic maps and Landsat image are concentrated between the BKF and the EPF. They show the contrasting difference in alignment and superficial size in comparison to ponds towards the west of BKF. The locations of GPR profiles and seismites near the EPF. The paleochannels of the Sone River (marked by white arrows) are clearly visible in the satellite image of the area.

pattern. Most of the water bodies towards east of the Sone River are confined

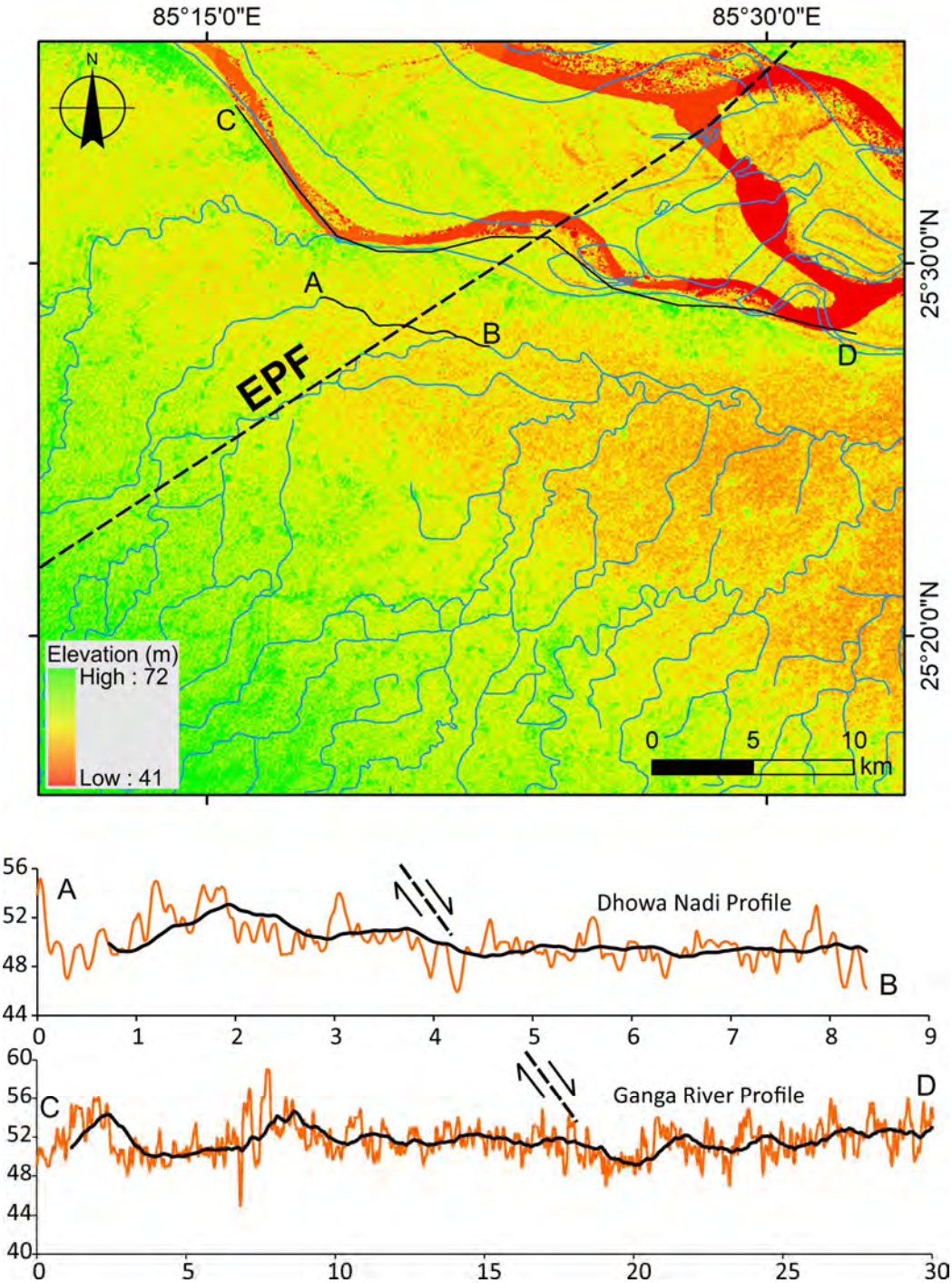

Figure 2.7 Longitudinal river profile of the Ganga River and Dhowa nadi indicating tectonically active nature of the EPF. The background image is a part of the SRTM DEM of southern Ganga plain with drainage network, general elevation of the area is decreasing from SW towards NE. The x-axis represents profile length in kilometers, and the y-axis shows elevation in meters. The black lines in the graph show best fir curve for the elevation profile by averaging 40 points on x-axis.

between the EPF and the present channel of the Sone River due to the confinement imposed by topographic barrier of Bishunpur-Khagaul Fault (BKF)

(Sahu and Saha, 2014) which also strikes parallel to the Sone River course (Fig. 2.6).

2.2.6 River Longitudinal Profile

Tectonic activity in an area owing to buried faults is also implied by the longitudinal profiles of rivers flowing across the trend of the fault. Seeber and Gornitz (1983) showed that a graded longitudinal profile of river indicative of the balance between rate of incision of the river and the rate of tectonic upliftment of the region. However, if the incision rate of river could not keep up with the uplift, a convex profile is observed (Whittaker et al., 2007). The longitudinal profile of river also provides first order information regarding the role of tectonics and climate to fluvial response (Hack, 1973; Merritts and Vincent, 1989). Pazzaglia (2013) concluded that this information can be used to ascertain the fluvial response to terrain stability/instability. The SRTM 1-arc second global DEM downloaded from USGS (https://earthexplorer.usgs.gov) has been used to obtain the longitudinal profiles of the Ganga River and Dhowa nadi (Fig. 2.7). Though smoothly gradient profiles of the river beds were expected in this alluvial plain, rather uneven river bed surface shown in the profiles infer that the area is neotectonically active and most possibly the presence of an active subsurface fault in stream paths.

2.3 DRAINAGE EVOLUTION

In context of alluvial plain such as the Ganga plain, the drainage morphology and satellite image analysis have an immense value in working out the evolution of landforms. The DEM is a vital tool to study topography of such plains with practically meagre relief differences because these models provide us the flexibility to enhance the elevation differences and hence even the minor variations can be detected.

In present study the satellite images helped to identify 4 geomorphic units (OdSP– Oldest Sone Plain, OSP– Old Sone Plain, YSP– Young Sone Plain, and AFP– Active Floodplains) (Fig. 2.8) and 3 generations of paleochannels of the same river. The oldest palaeochannel of the Sone River is traced in OdSP (Oldest Sone Plain) near Suryapura and Dumraon (Fig. 2.9).

The widespread paleochannels in both directions– east and west imply different episodes of fan building and its spatial limits.

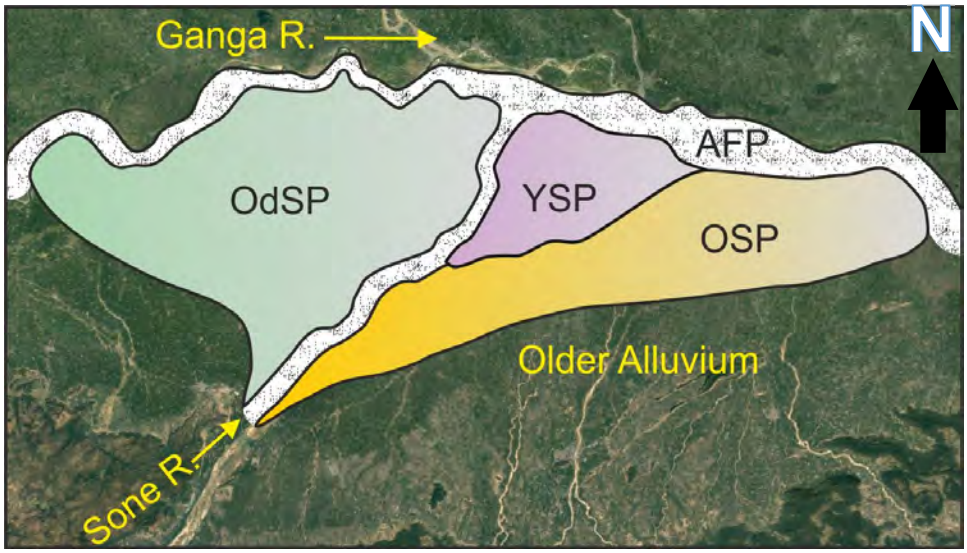

Figure 2.8 Four geomorphic units identified in the Sone megafan. OdSP- Oldest Sone Plain, OSP- Old Sone Plain, YSP- Young Sone Plain, AFP- Active Floodplain. Base image is obtained from Google Earth.

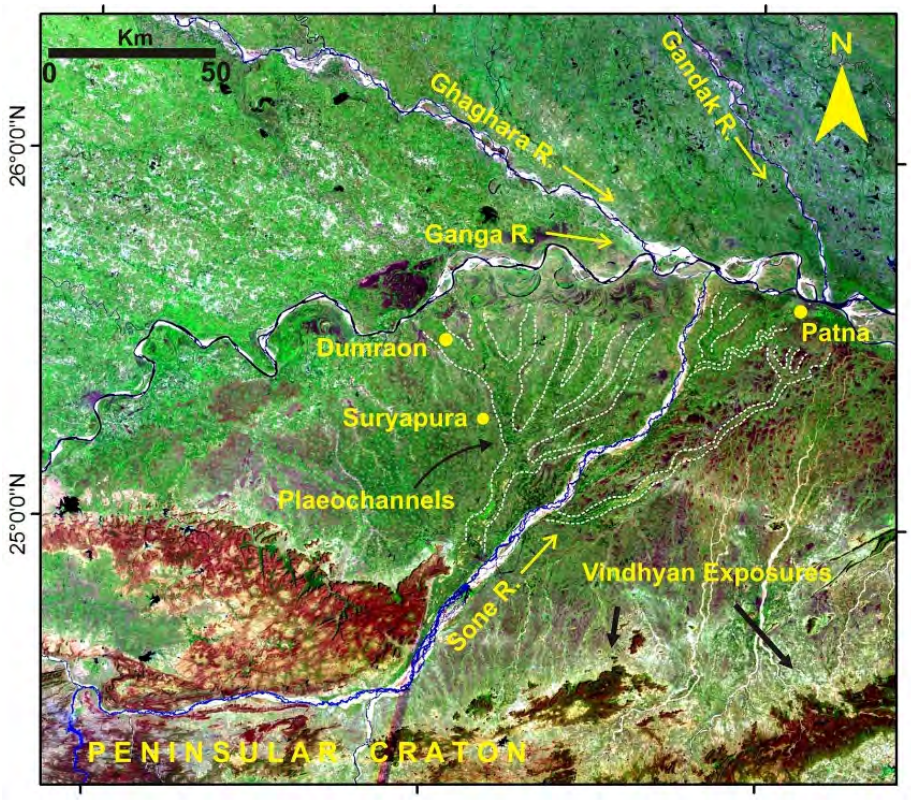

Figure 2.9 Standard FCC of Landsat ETM+ (R:7 G:4 B:2) showing braided network of paleochannels of Sone River. The darker tones show higher moisture towards the east of Sone and ponds appear as dark patches near the river.

Three lobes of the megafan could be clearly distinguished by the different generations of paleochannels. In the eastern part, the paleochannels are directed towards NW and few of them are now occupied by small streams. Other abandoned paleochannels are characterised by dissected small water bodies. Joining of adjacent water bodies may be useful for tracing the continuity of the paleochannels. These directional shifts of fan building front may be correlated with block tilting as the similar case has been established in the northern part of this present study area in the Gandak megafan (Mohindra et al., 1992). As the Sone megafan is restricted by active basement faults from both side and the block is being compressed between the peninsular and the Himalaya, block tilting could not be ruled out. The time and direction of tilting can be established with the help of OSL dating of sediments from the paleochannels and interchannel areas of the megafan. With the help of DEM, the morphology of the Sone megafan could be visualised in 3D which helped in understanding its nature more comprehensively. The surface elevation profiles extracted from DEM show the presence of active subsurface fault (EPF) towards south of the Ganga River, which has largely controlled the drainage morphology and formation of the megafan.

The streams towards east of the fault can be seen to be flowing northward initially. However, as those streams reach sufficiently close to the fault, almost all of the streams suddenly take a turn to follow a north-easterly trend i.e. parallel to the fault. This anomalous behaviour of streams implies that the subsurface fault forms a fault zone of effective deformation on the surface. It is also noticeable that as the depth of sediment fill decreases southward, the zone of deformation is narrower and towards the north where sediment fill is deep, the zone of hydrographic deformation is also wide. This observation agrees with the model of basement fault propagation as a deformation zone through the overlying soft sediment fill, shown by Gawthorpe and Leeder (2000). The observed anomalous stream behaviour in a tectonically active plain is entirely possible because of the unconsolidated sediment cover which allows the rivers and small streams to easily change their course in response to the

fault activity. Also, because the sediment is fairly loose to be remobilised and sediment sequences be readily disturbed, therefore finding the disturbed strata (as recorded by GPR) is clear evidence of very recent fault reactivation. The drainage towards the west of the Sone river is rather scarce. A few small streams originating on the downthrown block of WPF follow a northwest trend and fall into the river Ganga (Fig. 2.4). As discussed later in Chapter 4, the soils from the western part of the megafan provide older OSL dates as compared to the eastern counterpart. The soils are arid and situated at a higher elevation than the eastern plain. The satellite images also show the areas of low moisture content in the soil in lighter tones.

Chapter 3

SOFT SEDIMENT DEFORMATION STRUCTURES

3.1 INTRODUCTION

Normally, a sand deposit behaves as a 'solid' and is stable against applied shear stress as long as the depositional surface does not slope more than a critical angle of initial yield. However, in case where the sediment load is balanced by interstitial pore fluid pressure, the effective shear strength of the sediments is zero. Hence, when vibrations caused by cyclic earthquake shocks hit a water-saturated sand deposit, the grains tend to achieve a state of closest packing or minimum volume by compaction. If the pore fluid cannot escape, the pore water pressure can increase to a point where it reaches the overburden load, and then the sand *liquifies*. Tightly packed sand grains behave as a dilatant under shear stress, thus, for liquefaction to occur, the granular sediment must be loosely packed initially. The earthquake shocks of magnitude more than 5 on Richter scale are capable of causing liquefaction in sands, which may be at hundreds of kilometres distance from the epicentre. Due to liquefaction, the water tends to expel upwards in vertical pipes under high pressure (Leeder, 1982). The liquefaction often results in creating the deformation structures in water-saturated or freshly deposited sand bodies, which are sometimes preserved in section and referred to as "*soft sediment deformation structures"*.

The sufficiently strong vibrations needed to cause liquefaction may originate from a number of processes or sources. The sediment deformation structures which are produced by seismic shocks and are bounded by undeformed horizons on top and bottom are defined as *seismites* (Seilacher, 1969). Several authors (Amick et al., 1990; Galli and Bosi, 2003; Moretti and Sabato, 2007; Russ, 1982; Saucier, 1989; Sauret and Bousquet, 1984; Seed, 1979; Youd, 1977) have related the liquefaction-induced soft sediment deformation structures in sedimentary environments with the historical earthquakes. Recognition of liquefaction features can be anticipated as an indicator of strong past earthquakes (Tinsley et al., 1985). The liquefaction and soft sediment deformation require a water saturated basin and the factors,

which control the physical properties of sediments such as cohesion, porosity, and permeability, define the development of deformation (Berra and Felletti, 2011).

Soft-sediment deformation structures can be confidently used for interpretation of tectonic and seismic activities as well as can be significant in paleoenvironmental studies. Field observations show that, for given earthquakes of magnitude M, the occurrence of liquefaction is confined within a particular distance from the earthquake epicentre depending upon the suitability of the substrate, beyond which the liquefaction is not expected (Ambraseys, 1988; Galli, 2000; Kuribayashi and Tatsuoka, 1975; Papadopoulos and Lefkopoulos, 1993; Wang, 2007; Wheeler, 2002). The Indo-Gangetic foreland basin is filled with unconsolidated sediments deposited by mostly the Himalayan rivers and few rivers from peninsular craton. This vast alluvial plain provides a good natural laboratory for the seismic wave to cause liquefaction. Therefore, the deformation structures found in the present study in the sand -clay alternating strata to close proximity of the East Patna Fault have possibly been created by the seismic disturbances generated by the Great earthquake of 1934 (M–8.3) or any prehistoric unrecorded earthquake along the East Patna Fault. However, the exact time of occurrence of the earthquake event associated with these seismites can be revealed by dating the seismites.

3.2 SEISMITES IN THE MIDDLE GANGA PLAIN

The East Patna Fault is an active NE-SW trending basement fault in the middle Ganga plain (Dasgupta, 1993; Jain and Sinha, 2005; Sahu et al., 2010; Sinha et al., 2010). This fault together with other active basement faults in the region such as the West Patna Fault and Munger Saharsa Ridge Fault forms one of the several seismically active systems in the Ganga plain. Singh and Jain (2007) reported the development of fracture planes, bending and tilting of the beds and block movement in cliff section of the Sengar River, Kanpur (nearly 430 km west of the present study area). Gibling et al. (2005, 2008) provided sedimentological and paleoclimatic analysis for Belan river sections and the area around Kanpur city. Although those areas form part of the same southern Ganga plain, but in view of the present work, the areas differ

significantly in geology. Those areas fall under hard sandstone terrain and the upper Ganga plain while the present study includes unconsolidated sediment fill and alluvial plains of the middle Ganga plain. The normal and strike-slip component of the movement along the basement faults is known to have caused the earthquakes of 1833, 1906, 1934 and 1988 in the region (Banghar, 1991).

The epicentres of the great earthquakes (M > 8) in 1934 and 1988 (M = 6.7) are located along the East Patna Fault (GSI, 2000). Seeber and Armbruster (1981) and Chander (1989) reported the deformation structures impelled by liquefaction from the northern Ganga plain. Rajendran et al. (2016) reported the liquefaction records of the great earthquake of 1934 associated with the East Patna Fault from the north Bihar alluvial plains of India, but none from the south Bihar. Interestingly, besides the north Bihar being impacted by several seismic events in the historic past, these soft sediment deformation structures, so far, have never been reported from the south of the Ganga River. The reason for the ignorance of the seismites from the south Ganga plain can be attributed to the fact that none of the earthquake events in the historical past with M > 5 has been recorded to have an epicentre in this region.

In the present study, the soft sediment deformation structures (seismites), sufficiently close to the East Patna Fault (within the fault zone) have been reported for the first time from the south of the Ganga River in the middle Ganga plain. Mainly five types of liquefaction-induced seismites have been recognized from the study area along the bank of the Dardha River in Patna district, Bihar. As there are no records of any strong seismic activity originating from the southern Ganga plain, these evidence of deformation structures stands as a strong ground for the assumption that there has been a major (unrecorded) prehistoric seismic event in the region associated with the East Patna Fault. Ground Penetrating Radar study carried out in the vicinity of the location of seismites detected the subsurface secondary faults associated with the East Patna Fault. Development of the secondary faults confirms the active nature of the basement fault, which is the main source of seismic activity of the region. Activity along the East Patna Fault is controlled by the direction and

amount of stress accumulated due to the convergence along the Himalayan Frontal Thrust (HFT). Therefore, the seismites observed from the southern middle Ganga plain are actually the indirect imprints of the Outer Himalayan tectonics on the southern Ganga plain.

3.3 METHODOLOGY

The studied location covers a segment of the Dardha River and its nearby areas in the middle Ganga plain (Fig. 3.1). Though the Punpun and the Dardha are the two major rivers in the deformation zone of the East Patna Fault, but the Dardha River flows along the fault zone, consequently, acquiring the maximum possibility of being affected by seismic activity associated with the East Patna Fault. Therefore, the Dardha River banks were selected as the reconnaissance site for possible soft sediment deformation structures.

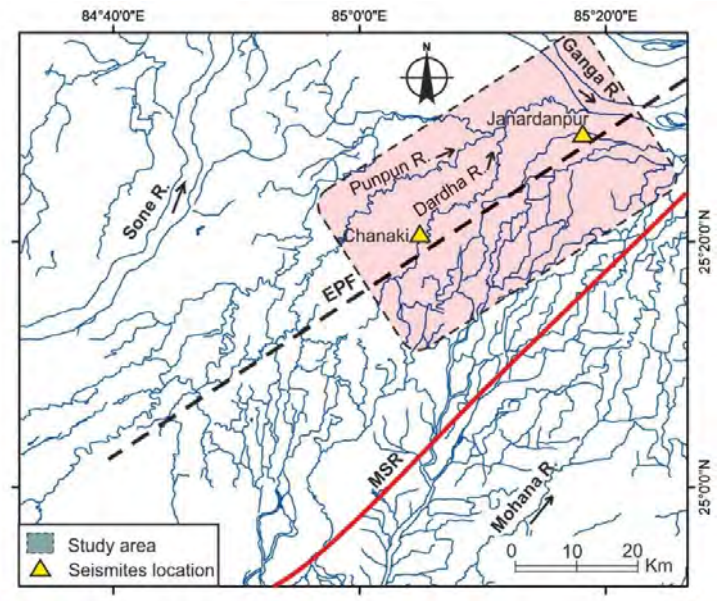

Figure 3.1 The study area is shown by a translucent rectangle in the southern part of the middle Ganga plain containing major river systems and the basement structures (EPF: East Patna Fault; MSR: Munger-Saharsa Ridge.

After mapping the fault zone by using remote sensing and GIS techniques, possible sites were chosen, and detailed field survey was carried out in the area. The exposed sections of the Dardha River banks were observed for the liquefaction and other deformation structures. One of the pits excavated near the river channel at *Chanaki* village (25°21′23.85″N, 85°05′21.02″E), provides a good vertical section of about 3–4 m depth from the surface, where several seismites were observed. Nature and extent of seismites, the associated lithology and the nature of deformation were studied in the field. For the convenience and clarity of presentation, cartography was prepared on the field photographs. Another excavation pit near the East Patna

Fault at *Janardanpur* village (25°21′23.85″N, 85°05′21.02″E), Patna district showed small scale normal fault; and the termination of clay beds against a fault plane.

The deformation and sedimentary structures have been studied at two locations (*Chanaki* and *Janardanpur* village) along the East Patna Fault to the south of the Ganga River and the respective observations have been reported below.

3.4 DEFORMATION STRUCTURES IDENTIFIED IN THE STUDY AREA

Location–1 Chanaki Village

Seismites such as small-scale listric fault and associated down-sagging, pillar and pocket structure, water-escape structures and thixotropic wedge and other deformation structures were observed in Chanaki village. As the southern Ganga plain has poorly defined seismicity, the occurrence of seismites from the southern middle Ganga plain provides interesting evidence of an earthquake event (of M > 5) in the southern middle Ganga plain. The required slip along the East Patna Fault to have caused an earthquake of M > 5 can only receive enough stress component from the corresponding Himalayan Zone near the north-eastern extension of the East Patna Fault. Soft-sediment deformation structures (i.e. seismites) identified in the strata of the Dardha River banks are defined in the following sub-sections.

Listric fault and tabular downsagging

The beds are affected by listric microfault, which occurs at 2–3 m below the surface. The fault is associated with tabular depression in the upper layer. (Fig. 3.2). The apparent dip of the fault near its tip is 40° towards west. The horizontally lying alternate clayey-silt and sand layers tend to bend along the fault or end abruptly against the fault surface. The vertical displacement of layers is about 7 cm.

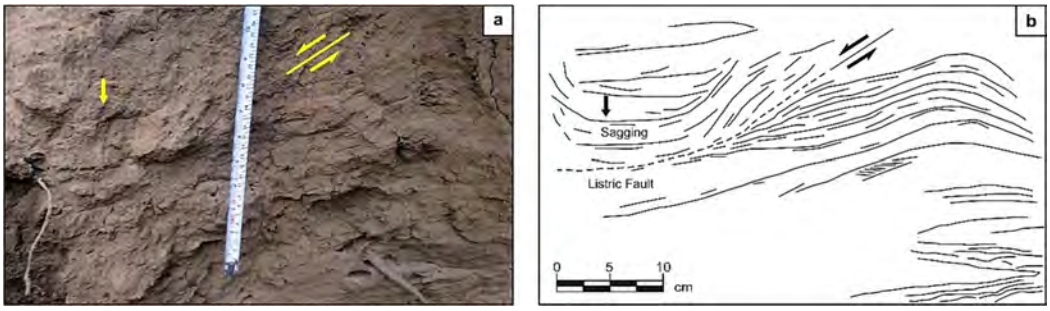

Figure 3.2 (a) Listric microfault and associated sagging of the sand beds observed on the bank of river Dardha (shown by yellow arrows), (b) figure redrawn and labelled from the actual photograph.

Pillar and pocket structure

The pillar structure has been formed by the injection of clayey silt layer up to 27 cm into the overlying sand beds. The area between the adjacent almost round crested pillars forms an upward concave flat-base pocket structure. Along one of the steep walls of the pillar, the clayey silt layers alternating with fine sand layers cease abruptly. Sand pseudonodules and disturbed laminites with the thickness of about 2–5 cm were also observed about 8–10 cm below the pocket base (Fig. 3.3).

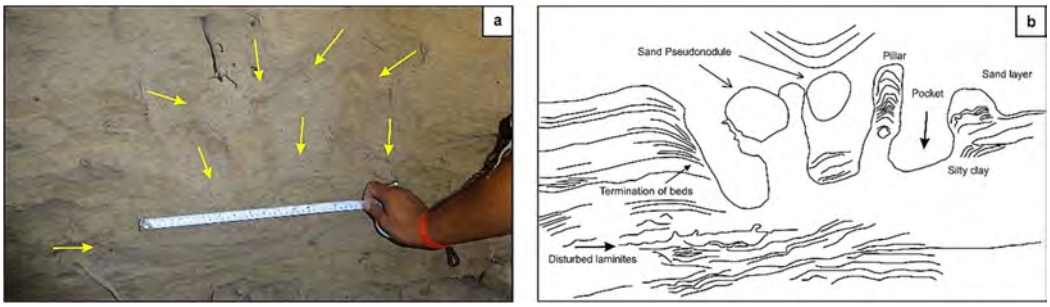

Figure 3.3 (a) Pillar and pocket structure formed by the upward movement of water saturated sediments by intense shaking of the region due to earthquake event (marked by yellow arrows), (b) deformation structures redrawn, marked and labelled by black arrows.

Water escape structures

Rossetti (1999) defined the water escape structures as deformation structures morphologically similar to the flame structures, which occur in mud only. Structures observed in the present work are cusps of deformed masses of fine sands intruding into the overlying undeformed sand layers (Fig. 3.4). The presence of deformed beds trapped between the undeformed sand strata

strongly supports the seismic origin to the formation of these deformation structures.

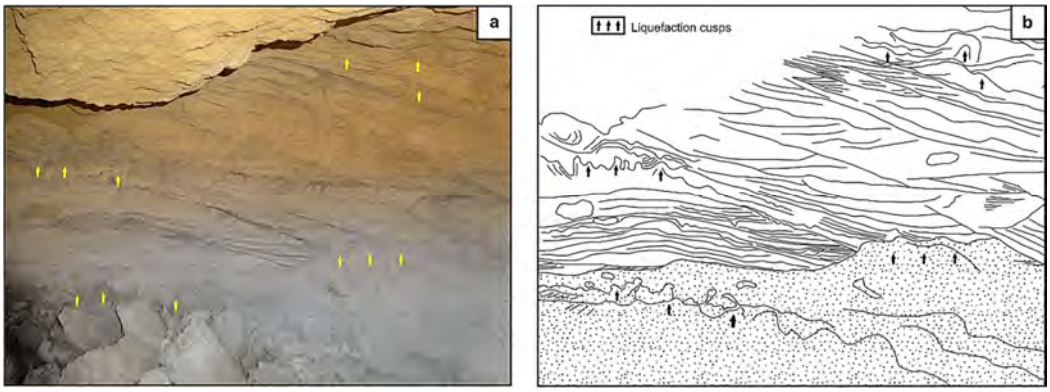

Figure 3.4 (a) Water escape structures preserved in the riverine sand bed as liquefaction cusps and disturbed laminae (shown by yellow arrows in actual photograph), (b) structures redrawn from the photograph (marked by black arrows).

Thixotropic wedge

Thixotropic wedges are developed in fine sandy deposits which are usually underlined by a very fine-grained dark sediment (silt and iron oxide) (Montenat et al., 2007). Similar V-shaped layers in the fine alternating sand and dark sediments are observed in the present study area (Fig. 3.5).

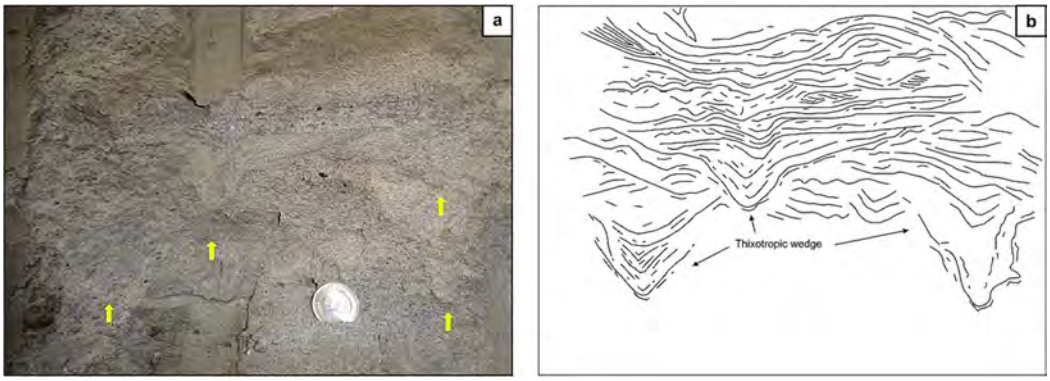

Figure 3.5 (a) Alternating sand and dark colored fine sediment layers deformed into V-shaped wedges identified as thixotropic wedges observed on the eastern bank of the river Dardha (shown by yellow arrows), (b) prominent features redrawn and labelled from the actual photograph.

Folds and sagging structures

Over the riverbank, the coarse sand horizon is characterized by the presence of antiform due to soft sediment deformation event lying over the undeformed inclined sand beds (Fig. 3.6). A deformed recumbently folded clay layer was also observed in the vicinity (Fig. 3.7).

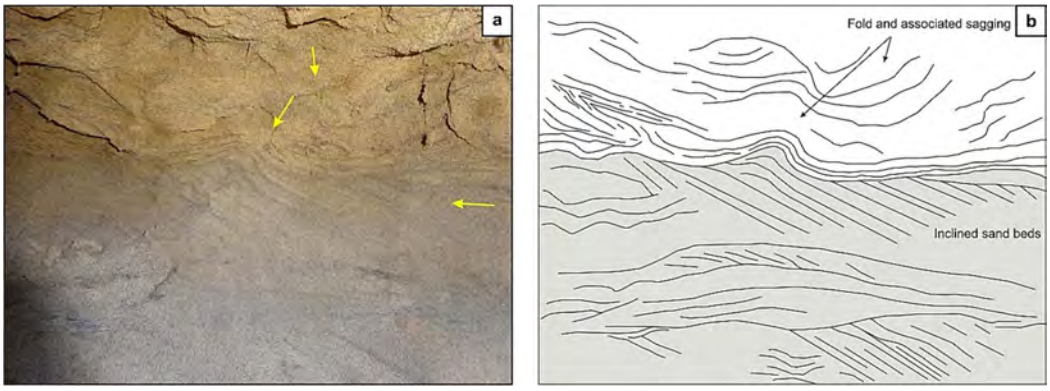

Figure 3.6 (a) The actual photograph showing fold and associated sagging observed in the overlying sand layers underlain by undeformed inclined sand beds resulting from impact by cyclic shear waves (shown by yellow arrows), (b) structures redrawn and labelled from the photograph.

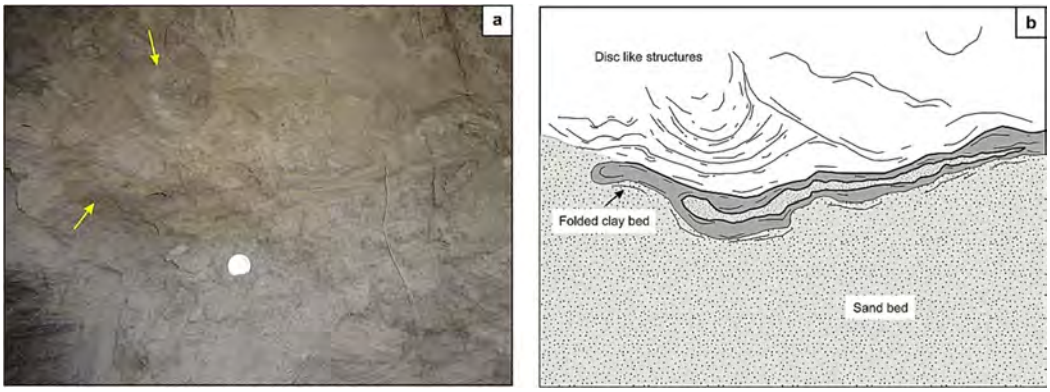

Figure 3.7 (a) The refolding of intensely folded clay layer between sand beds associated with the downsagging of overlying sand beds occurring with other seismites in the same location (marked by yellow arrows in the photograph), (b) features redrawn and labelled from the actual photograph.

Location–2 Janardanpur Village

Another pit excavated in Janardanpur village in Patna district of Bihar shows small-scale normal fault in the alternating sand and clay beds (Fig. 3.8). This site is located very close to the East Patna Fault to the south of the Ganga River. The other exposures in the excavation pit show the cross-bed structure with foreset dipping by 22° and topset dipping 3° towards NE (Fig. 3.9). A surface of erosion representing the flooding event was also observed in between the cross beds. The cross bed sedimentary structures and clay beds trapped in between the sandy depositions is suggestive of the active channel

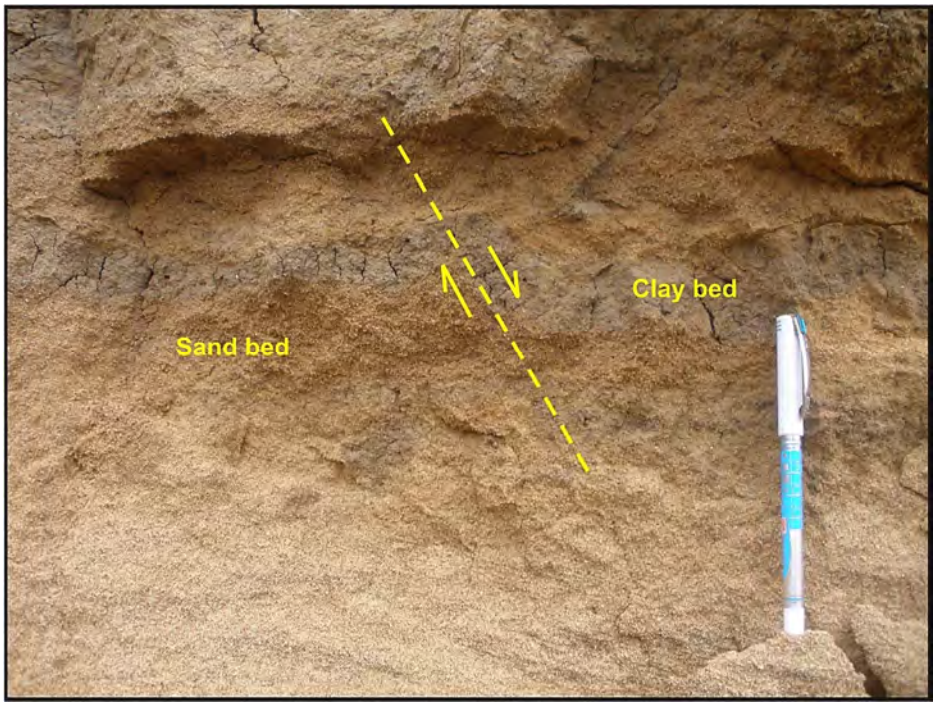

Figure 3.8 Exposure at Janardanpur showing the deformation by small-scale normal fault causing localized drag fold in clay bed trapped in the sand bed.

Figure 3.9 The cross-stratification structures are shown by the sand beds deposition indicating fluvial environment. Topset and foreset dipping 3° and 22° respectively towards NE direction. Location – Janardanpur.

and the stagnant water (fluvio–lacustrine) environment. The clay beds of ~10 cm thickness lying in the sand deposition were observed to be abruptly terminating against an inclined plane (Fig. 3.10).

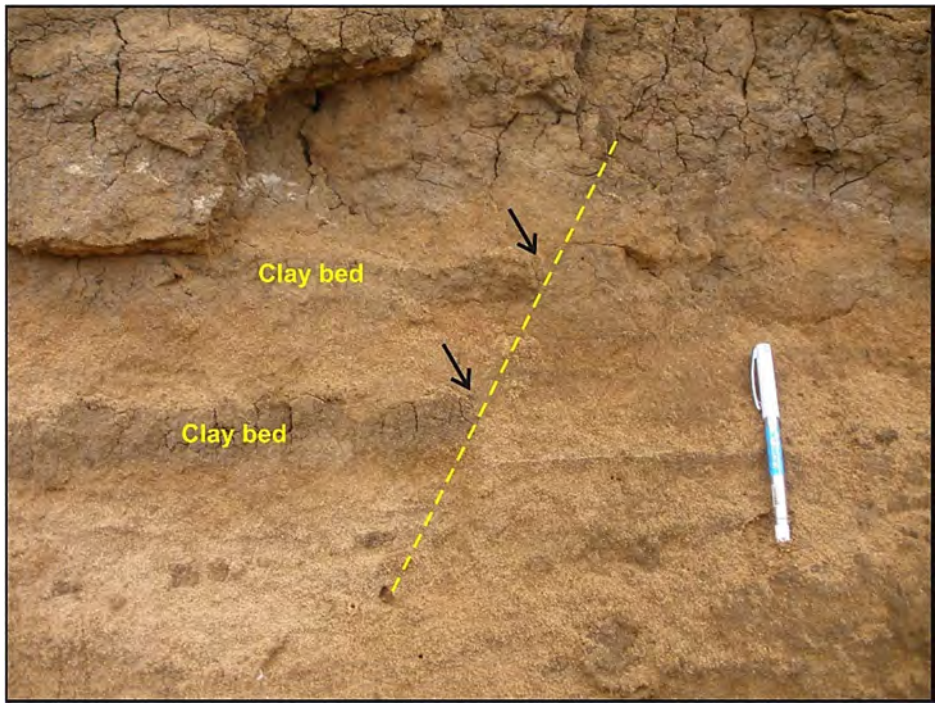

Figure 3.10 Abrupt termination of clay beds against a steep plane. Often during earthquake-induced downsagging of the sediments, the adjacent beds tend to abruptly terminate against the steep walls of the sagging structure thus formed. Exposure at Janardanpur.

3.5 MECHANISM AND IMPLICATIONS OF SEISMITES

The water-saturated sediments in an unconsolidated deposit are primarily required for the formation of soft sediment deformation structures (Allen, 1982; Owen, 1987). Strong cyclic shear waves increase the pore water pressure in the water saturated sediments and sediments move into the liquid-like state (Obermeier, 1996a). This liquefaction creates the deformation structures through relative movement between sediments and such sedimentary environments containing less than 15% clay preserve these structures (Berra and Felletti, 2011). The sand strata confined by clay layers are more vulnerable to increased pore pressure in water saturated sediments (Obermeier, 1996b). The similar setting was observed in banks of the Dardha River.

Different mechanisms such as impulsive stress (rapid sediment deposition, slope failure in response to undercutting or over-steepening, breaking waves and flood surges), bioturbation and seismic shaking can trigger the deformation in the soft sediments. Besides the triggering mechanisms,

various controls such as different physical properties of confining strata and slope instability are paramount for the formation of seismites, though, the seismic shocks are cardinal for the occurrence of liquefaction (Obermeier, 1996a). The seismites are not indicative of any particular triggering mechanism by themselves but given the tectonic activity, structural controls, geographic location, geomorphology and sediment cover of the region, other mechanisms such as great storms, traction processes, high paleoslope of beds for gravity sliding, burrowing and biogenic activities, bottom currents, etc. imperative for observed deformation structures are highly unlikely. The frequent repetition of deformed layers in the vertical distribution (Fig. 3.4) is strongly suggestive of earthquakes with close aftershocks (Bose et al., 1997; Owen, 1995; Seilacher, 1984). The occurrence of deformed layers between the unaffected beds of similar grain size is one of the strongest arguments for earthquakes as triggers for the deformations interpreted as seismites. Some of the best-developed stratigraphic sections from the study area including that of the Chanaki village excavation pit (Fig. 3.11c) where the seismites were observed have also been provided here (Fig. 3.11). These sections imply the prevalence of fluvial environment and that the host sediments preserving the seismites were deposited by the Dardha River itself. Triggered by rapid sedimentation, groundwater movement, earthquake shaking, storm currents and gravity flows (Lowe, 1975; Obermeier, 1996a; Owen and Moretti, 2011), the deformation of clastic sediments occurs by liquefaction, fluidization, and thixotropy (Owen, 2003). For the development of the soft sediment deformation structures, liquefaction and fluidization are the most common mechanisms responsible in unconsolidated sediments after the earthquake of magnitude, $M \geq 5$ (Obermeier, 1996b).

The seismic liquefaction processes have been connected to seismic shocks with $M > 5$ (Ambraseys, 1988) and with critical acceleration (a) depending on the actual magnitude of the earthquakes (for $M = 5$, $a = 0.20g$; for $M = 8$, $a = 0.03g$; Carter and Seed, 1988). The coexistence of the deformation structures such as bending of laminae, down-sagging of a sequence of alternating sand and silty clay beds and small scale listric fault is suggestive of the ductile-brittle transitional regime. Rodríguez-López et al.

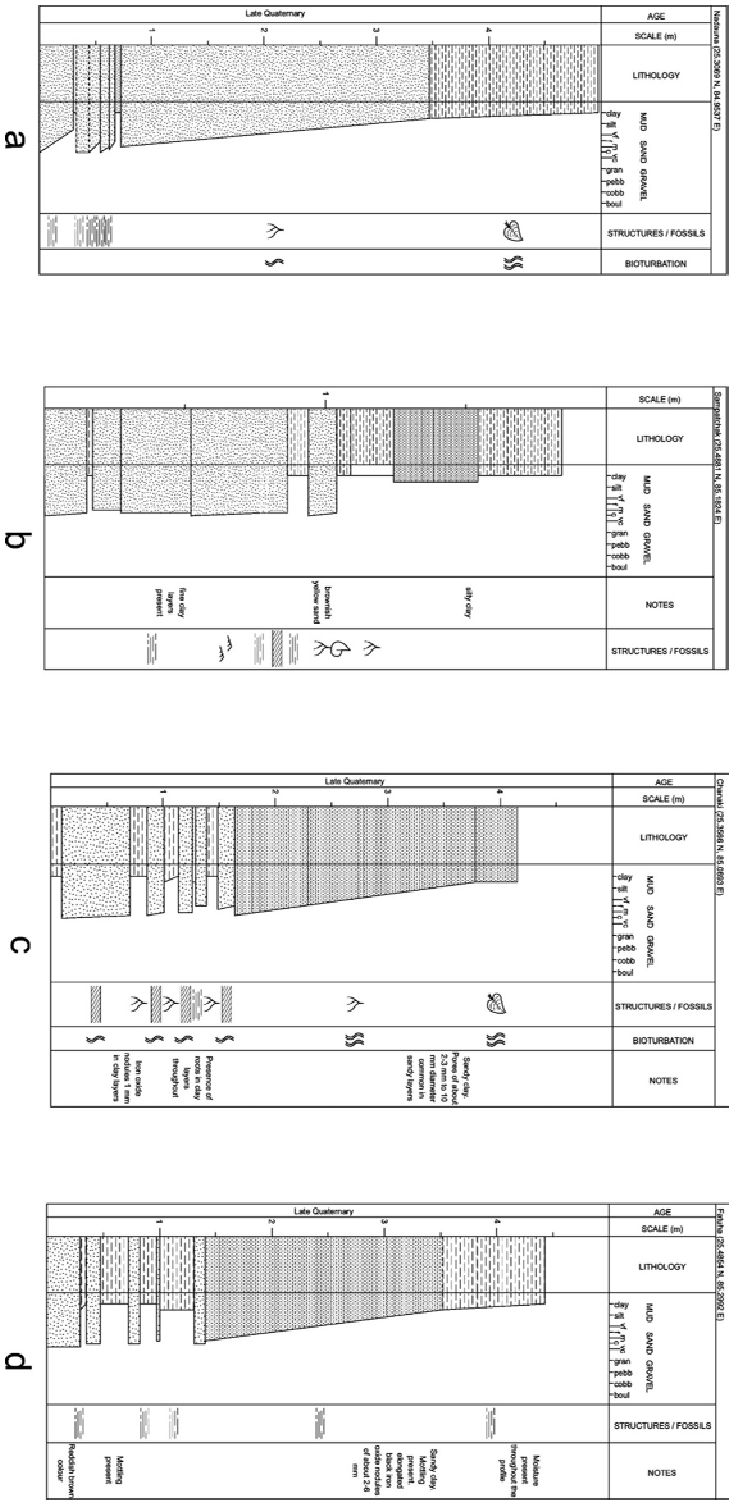

Figure 3.11 Sedimentary logs showing some of the best-developed soil profiles indicative of fluvial environment in the study area.

(2007) and other workers have described such coexistence from deformed unconsolidated sediments as the consequence of earthquake tremors.

As described by Lowe and LoPiccolo (1974), the unconsolidated sediments when undergo compaction and dewatering, the deformations such as pocket and pillar structure originate. The pillars are formed with the sudden expulsion of the water along vertical or sub-vertical columnar flow path during compaction of the sediments. That parallel vertical columnar ejection forms pocket-like structure in between the pillars. Lowe and LoPiccolo (1974), Lowe (1975), Allen (1982) and few authors suggested sediment gravity flows and overloading as triggering mechanism for the formation of such structures. However, other workers (e.g. Moretti et al., 1999) related them with seismicity. In the study area, deformed beds are often over- and underlain by undeformed horizontally lying strata, the deformation was penecontemporaneous with deposition and the deformation took place under dominantly hydroplastic behavior (but close to brittle-ductile field transition) in short time interval. The disturbed laminations or thinning and thickening of laminae also reflect ductile-brittle behavior. Owen (1996) interpreted that water escape cusps originate with water escape process and localized fluidization of lower sand layers. The thixotropic wedges are characteristics of periodical occurrence of liquefaction because of seismic quivers. Black (1983) and Thorson et al. (1986) described thixotropic wedges from Eastern Connecticut (late Quaternary deposits) as extension and collapse features resulting from the development of conduits of water and liquefied sediments. The cause of dewatering and liquefaction are believed to be due to the seismic shakes. Other deformation structures include deformed recumbent fold associated with slump and anticline underlain by undeformed inclined sand beds.

Development of small–scale fault and the associated bends in the clay beds at Janardanpur village (~20 km NE of Chanaki village) could most possibly be the result of deformation due to seismic activity as the other factors responsible for deformation are absent and the site is located close to the fault. This micro faulting structure supports the occurrence of seismic shock due to movement along the East Patna Fault. The abrupt termination of clay beds against a steep wall of sand bed due to liquefaction is often found in the seismic deformation structures. Such deformation has been observed at both locations (Fig. 3.3 and Fig. 3.10), though at the Janardanpur village, the sand bed

intrusion cannot be observed due to possible destruction. In view of the observations from both locations, it can be implied that the earthquake event may have occurred towards the southern reaches of this marginal alluvial plain and therefore the effect of the seismic shocks is seen to be diminishing towards the NE direction (i.e. from Chanaki to Janardanpur village). However, the formation of such deformation structures also depends upon the physical properties of the material constituting the section under question. East Patna Fault is a basement fault, which lies underneath 400–500 m thick sediment cover and hence, the direct detection of the main fault is highly implausible, but occurrence of the seismites provides an important evidence to substantiate the subsurface active fault in southern middle Ganga plain.

The type and dimension of seismites have been interpreted as a function of the magnitude of palaeo-earthquakes (Guiraud and Plaziat, 1993; Rodríguez-Pascua et al., 2000), and their spatial distribution can be used to locate main active faults (Alfaro et al., 2010). In the present study, the location of seismites is within the fault zone of East Patna Fault and the nearest recorded earthquake epicenter capable of causing liquefaction in such sedimentary environment is ~200 km away from the location of observed seismites. Therefore, the present observance of seismites from the middle Ganga plain to the south of the Ganga River (together with the evidence of recent activity of the East Patna Fault obtained by GPR study) is very conclusive of association of the earthquake event with East Patna Fault. It also provides the evidence of the influence of Himalayan tectonics to the southern Ganga plain towards the peninsular region. Although the documentation of soft sediment deformation in Holocene sediments and their formation mechanism exists from several parts of the world but the presence of the seismites from southern middle Ganga plain bears significance because these structures indicate neotectonic activity or reactivation of the East Patna Fault i.e. the most probable channel of stress migration from the Himalayan belt to peninsular India. The minimum slip potential values observed towards the northern end of the East Patna Fault (Bilham et al., 2001) also indicate the same stress dissipation mechanism.

The frequent seismic events associated with the East Patna Fault released the strain accumulated along the southern edge of the Himalayas. The expulsion of stored energy due to earthquakes reduced the slip potential in the region (Fig. 3) through the propagation of stress along the fault from the Himalayan front towards the peninsular region. This transfer of stress regime of the Himalayas, along the East Patna Fault to the south of the Ganga River, is an implication of possible prehistoric earthquake in the middle Ganga plain. This pre-historic earthquake event along East Patna Fault is well documented by the seismites observed in the southern Ganga plain close to the fault.

Although the deformed horizons could not be traced at other locations (due to lack of larger exposures), the studies may further be carried out, in future, in other parts of the southern Ganga plain as well. The dating of suitable horizons can prove to be valuable in determining the exact ages of events and the long-term sediment accumulation rates in the middle Ganga plain.

The present study reports the seismites associated with the East Patna Fault from south of the Ganga River in the middle Ganga plain for the first time. In the absence of any other potential triggering mechanism in the region, the well-preserved liquefaction structures 3–4 m below the surface owe their origin to the prehistoric earthquake event and its aftershocks. Their proximity to the EPF indicates moderate-size earthquakes (or aftershock triggered by major earthquakes) on the fault in the past or mega earthquake in the nearby Himalaya. The signatures of the Outer Himalayan tectonics and associated seismic activity extend to the southern marginal Ganga plain. The seismites observed from southern middle Ganga plain also provide evidence of the propagation of stress regime from the Himalayan front to the Indian Peninsula through the transverse basement faults.

Chapter 4

OPTICALLY STIMULATED LUMINESCENCE DATING OF SEDIMENTS

4.1 INTRODUCTION

The exact time of formation of various organic and inorganic materials can be established by a number of techniques available today such as carbon dating. Comparatively, there are fewer methods to know the time of last deposition or burial of sediments. From available methods, the optical dating is the most advantageous for the Late Quaternary sediments. This method is important especially for geoscientists and archaeologists working with sedimentary deposits because of its one characteristic nature that its 'clock' can be set to 'zero' by exposing the sediment to the light. Almost all grains of a sedimentary deposit in fluvial environment are exposed to daylight (called bleaching event) during their course of deposition. The event of their last exposure is dated using optical dating. The sediment may, however, have comminute from the parent rock at any geological period. The optical dating of sediments, mainly quartz, can be used to correlate spatially separated sediments, environmental reconstruction and extinction events (Jaiswal et al., 2008; M. Jaiswal et al., 2009; M. K. Jaiswal et al., 2009; Singh et al., 2017, 2016; Wu et al., 2010).

There are two main types of dating in luminescence technique i.e. optical and thermoluminescence dating. However, out of the two, optical dating has been found to be more effective. In both of the methods, the clock can be set to zero by heating the sediment. The quartz or felspar grains are used for both dating techniques. After the zeroing event, the latent signal is acquired by the grains in geological time-period until it is thermally or optically stimulated for measurement in the laboratory. The limits of age that can be measured with luminescence techniques depends upon samples and upper and lower bounds can range between a million to a few decades. The type of dating technique to be used depends upon the type of sample as each chronology method is

suitable for a given time range (Fig. 4.1) and can be used with particular type of sediment or circumstances (Fig. 4.2).

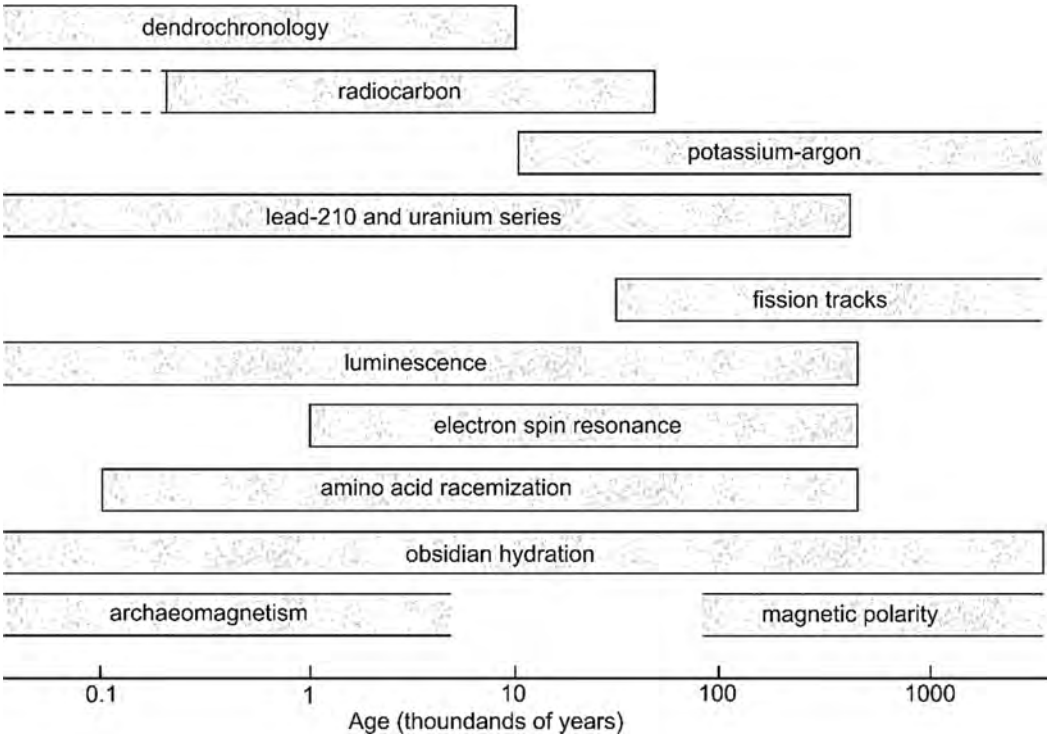

Figure 4.2 Age range of various methods. Actual limits are dependent on circumstances such as state of sample preservation (Aitken, 1998).

In optically stimulated luminescence, the dating signal of emitted

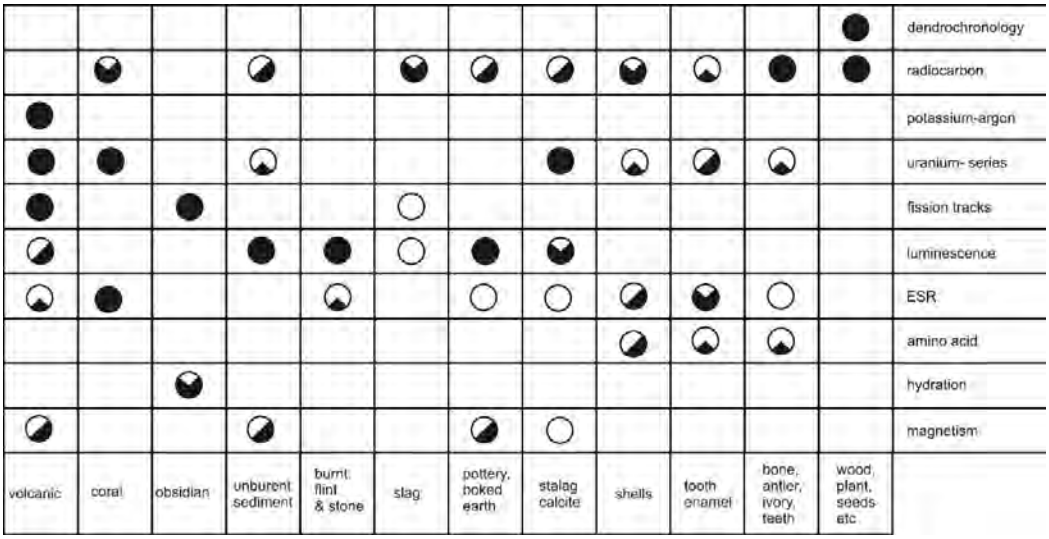

Figure 4.1 Types of samples to which different dating techniques can be applied (Aitken, 1998).

luminescence is obtained by shining a beam of light on it and then the emitted signal is counted by a photomultiplier. In nature, when mineral grains are exposed to light, the latent signal becomes zero in the grains (Fig. 4.3). Later,

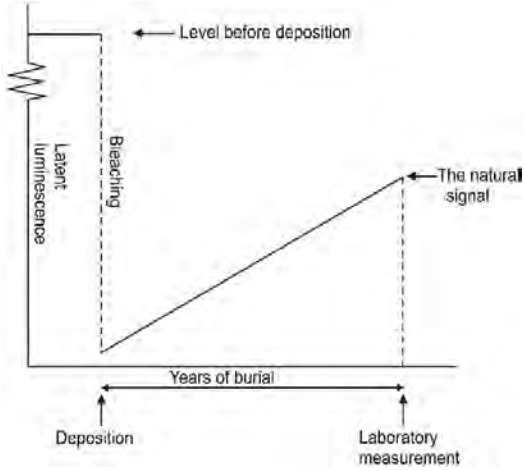

Figure 4.3 The event dated in optical dating is the setting to zero, or near zero, of the latent luminescence acquired at some time in the past (Aitken, 1998).

when it is buried under other sediments and the light is completely blocked, the latent signal again starts building up due to ionizing radiation emitted by uranium, thorium and potassium–40. Almost all sediments contain these radioactive elements in trace amounts. Mainly quartz is used in this technique which is separated from the sample and processed to reduce the grains to a given size range. The grains are given nuclear radiation from a calibrated radioisotope source and the signals obtained are compared with the dating signal to calculate *paleodose*. Paleodose is the dose of nuclear radiation artificially given to the grains in the laboratory which indices the luminescence equal to that found naturally in the grain. "The rate at which the energy is absorbed from the flux of nuclear radiation is called *dose rate"*. The age is then calculated by the formula

$$Age = \frac{Paleodose}{Dose\ rate}$$

The optical luminescence dating was initially used for dating aeolian sediments but later the techniques have been modified and fluvial sediments could also be suitable dated. Several workers have used optically stimulated luminescence (OSL) dating in fluvial sediments to evaluate the time of tectonic activity or paleoclimate change (Kale et al., 2000; Pati et al., 2012, 2011a; Rao et al., 1997).

4.2 EVALUATION OF PALEODOSE

The paleodose is obtained by comparing natural signal acquired during the burial period with the artificial signal obtained in the laboratory from known doses of radiation. There are two approaches to achieve this– the additive method and the regeneration method.

4.1.1 The additive method

In this method, the portions (or aliquots) are divided into groups of six or more members. The groups are given different dose of radiations except one group which is used to measure the natural luminescence or signal. All members in a single group are subjected to exactly same dose of radiation. All the members are preheated before subjected to radiation including the group reserved for measurement of the natural signal. The OSL is then plotted against laboratory dose to obtain the growth curve from which the paleodose can be calculated by extrapolation. However, in this method, the response curve is not linear at high doses because the rate of growth increment falls off with increment in doses. This is the disadvantage of this method. (Fig. 4.4).

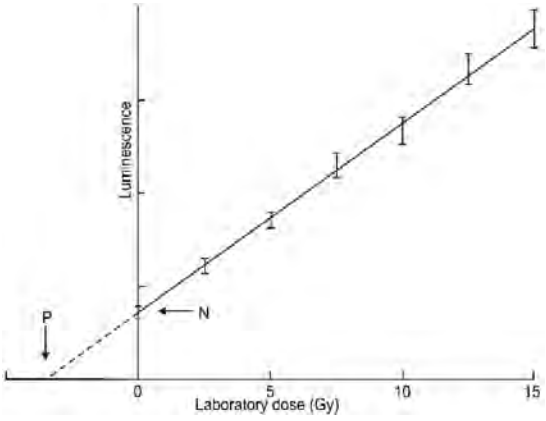

Figure 4.4 Additive method of paleodose evaluation. Each data point is average OSL from a group of aliquots. Laboratory dose is zero for N. P is read off as paleodose (Aitken, 1998).

4.1.2 The regenerative method

In this method, the natural signal is compared directly with the artificial signal (obtained from laboratory irradiation). However, the aliquots, except natural, are bleached before giving artificial radiation dose. There is no need to extrapolate the growth curve in regenerative method and hence, the complications of non-linearity are reduced (Fig. 4.5).

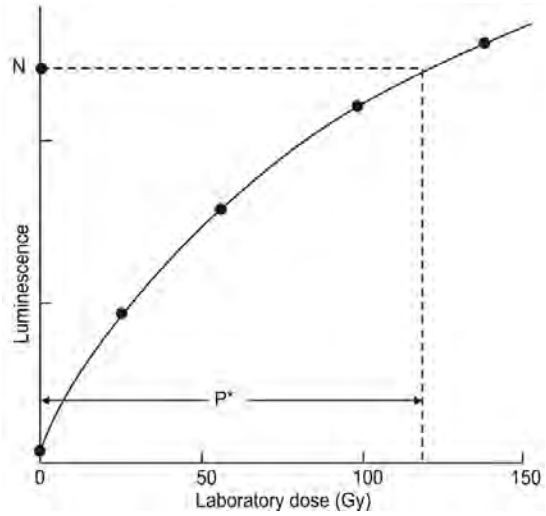

Figure 4.5 The regeneration plot. The aliquots have been bleached and dosed. N is the natural OSL. P is read off as paleodose by regeneration.

4.2 MECHANISM

The most common minerals found in the sedimentary deposits are quartz and feldspar. The crystal lattice of these minerals often contains defects which are created during crystallization or by exposure to the ionizing radiation. These charge defects are potential sites of electron storage with a variety of trap-depth energies. A subpopulation of stored electrons with trap depths of ~1.3 to 3 eV is a subsequent source for time-diagnostic luminescence emissions. The radioactive isotopes (^{235}U, ^{238}U, ^{232}Th and ^{40}K) within the minerals ionize the minerals which creates free electrons. The radiations from cosmic sources and Rb^{85} do not contribute to a large extent in this. Most of the high energy Gamma radiation is produced from ^{40}K while ^{238}U and ^{232}Th are responsible for Alpha particles and some Gamma and Beta radiation. Alpha particles are about 90 to 95% less effective in inducing luminescence compared to Beta and Gamma radiation. Thus, the luminescence increases with time as electrons in traps increase with continuous exposure to ionizing radiation over a long period of time. The luminescence of mineral grains reduces, when subjected to heat (~300˚C) or light, to a low and definable residual level. In many depositional environments over the geological time, most of the sediments get buried, eroded and transported several times. Thus, the mineral grains acquire signal during their burial period and the signal resets to zero after exposure to light during erosion and transportation. This luminescence “cycle" occurs repeatedly. Fresh sediments from bedrock, which are not subjected to this cycle have lower luminescence emissions per radiation dose. OSL dating provides a depositional age of grains since the latest event of burial.

4.3 SAMPLE COLLECTION AND PREPARATION

The samples for OSL analysis were collected in one-end-closed opaque tubes by pushing the tube into the freshly exposed sediment exposure of a natural or man-made section. The size of the tube measures 5 cm (dia) x 20 cm (length). Tubes were sealed after extraction and care was taken so as not to expose the sample to any light until the sample is extracted in the dark room for further processing.

The locations of the collected sample are given in figure. Appropriate sites for sampling were identified after preliminary analysis of the area using remote sensing techniques. Later, a fieldwork was carried out and samples were collected from C-horizons. The targeted locations were paleochannels of the Sone River, interchannel areas and floodplains because channel avulsion in the study area is an outcome of the active tectonics along the subsurface fault. The selected samples were processed for OSL dating.

The sediment extraction, chemical treating and physical separation- all the processes were carried out in dark room with only subdued red light used when necessary. About 3 cm of material from either side of the tube (which may have got exposed to scattered light directly or indirectly causing bleaching of grains) was removed and kept aside for estimation of ^{238}U, ^{232}Th and ^{40}K content in the sample. The sample obtained from centre of the core tube was treated with 1N HCl (hydrochloric acid) repeatedly to remove carbonates, followed by 37% H_2O_2 (hydrogen peroxide) treatment to remove the organics. The sample was kept for 6 hours in the acid in a glass beaker and then it was washed, and new acid was added again. This cycle was repeated 3-4 times. The sample was then washed with ultra-pure distilled water and the same cycle was repeated with H_2O_2. This is followed by sieving to concentrate the quartz grains fraction size of 90–150 μm size. This was followed by heavy liquid density separation using sodium polytungstate (density = 2.58 g/cm^3) to separate quartz and feldspar. The quartz grains thus obtained were dried in oven at 50°C. Finally, the grains are etched with 40% HF (hydrofluoric acid) for 80 min to dissolve any feldspar left and remove the outermost “rind” of the quartz grain which may have been affected by the alpha radiation. This was followed by treatment with 12N HCl so that the fluorides which may have formed during etching could be dissolved. All the samples were checked for feldspar contamination with the help of infrared stimulated luminescence. The sample preparation and OSL measurement was carried out at Indian Institutes of Science Education and Research (IISER) Kolkata, India.

4.4 OSL MEASUREMENT

The quartz grain obtained after processing were mounted on 10 mm stainless steel discs using Silko-spray silicone oil. The sediments are subjected to blue light (λ = 458 nm) (using light emitting diode) to release the trapped electrons. Calibration quartz supplied from the Risoe National Laboratory, Denmark Technical University, Denmark was used to calibrate the beta dose rate of the instrument. The released electrons emit a photon of light upon recombination at a similar site. To obtain an age from the luminescence given off by the sample, first the dose equivalent to burial dose needs to be found. As described by Murray and Wintle (2000), the single-aliquot regenerative (SAR) method is followed in which first the natural luminescence of the sample is measured. Then, the bleached sample is exposed to known doses of radioactive radiation (regenerative doses). The counts (number of photons emitted from the sample upon exposure to the radioactive radiation) is measured by the 'reader' (Lexsygsmart TL-OSL) and the number of counts obtained for each artificial dose is plotted against the doses given to obtain the dose-response curve. The detection window consists of a combination of optical filters Hoya U340 and Delta BP 365/50 EX mounted on a solid-state photomultiplier tube (PMT) designed to have very low background counts. A $^{90}Sr/^{90}Y$ beta source is used for irradiation (Singh et al., 2017). The intersection of the curve by natural luminescence signal provides De. A curve is generated for each aliquot (subsample), multiple aliquots are needed to obtain an accurate De. Also, each sample is given a preheat (160–300°C) before bleaching the grains so that the errors imparted from electrons trapped in shallow traps which are light sensitive but do not contribute to the natural luminescence are removed.

4.5 ANNUAL DOSE-RATE

An estimation of annual dose rate is required to obtain an OSL age. It involves determination of exposure of the grain to the ionizing radiation from ^{238}U, ^{232}Th, ^{40}K and cosmic rays during the burial period. The radionuclides content of the sediments was determined by inductively coupled plasma-mass spectrometry (ICP-MS) at Institute Instrumentation Centre of Indian Institute of

Technology Roorkee. A secular equilibrium in the ^{238}U and ^{232}Th decay series was assumed. To estimate the OSL age, efficacy of cosmic rays was also considered by including geographic position, elevation, depth of burial, density of burial material and moisture content (with 15% uncertainty) in the calculation (Prescott and Hutton, 1994).

4.6 AGE ESTIMATION

A measurement of paleodose or equivalent dose (De) and annual dose is required to estimate the OSL age of the sediment. The equivalent dose was obtained from the dose response curve. The concentrations of radioactive elements (^{238}U, ^{232}Th and ^{40}K) were determined by ICPMS. The moisture content was calculated from the samples and an uncertainty of 15% was included. Knowing the geographic locations of each sampling point, depth of burial from where sample was collected, the OSL age was computed as per the protocol described by Aitken (1998).

4.7 RESULTS

A total of 16 OSL dates have been included here to date the geomorphic units of the Sone megafan (Fig. 4.6). The error in ages of these samples was

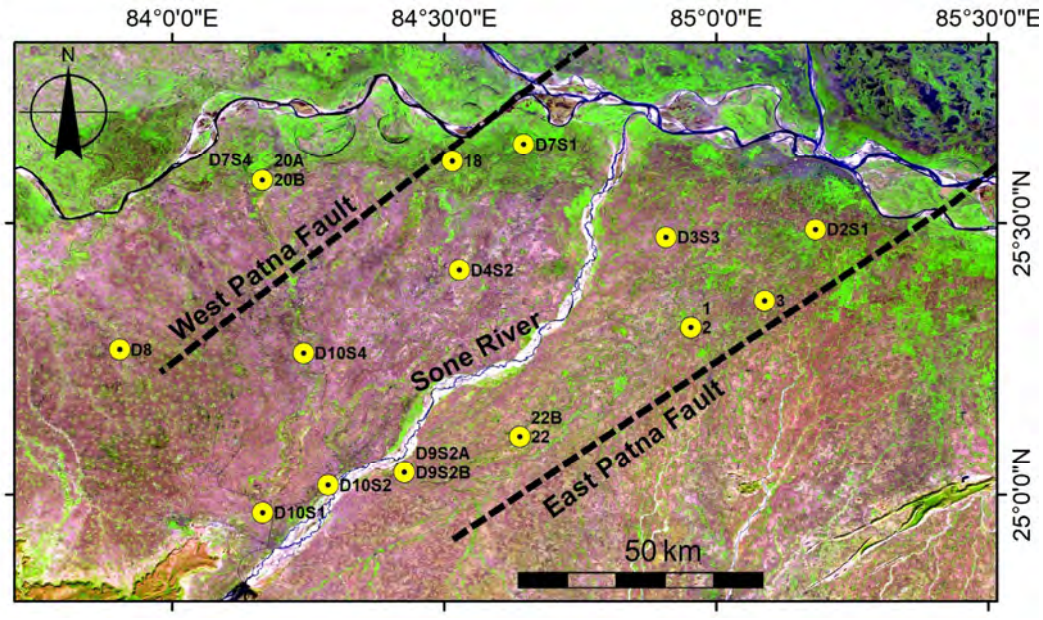

Figure 4.6 Sample numbers and their locations in the study area. Base map is a Resourcesat2 satellite image: AWiFS (R: 5 G:4 B:3).

not found to be too high. However, many aliquots could not be accepted for reliable dating due to changing sensitivity and poor fitting of the luminescence data (high recuperation value, poor recycling ratio and high test dose error). The selected OSL ages indicate that ages can be categorised into 3 groups. The western plain apparently developed around 20 Ka which makes the oldest part of the megafan. The eastern parts of the megafan seem to have deposited around 8 Ka (8.0 ± 0.7 Ka to 7.31 ± 0.55 Ka). Though, earlier evolution of the central part took place somewhere between 20 and 14 Ka, due to unavailability of deeper sediments as the surface is occupied by recent sediments of floodplain of the Sone River. These sediments are less than 0.8 Ka old.

Based on the OSL ages the geomorphic units of the Sone megafan has been classified as Oldest Sone Plain (OdSp) in the west, the eastern part is divided into two units i.e. Old Sone Plain (OSP) and Young Sone Plain (YSP). Apart from these, distal parts of the megafan covered by the floodplain sediments of the Ganga were also dated. Apparently at ~2.4 Ka the sediments of the Ganga encroached farthest into the Sone megafan. The details of sample and the age data are given in Table 4.1.

Table 4.1 OSL age of the sediments from Sone megafan

Sl. No.	No of Discs	Name	ED (Gy)	K (%)	Th (ppm)	U (ppm)	Dose Rate (Gy/Ka)	Age (Ka)
1	5	1	3.06±0.66	2.997	11	4	4.63±.08	0.66±0.14
2	13	2	2.74±0.48	3.16	11	4	4.79±.08	0.57±0.10
3	8	3	2.79±0.92	3.917	8	4	4.62±0.08	0.60±0.19
4	19	18	3.67±0.47	1.769	8	2	2.82±0.05	1.3±0.16
5	21	22	18.78±1.62	1.542	10	1	2.52±0.04	7.46±0.65
6	12	22B	18.40±1.36	1.542	10	1	2.52±0.04	7.31±0.55
7	18	D3S3	4.84±.13	3.318	22	3	5.45±0.1	0.89±0.02
8	14	D2S1	0.66±0.21	2.564	21	7	5.55±0.09	0.12±0.03
9	17	D4S2	70.38±3.57	2.553	22	4	4.94±0.09	14.25±0.76
10	12	D9S2A	26.43±2.26	2.318	4	3	3.304±0.063	8±0.70
11	28	D9S2B	22.26±1.97	1.493	12	3	3.045±0.055	7.31±0.66
12	27	D10S1	59.16±13.66	1.625	7	4	3.063±0.056	19.32±4.47
13	29	D10S2	10.69±1.47	2.637	16	4	4.622±0.084	2.31±0.32
14	15	D10S4	22.02±3.46	2.341	12	3	3.854±0.071	5.71±0.90
15	17	D7S4	11.62±0.65	2.361	23	4	4.822±0.086	2.41±0.14
16	12	D8	119.74±9.79	2.641	25	5	5.443±0.097	22±1.84

Chapter 5

MICROMORPHOLOGICAL STUDY OF SOIL PROFILES

5.1 INTRODUCTION

The pedofacies establishment requires rigorous micromorphological observations under the microscope. It could be erroneous to establish pedogenesis only on field-based observations. The development of interfluve successions is a complex process; various allogenic and autogenic controls create a hierarchical record of geological and pedological events in response to the interplay of climate, tectonics, and sedimentation (Atchley et al., 2004; Cleveland et al., 2007; Kraus, 1987; Mccarthy et al., 1998; Shanley and McCabe, 1994). The sedimentology and stratigraphy of several sedimentary basins have been studied on the basis of the study of interfluve successions (Kraus, 1987; Kraus and Gwinn, 1997; McCarthy et al., 1997; Platt and Keller, 1992). Stratigraphic details of the interfluves suggest that paleosols occur extensively in such fluvial successions and are marked by a varying degree of pedogenesis. These paleosols provide critical information about landscape evolution and paleoclimatic changes, and they serve as bounding surfaces or stratigraphic markers (Cleveland et al., 2007; Mccarthy et al., 1998; Pal et al., 2012; Shanley and McCabe, 1994; Srivastava et al., 2010).

The pedological fieldwork generally involves investigation of soil profiles exposed in the excavation pits. The profiles are identified broadly with horizon A, B and C, where A represents the topmost soil layer composed of humus mixed with microbial biomass, B-horizon is characterised by clay and minerals percolated down through A-horizon with the water, and different soil structures, and C-horizon is basically the parent material which lacks structures and shows little to no alteration of sediments which formed the overlying A and B horizons. The soil cover exposed on the surface which usually contains litter and decomposed organic matter is sometimes recognized as O-horizon. In regions of high rainfall, the layer immediately below A-horizon extensively leached by downward percolating rainwater is known as *zone of eluviation* or E-horizon,

whereas the subsequent deposition of leached material forms another layer below it called the *zone of illuviation*.

Table 5.1 Soil horizon letter designations (source: Encyclopædia Britannica, Inc)

	Base symbols for surface horizons
O	organic horizon containing litter and decomposed organic matter
A	mineral horizon darkened by humus accumulation
E	mineral horizon lighter in colour than an A or O horizon and depleted in clay minerals
AB or EB	transitional horizon more like A or E than B
BA or BE	transitional horizon more like B than A or E
B	accumulated clay and humus below the A or E horizon
BC or CB	transitional horizon from B to C
C	unconsolidated earth material below the A or B horizon
R	consolidated rock
	Suffixes added for special features of horizons
a	highly decomposed organic matter
b	buried horizon
c	concretions or hard nodules (iron, aluminum, manganese, or titanium)
e	organic matter of intermediate decomposition
f	frozen soil
g	gray colour with strong mottling and poor drainage
h	accumulation of organic matter
i	slightly decomposed organic matter
k	accumulation of carbonate
m	cementation or induration
n	accumulation of sodium
o	accumulation of oxides of iron and aluminum
p	plowing or other anthropogenic disturbance
q	accumulation of silica
r	weathered or soft bedrock
s	accumulation of metal oxides and organic matter
t	accumulation of clay
v	plinthite (hard, iron-enriched subsoil material)
w	development of colour or structure
x	fragipan character (high-density, brittle)
y	accumulation of gypsum
z	accumulation of salts

The transitional layers which show intermediate properties are labelled by two symbols of the adjacent horizons. Sometimes, the layers are observed with special features that form with the soil development. These additional features are important as they provide clue to climatic conditions during soil development. Thus, these features are designated as suffix to the base symbol for the horizon.

The combination of A, E and B horizons is known as the solum. The soil forming processes and degree of soil development can be deduced from the study of solum. In general, under uniform rate of sedimentation, the thicker solum represents older soil. However, it is rather difficult to identify all features in the field, therefore, micromorphological study of soil in laboratory is important. The laboratory analyses may help to accurately measure the percentage of sand, clay and silt present in a sample, salinity, clay illuviation, identify parent material, etc. The appropriate analysis is carried out depending upon the requisites of the study. In the present study, soil study was mainly aimed to help us in identifying the older soils and the younger ones, and to estimate the degree of soil development in different parts of the megafan with increasing time. The profiles have been identified with loam, sand, clay, sandy loam, clay loam and gravel which are shown in fig. 5.1. During fieldwork, a

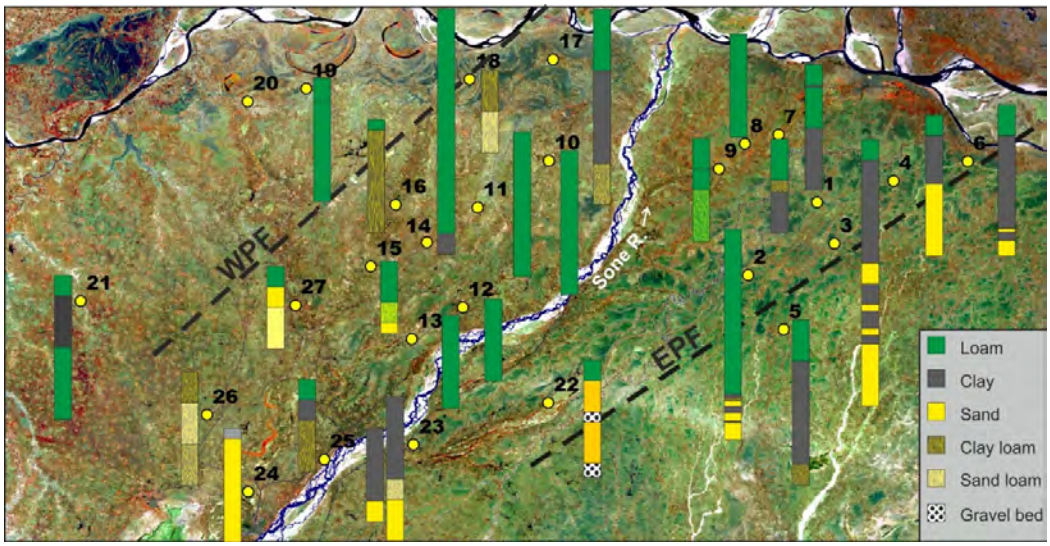

Figure 5.1 Relative thickness of different types of soil identified in field observation and their respective locations shown on satellite image. The base image is a standard FCC of Landsat ETM+ image (R:7 G:4 B:2).

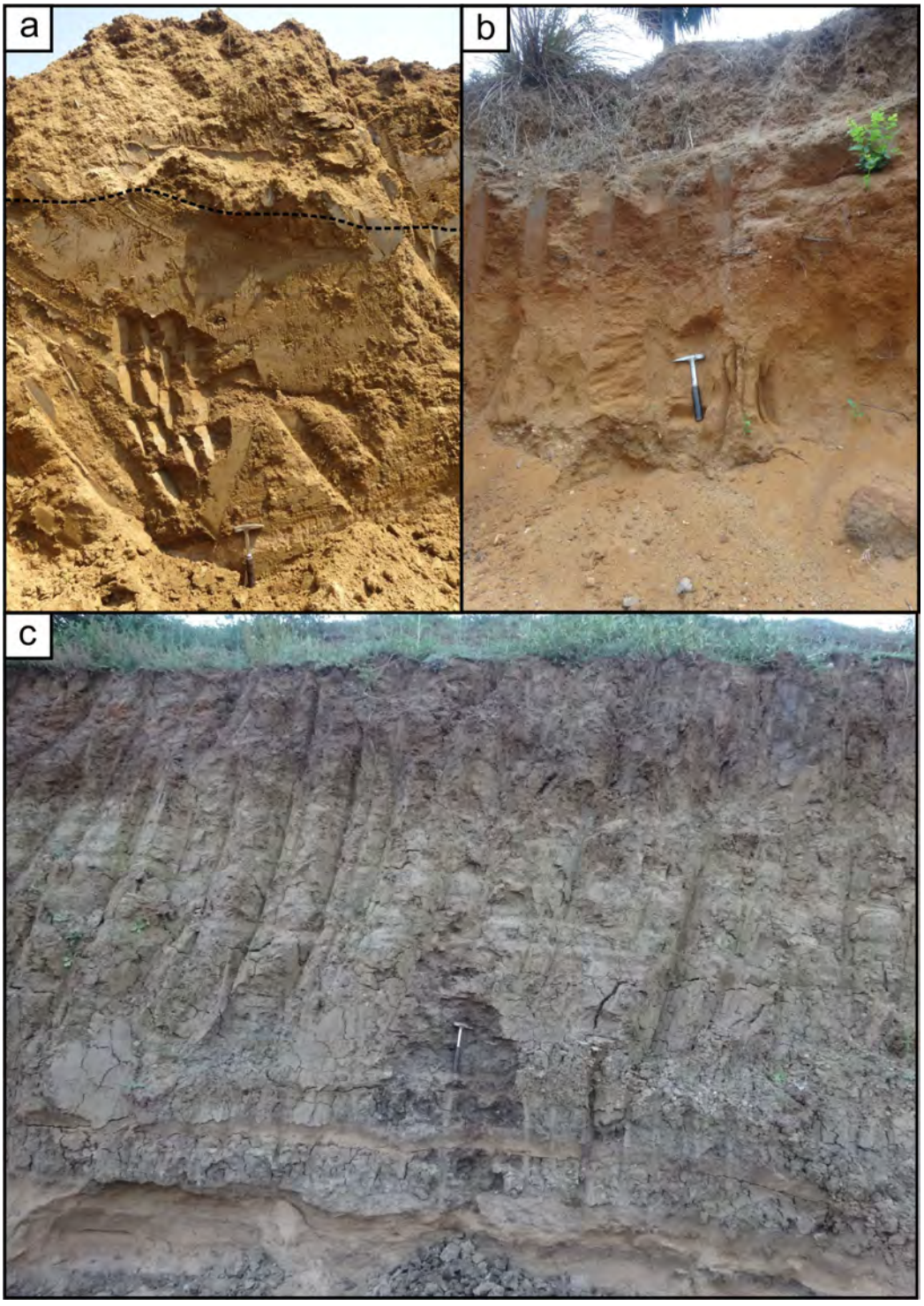

Figure 5.2 (a) Section from YSP showing sand deposit with no soil development, 2 (b) Section from YSP, gravel and sand beds in paleochannel of Sone River, 22 (c) Section from distal part of Sone megafan, gray sand desposit by Ganga River, 6. Numbers show the section location (refer to figure 5.1).

number of macro features characteristic of their location (in OdSP, OSP, and YSP) in the Sone megafan were recognised such as west dipping floodplain in OSP, compact and hard, whitish B-horizon due to calcium carbonate

accumulation in OdSP, gravel beds from paleochannels of Sone River, and sand beds of YSP (Fig. 5.2, 5.3 and 5.4).

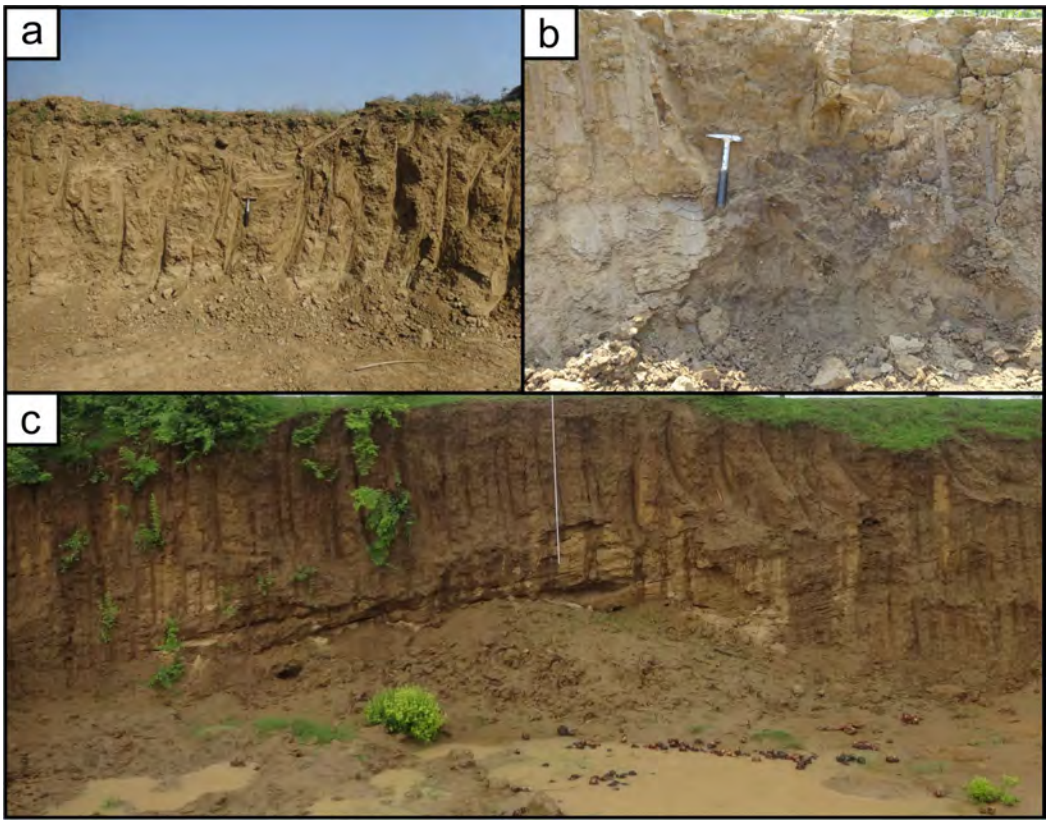

Figure 5.3 (a) Moderately developed soil section from OSP, 5 (b) weakly developed B-horizon of soil section from OSP, 4 (c) Section from OSP, shows thick sand deposition dipping towards the river paleochannel, 3. Numbers show the section location (refer to figure 5.1).

5.2 SOIL MICROMORPHOLOGY OF THE STUDY AREA

The study of soil micromorphology involves finding the arrangement of structures, grains and groundmass. These microfeatures develop during pedogenesis and are not visible in the field observation. Thus, thin sections of intact soil mass were prepared and studied under microscope. A selective study of 19 thin sections from 3 geomorphic units was done. The objective of present study was to understand the degree of soil development and its relationship with the relative increase in age of soils.

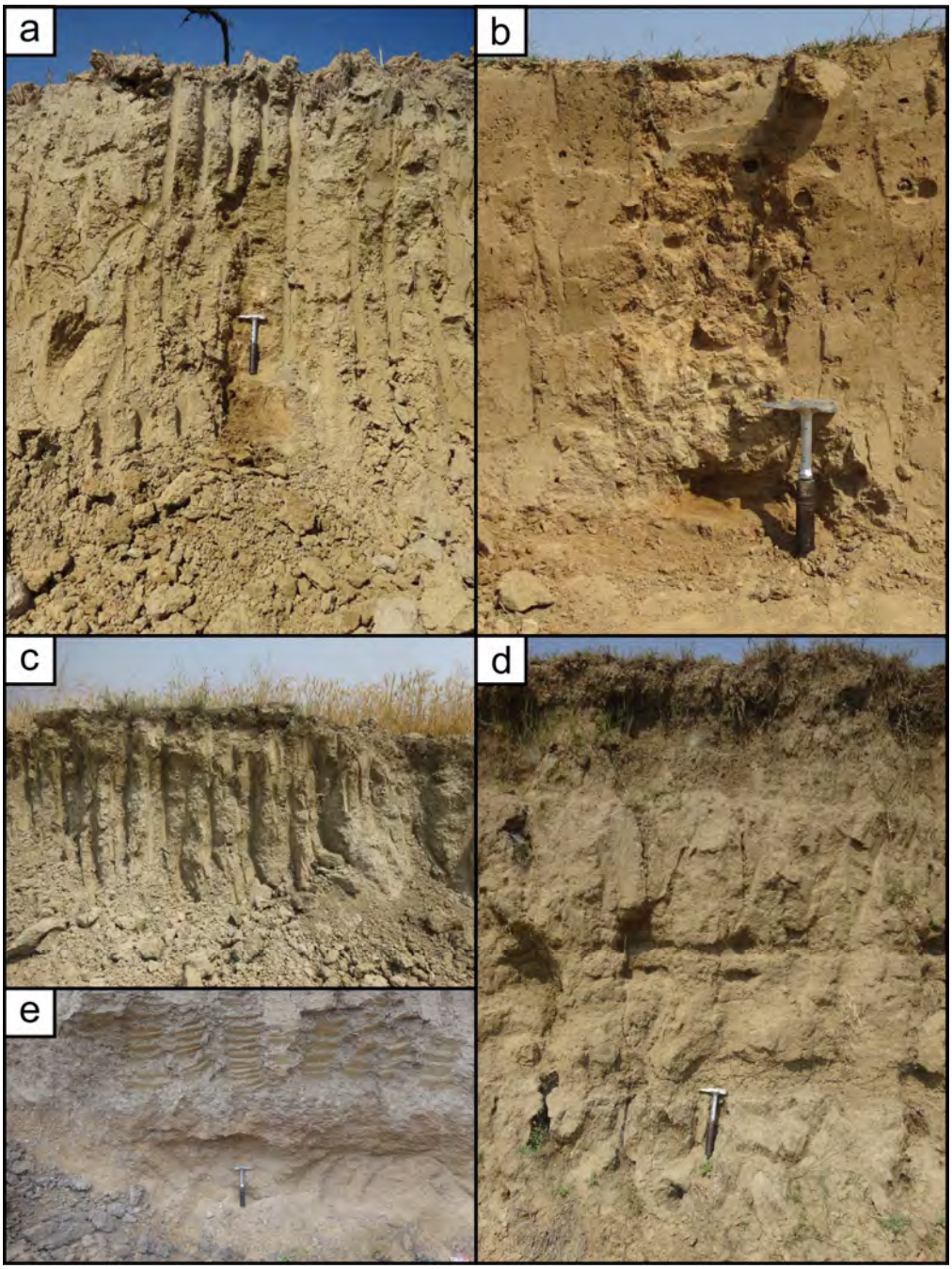

Figure 5.4 Some of the sections from OdSP. (a), (b), (c) and (d) show the hard and compact, well-developed loamy soil profiles from OdSP at locations 10, 15, 21 and 17, respectively. (e) a section from the paleochannel of Sone River, 23. Refer to figure 5.1 for locations in the study area.

5.2.1 Preparation of thin sections

The soil samples for thin sections were collected from B-horizon of the fresh profile exposures in metal boxes (7.5 x 5 x 5.5 cm) from different

geomorphic units. The methodology as suggested by Miedema et al. (1974) and Jongerius and Heintzberger (1975) was adopted to prepare the thin sections. The collected samples were soaked in acetone and placed in vacuum desiccator for 4 hours. The samples were then impregnated with a mixture of crystic resin, thinner, catalyst and hardener in a fixed proportion as follows: a) crystic resin (synolite 544) 750 ml, b) thinner (isopropyl alcohol) 250 ml, c) catalyst (cyclonox LNC) 6-7 ml and d) hardener (Co-octate) 3-4 drops. It was taken care than no air bubbles remain in the mixture. The mixture thus prepared was added to the samples in metal boxes, followed by placing them in the vacuum chamber for 12 hours to allow the mixture to penetrate the pore spaces. The samples were left at room temperature for 6 weeks for hardening. These solid blocks were later used to prepare thin sections (30 µm thickness) by cutting and polishing into sections of 9x6 cm size. These sections were used for the study of pedo-features.

5.3 MICROMORPHOLOGICAL FEATURES

The micromorphological features of the soil have been described as suggested by Bullock et al. (1985). The main features observed in the thin sections were pedality, voids, cutans, b-fabrics, degree of alteration and concretions or nodules. The pedality is defined in terms of the shape of peds which may be angular, sub-angular, blocky, prisms, etc, and the degree of pedality which may be apedal, weak, moderate or strong depending upon the voids in between them. Voids are described in shape, size, degree of smoothness/roughness. Cutans have been defined on the basis of mineralogical composition as argillan for clay, ferriargilan for clay with iron oxides, calcetan for calcium carbonate rich clay. Morphological relation of cutons and coatings with pores or grains are described in terms of typic–, hupo– and quasi–coating. The orientation and distribution pattern of interference colours of soil micromass birefringence fabric or b-fabric. These are termed as unistrial–, crystallitic–, cross–, reticulate–, poro–, grano–, circular–striated, stippled–. The degree of development of b-fabric is described as weakly, moderately, and strongly developed. Three minerals, namely, quartz, feldspar and biotites were studied for degree of alteration. The alteration patterns are

defined as pellicular, linear (irregular, parallel and cross) and dotted alterations. The degree of alteration can also be expressed as weak, moderate and strong. The concretions and nodules may be sesquioxidic (Fe/Mn), mottles and calcite nodules and have been described as weakly, moderately and strongly impregnated nodules.

5.3.1 Microstructures and alterations

Micromorphological investigations show that the soils of OdSP have moderately to strongly developed subangular blocky microstructures in B-horizons. The soils of AFP, YSP show no to weak soil development features whereas the soils of OSP show moderately developed pedo-features (Fig. 5.5 and 5.6). Average ped diameter, void diameter, channel width and porosity ranges between 200 µm – 3.5 mm, 50 µm – 3 mm, 50 µm – 1 mm and 5–20% respectively. The roughness of voids decreases from YSP to OdSP. The pellicular alteration of biotites and feldspar along with irregular linear alteration of feldspar and fracturing of quartz are observed in the older soils i.e. degree of alteration increases from YSP to OdSP. As seen in the soil sodicity and salinity map of the area (Fig. 1.5), the soils of OdSP are more sodic and saline than the OSP and YSP.

5.3.2 Groundmass

The groundmass is generally yellowish brown, yellowish red to reddish brown and in some thin sections it is yellowish brown to gray. A few thin sections show linear accumulation of yellowish to orange colour of lepidochrosite. Reddish brown colour occurs due to the presence of Fe_2O_3 formed in the oxidising environment of well drained soils. The sesquioxides released by weathering of biotite gets precipitated close to these grains and biotite exhibits discolouration on weathering. Micromass of soils in different soil geomorphic units exhibit random circular–, reticulate striated and mosaic speckeled b-fabrics. In general, the degree of development of b-fabric is stronger in younger soils.

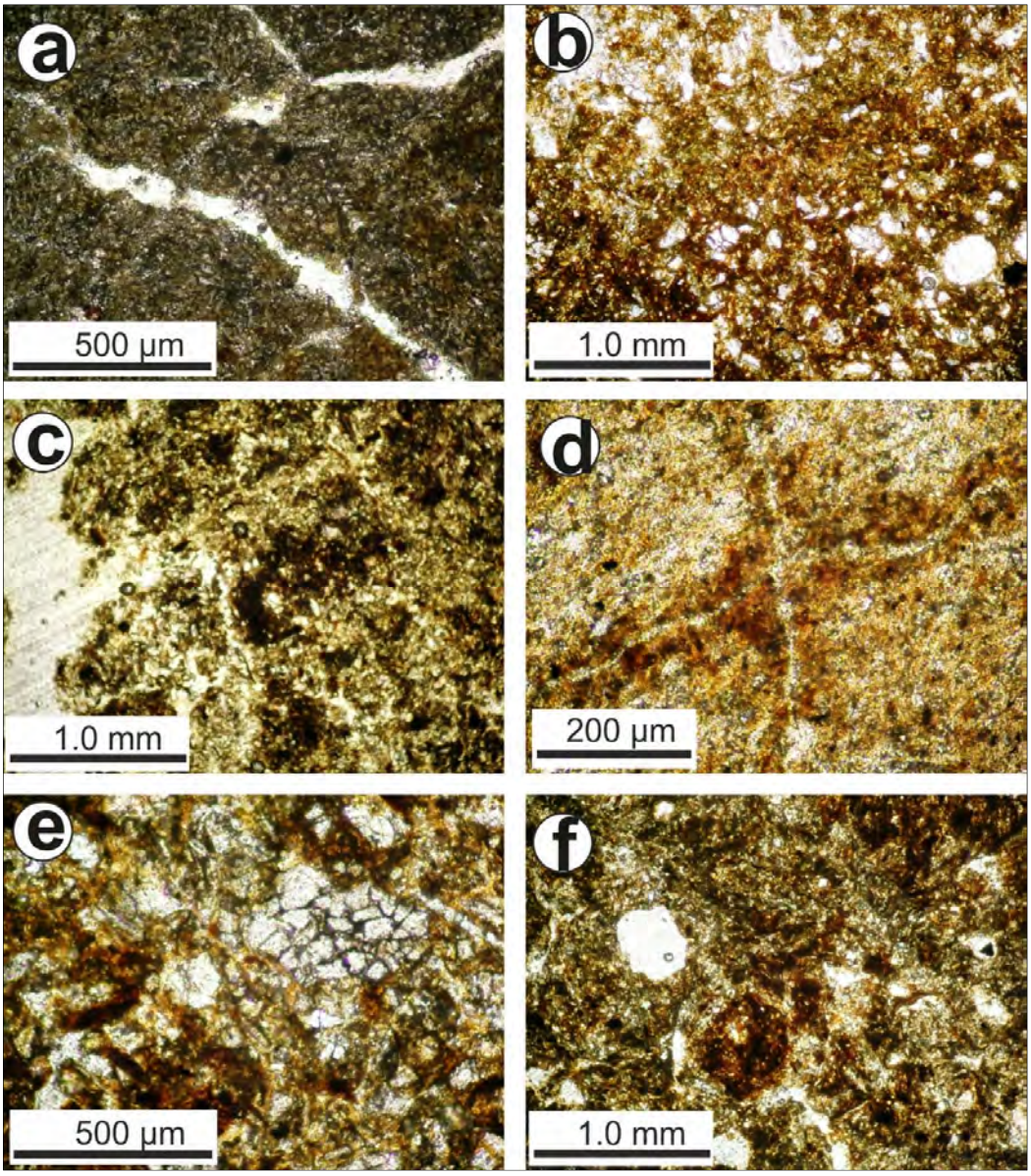

Figure 5.5 (a) Apedal,Fe-Mn impregnated dense ground mass, rootlets filled with silica, YSP (b) Weakly developed sub angular blocky structure, OSP (c) Moderately developed sub angular blocky structure, OSP (d) Stipple-specled b-fabric,cross cutting void, YSP (e) Fractured Quartz grain(QZ) and accumulation of Fe-Mn rich material, YSP (f) Moderately developed reticulate striated b-fabric, OSP.

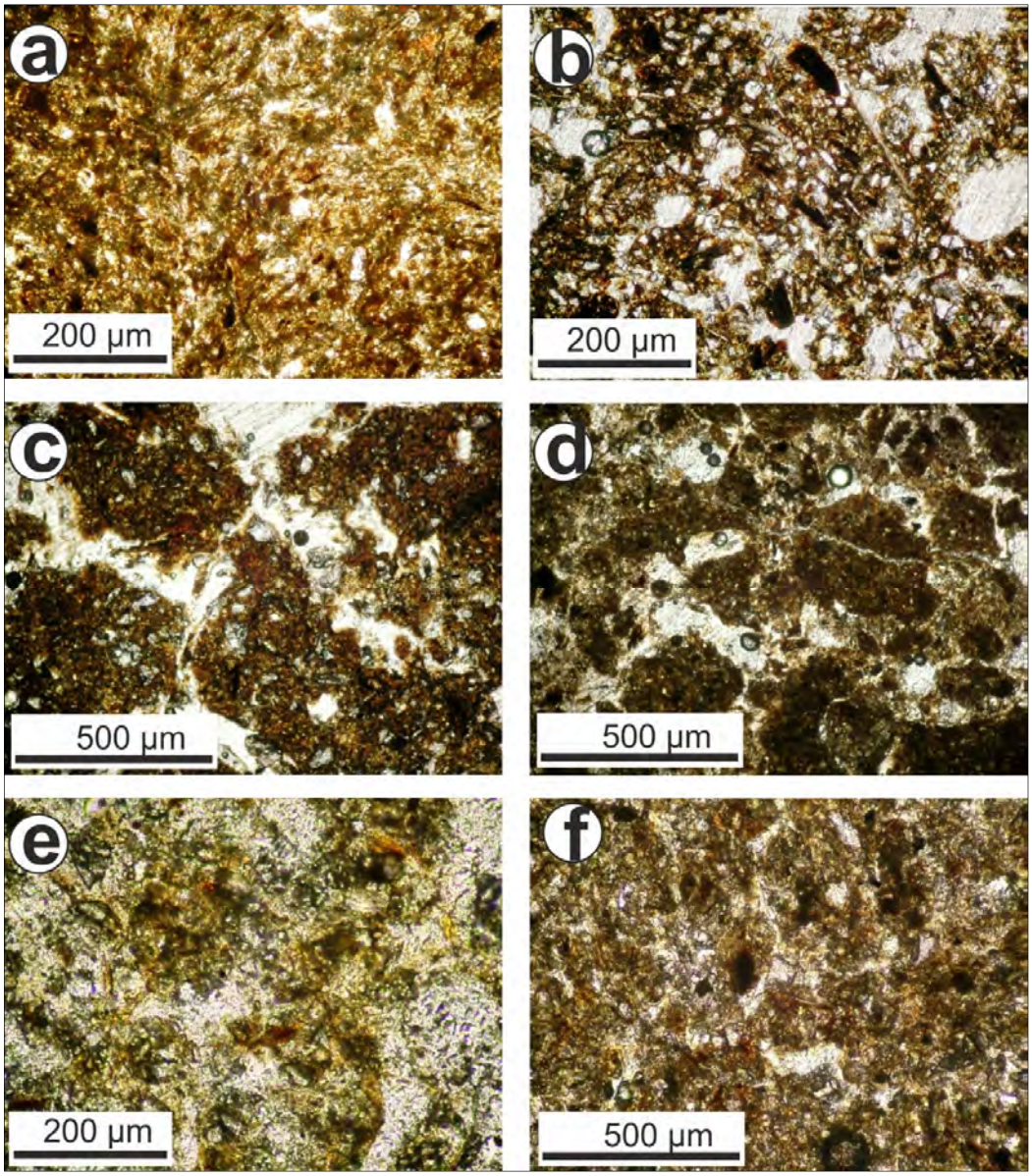

Figure 5.6 (a) Deformed reticulate striated b-fabric, OdSP (b) Muscovite laths and Fe-Mn impregnated dense ground mass, OdSP (c) Strongly developed spheroidal blocky peds, OdSP (d) Very strongly developed spheroidal blocky peds, OdSP (e) Strongly developed peds with altered Biotites, OdSP (f) Moderately developed sub angular blocky peds with Channels filled with secondary materials, OdSP.

5.3.3 Pedofeatures

The major pedofeatures observed are coatings like argillans, ferriargillans, Fe-Mn coatings, mottles and Fe-Mn nodules. Ferriargilan and argillan occurring as typic and hypo coatings are present in all soils. The thickness of cutans show a general increment from YSP to OdSP. Fe-Mn coating were also find in some the thin sections from younger soils. Decomposed rootlests and stems partially

filled with Fe-Mn rich materials are seen in all the soils. Micromorphologically sesquioxides are observed as dense groundmass and as coating with variable thickness along ped, voids and channels. Fe/Mn features are more commonly observed in wetlands irrespective of the age of the soil. The OdSP shows concretions of both Fe-Mn and calcite <10 mm diameter.

5.4 INFERENCES

Most of the soil in the study area are classified as sandy loam. The soils of the YSP show thick caps of clay deposit on surface because of many closely spaced ponds covering the area, underlain by none to low thickness of B-horizon development. Most of profiles show clay cap underlain by coarse sand beds of paleochannel of the Sone River. Alternating clay and sand layers suggest frequent flooding in the area. A very few soil profiles from OSP show thick loam development in B-horizon (~0.3 – 1.5 m), while most of the profiles show thin loam/clay beds underlain by sand beds. Most of the profiles in OdSP reveal thick solum development (~0.5 – 3 m). The solum variation of various soil profiles observed in the field have been shown in fig. 5.1. The B-horizon mainly consists of thick loam layer underlain by sandy loam or clayey loam. The profiles across the paleochannels show distinct gravel beds. The gravel beds separated by sand beds show meandering of the Sone River. The micromorphological study also shows that soils of YSP and OSP, have weak pedality and soils of OdSP show moderate to well-developed sub-angular blocky microstructures. Thus, the field observations coupled with micromorphological studies suggest increasing degree of soil development, alteration of minerals, pedality and solum thickness from younger to older soils i.e. YSP, OSP and OdSP.

Chapter 6

GROUND PENETRATING RADAR STUDY

6.1 INTRODUCTION

To determine the features in shallow subsurface, ground penetrating radar (GPR) survey has been proved to be a well-established geophysical technique for high resolution imaging (Bristow and Jol, 2003). The GPR is very useful in interpreting sedimentary architecture, stratigraphic sequence and geometry of the subsurface deposits. This is particularly important in correlating concealed soft sediment structures and identification of breaks in structures in the Quaternary sediments (Bristow and Jol, 2003; Gawthorpe et al., 1993). In past few decades, the GPR study has been carried out in many geological as well as non-geological problems. It has been put to use in different environments such as lacustrine delta, fluvial, aeolian, peat deposits, glacial, etc. (Jol and Smith, 1991). GPR has found application in engineering, environmental management and geology (Mellett, 1995). The areas of application for ground-penetrating radar are diverse (Bhatt et al., 2006; Bhatt and Bhonde, 2003; Maurya et al., 2005; Prizomwala et al., 2016; Sharma et al., 2017; Shukla et al., 2013). The method has been used successfully to map ice thickness, water depth in lakes, bedrock depth, soil stratigraphy, and water table depth. It is also used to delineate rock fabric, detect voids and identify karst features (Davis and Annan, 1989). The technique has been applied to hydrogeology, petroleum reservoir modelling, groundwater contamination and archaeological studies also (Dolphin et al., 1978; Jol et al., 1996; Knight and Endres, 1990; Thompson et al., 1995). A GPR works within a wide range of frequency between 20 MHz to 2.5 GHz or even higher. Unlike seismic reflection profiling, it uses electromagnetic radiation to image subsurface and thus it depends upon the dielectric constant of the material it is investigating. The dielectric constant is a critical GPR parameter because it affects the horizontal and vertical imaging resolution (Martinez and Byrnes, 2001). GPR is a non-destructive near surface geophysical imaging technique. The GPR has been extensively used in fluvial environment due to widespread distribution of river deposits, ease of access, heterolithic character of fluvial sediments and their

large-scale depositional forms (Bristow and Jol, 2003). GPR can also be used to assess the evolution of an alluvial fan in association with geochronologocial data (Ékes and Friele, 2003).

In the present study, GPR survey was carried out using a 100 MHz antenna which is suitable for identifying discontinuities in soil. The profiles were taken across the inferred faults to assess their subsurface nature and to obtain an evidence of recent fault activity.

6.2 PRINCIPLES

The ground penetrating radar is based on the properties of wave nature of electromagnetic (EM) radiation. GPR exploits the electrically conducting band of EM spectrum. The electrical discontinuities in the subsurface, typically < 50 m, are detected by generation, transmission, propagation, reflection and reception of discrete pulses of high-frequency (MHz) electromagnetic energy (Neal, 2004). A GPR system consists of three main components: (1) Control Unit (2) Antenna (3) Power Supply. The power supply may be either small rechargeable batteries or normal 110/220–volt. The *control unit (C/U)* is an electronic instrument that interfaces a transducer to recorders, processes, displays, survey wheel, power supply, etc. It also has controls to allow radar functions such as range, gain and filtering to be adjusted. A control unit can be analog, digital, or hybrid. An *antenna* is a component of an impulse radar system designed to radiate radio waves (electromagnetic radiation) from Applied voltage impulses (transmitting antenna), or conversely, to intercept radio waves and convert them back into electrical impulses (receiving antenna). Antennae radiate or receive electromagnetic energy.

The control unit triggers discrete electrical pulses of a particular frequency that antenna amplifies and transmits into the ground. The depth penetration depends upon the frequency of the signal. The lower the frequency of the antenna, the deeper into the ground it will penetrate. A higher frequency antenna is chosen for detection of smaller targets and vice versa. The distance between the antennae (transmitter and receiver) can also be varied depending upon the type of survey and target under study (Fig. 6.1).

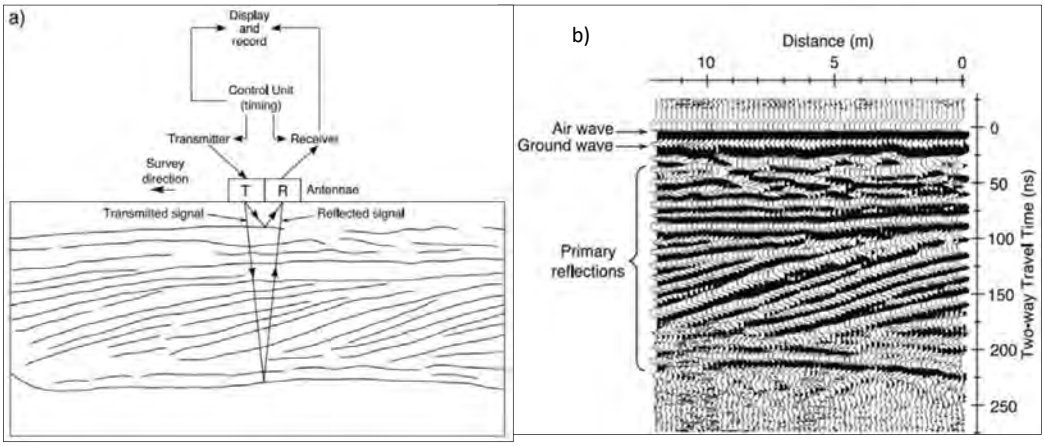

Figure 6.1 GPR data acquisition and resulting radar reflection profile (a) Data acquisition at a single survey point, showing GPR system components and subsurface reflector configuration (b) radar reflection profile resulting from sequential plotting of individual traces from adjacent survey points. Positions of air wave, ground wave and primary reflections are indicated (Neal. 2004).

GPR works by sending pulses of energy into the ground or any material and records the strength and time required for the reflected signal to return. Reflections are produced whenever the signal meets the boundary between two materials of different electrical conductivity or dielectric permittivity. The higher the contrast between the two, stronger the reflections are produced. While some of the energy is reflected back to the system, a part is attenuated into material.

Materials of high dielectric such as the water saturated strata slow down the radar waves and penetration depth decreases. Dielectric values for some common materials are given in table 6.1. Highly conductive rapidly attenuate the signal. The radar energy is emitted in a cone shape. Since the leading edge of the cone is farther away from the target, it will take a longer time to return than the time taken by the wave directly beneath antenna. The energy received later is recorded farther down in the profile on a radargram. Therefore, as a GPR is moved over a single target, it appears as a hyperbola in the profile. The target is actually at the peak amplitude of the positive wavelet.

Table 6.1 Dielectric values for common materials (Reynolds, 1997)

Material	Dielectric	Velocity (mm/ns)
Air	1	300
Water (fresh)	81	33
Water (sea)	81	33
Polar snow	1.4 – 3	194 – 252
Polar ice	3 – 3.15	168
Pure ice	3.2	167
Freshwater lake ice	4	150
Sea ice	2.5 – 8	78 – 157
Permafrost	1 – 8	106 – 300
Coastal sand (dry)	10	95
Sand (dry)	3 – 6	120 – 170
Sand (wet)	25 – 30	55 – 60
Silt (wet)	10	95
Clay (wet)	8 – 15	86 – 110
Clay soil (dry)	–	173
Granite	5 – 8	106 – 120
Limestone	7 – 9	100 – 113
Basalt (wet)	8	106
Shale (wet)	7	113
Sandstone (wet)	6	112
Coal	4 – 5	134 – 150
Quartz	4.3	145
Concrete	6 – 8	55 – 112
Asphalt	3 – 5	134 – 173
PVC	3	173

6.3 METHODOLOGY

The area for GPR study was identified through preliminary studies carried out using remote sensing and GIS techniques (Fig. 6.2 and 6.3). A field

study was carried out around the EPF for identification of deformation structures related to faulting and locating suitable places for GPR surveying to probe the subsurface discontinuity.

Figure 6.2 Location of ground penetrating radar (GPR) survey carried out across East Patna Fault (EPF) near Daniawan village in Patna, Bihar. The base image is obtained from Google Earth.

Figure 6.3 Location of ground penetrating radar (GPR) survey carried out across East Patna Fault (EPF) in Jehanabad distrct of south Bihar. The base image is obtained from Google Earth.

As EPF is the most active fault in the middle Ganga plain, therefore it has remained the focus of the exploration for signatures of active tectonics in the area. GPR survey was carried out in other parts of the Sone megafan also but the radargrams obtained at other locations did not show new or interesting features. The reason for this could be the monotonous nature of thick sand cover for most of the megafan surface.

6.4 DATA ACQUISITION

The device used in the present study was a subsurface interface digital GPR system (SIR-3000) manufactured by Geophysical Survey Systems Inc (GSSI). The transmitter and receiver were separated by a distance of 1 m and the profiles were taken in point mode and distance mode using the survey wheel (Fig. 6.4).

Figure 6.4 Ground penetrating radar (GPR) setup with survey, shielded antennae, control unit and fibre cables for survey in distance mode.

The best balance of data resolution with the optimum depth of penetration can be obtained by using antennae of 100 MHz frequency (Bristow and Jol, 2003). As suggested by (Audru et al., 2001), antennae were shielded

to avoid ringing innate to hardware. The GPR profiles were taken in distance mode along straight lines transverse to the strike of EPF. The fiber optic cables were used to transfer all data from antennae to control unit. The most appropriate data could be obtained by adding Automatic Gain Control (AGC) (Neal, 2004). Gain is the artificial addition of signal in order to counteract the natural effects of attenuation. As a radar scan travels into the ground, some of the scan is reflected, some of it is absorbed, and some of it keeps travelling down. As the scan gets deeper, it becomes weaker. Thus, gain is applied to the scan at particular points to make the subtle variations in weaker data more visible. All sources of electromagnetic waves such as mobile phones, hypertension lines, electric poles, etc. were avoided to the best possibility in order to avoid any signal interference with the working of the equipment. Running vehicles, passing trains or other heavy traffic which cause vibrations and induce noise in the data were also obviated. The GPR was moved onto the plain surface with no grits or gravels as they add noise to the data.

As the basement fault lies at about 400−500 m depth, it is beyond the detectable limit of GPR. Hence, GPR profiling was carried out to perceive the near surface nature of the secondary faults associated with the basement fault (EPF). The profiles were taken from different locations across the expected fault (located using geomorphic evidence), each profile being about more than 1 km length. The range of the signal for depth penetration was kept at 800–1000 ns.

6.5 GPR DATA PROCESSING

The collected data were processed with RADAN software as suggested by Fisher et al. (1996) and GPR manual provided by Geophysical Survey System Instruments (GSSI). The tools and filters were used in the software such as Finite Impulse Response (FIR), Infinite Impulse Response (IIR) filter, gain control, 2-D spatial fast Fourier transform filters, distance normalization, deconvolution, surface normalization, hyperbola migration and band pass filtering. For the processing of data obtained from GPR at 100 MHz frequency, the filter bandwidth applied was 40/50 and 150/180 MHz as suggested by Fisher et al. (1996). The reflection of the waves caused by the air and other

surficial matters was removed. Some of the important functions and filters are briefly described below.

Horizontal scaling: Data may be modified by adjusting the horizontal scale using the Stacking, Skipping and Stretching functions.

Stacking: Stacking applies a simple running-average to stack the data. It combines the adjacent selected radar scans to remove minute amount of high frequency noise and outputs a single scan.

Skipping: Skipping is used to specify the number of scans needed to be skipped over from the previous scan.

Stretching: Stretching is used to expand the horizontal scale. This function will calculate the simple average of two adjacent scans (or specified number of scans) and place the average scan in between the existing scans.

Infinite Impulse Response (IIR) filters: When an IIR filter encounters a feature in the radar data, it produces an output that decays exponentially towards zero but never reaches it, hence the name “infinite”. IIR filters are not necessarily symmetrical and while they achieve excellent amplitude response, their phase response is non-linear and so they can cause slight phase shifts in the data. The IIR filter parameters allow to define the high and low pass horizontal and vertical filters as well as the time interval that will be processed, defined by the start and end sample number. The cut-off frequencies are defined in number of scans horizontally and in MHz vertically.

Finite Impulse Response (FIR) filters: FIR filters have a finite duration impulse response. FIR filters, when encounter a feature in the data, are guaranteed to output a finite filtered version of that feature. FIR filters produce symmetrical results, so reflections will not be shifted in time or position. There are two types of FIR filters available, Boxcar and Triangular Filters.

Boxcar filter: The Boxcar filter is a rectangular window function that performs a simple running average on the data. A portion of the data, determined by the filter length, is averaged, and the average is output as a single point at the

centre of the active portion of the filter window. The filter moves on to the next sample and the process is repeated. The Boxcar filter assigns equal weight to the data all along the filter length.

Triangular filter: The Triangular filter emphasizes the centre of the filter more heavily than the ends of the filter. This type of filter is a weighted moving average, with the weighting function shaped like a triangle. A portion of the data, determined by the filter length, is multiplied and summed by this function. The result is output at the centre of the triangle. The filter then advances one sample and the process repeats.

Horizontal High Pass (Background Removal) Filter: Flat lying ringing system noise is usually most prevalent when the range (the time window in nanoseconds that the instrument will record from a single pulse) is set near the maximum limits for the antenna. It is characterized by flat-lying or horizontal bands usually of a vertical frequency lower (shown by wider bands) than that of real reflections in the data set. This type of noise can obscure or mask real reflections at greater depths. This type of low frequency noise is removed by using Background Removal Filter. When a non-zero value is used, thigh pass filtering will occur in the horizontal direction. Low frequency features in the data will be removed, such as antenna ringing. This filter will also remove the surface reflection (direct coupling) pulse.

Low Pass filters: High frequency noise is usually most prevalent when the range is set near the limits for the antenna in use, and large amounts of gain are used. It is characterized by “snow-like” noise in the data at depth. This type of noise can make it difficult to map real reflections at depth. Both Vertical and Horizontal Low Pass Filters are effective for removing high frequency noise. A Vertical Low Pass Filter will reject frequencies above an established threshold. When a non-zero value of Horizontal Low Pass Filter is used, low pass filtering will occur in the horizontal direction and reduce the “snow” noise and smooth the data. A number of scans on either side of the centre are averaged and the results placed in the centre scan.

Spatial Fast Fourier Transform (FFT) Filter: The spatial FFT filter, which is a two-dimensional frequency filter, takes place in the time-space domain. It is often called a frequency-wave number, or F-K, domain. This approach generates a two-dimensional matrix, the complex element of which represent the phase and amplitude of various spatial waves present in the radar data. It allows to develop a two-dimensional filter to attenuate the noise. Performing the inverse Fourier transformation of the product matrix from the transformed data and the filter yields a data with reduced noise. Technically, at this stage the frequency domain data is reconstructed back to the time domain. The advantage of F-K filtering over successive vertical and horizontal one-dimensional frequency filtering is that it enables a better distinction to be made between the signal and the noise. The signal and noise spectra may overlap in one-dimension, which makes their separation impossible, but this is less likely in the F-K domain.

Deconvolution: Multiples or “ringing” occur when the radar signal bounces back and forth between an object (such as a piece of metal or a layer of wet clay) and the antenna, causing repetitive reflection patterns throughout the data and obscuring information at lower depths. Multiple reflections may also be observed when mapping water bottom, bedrock, or voids. Deconvolution is the filtering method used to remove this type of noise. The earth behaves as a filter by removing high frequency information from the data. Deconvolution can also be used to restore the vertical resolution of the radar wave before it underwent this filtering process by compressing the reflected wavelets. Hence, in addition to removing unwanted multiples, deconvolution can be used to resolve closely spaced layers.

6.6 SHALLOW SUBSURFACE SECONDARY FAULTS

The data collected with the help of GPR survey was processed and the profiles then obtained are shown in the Fig. 6.5 and 6.6. Given that the GPR could record shallow subsurface discontinuity up to ~40 m depth at maximum in present GPR settings and selected terrain conditions, the discontinuity recorded at a couple of locations show both of the synthetic and antithetic nature of the secondary fault of EPF.

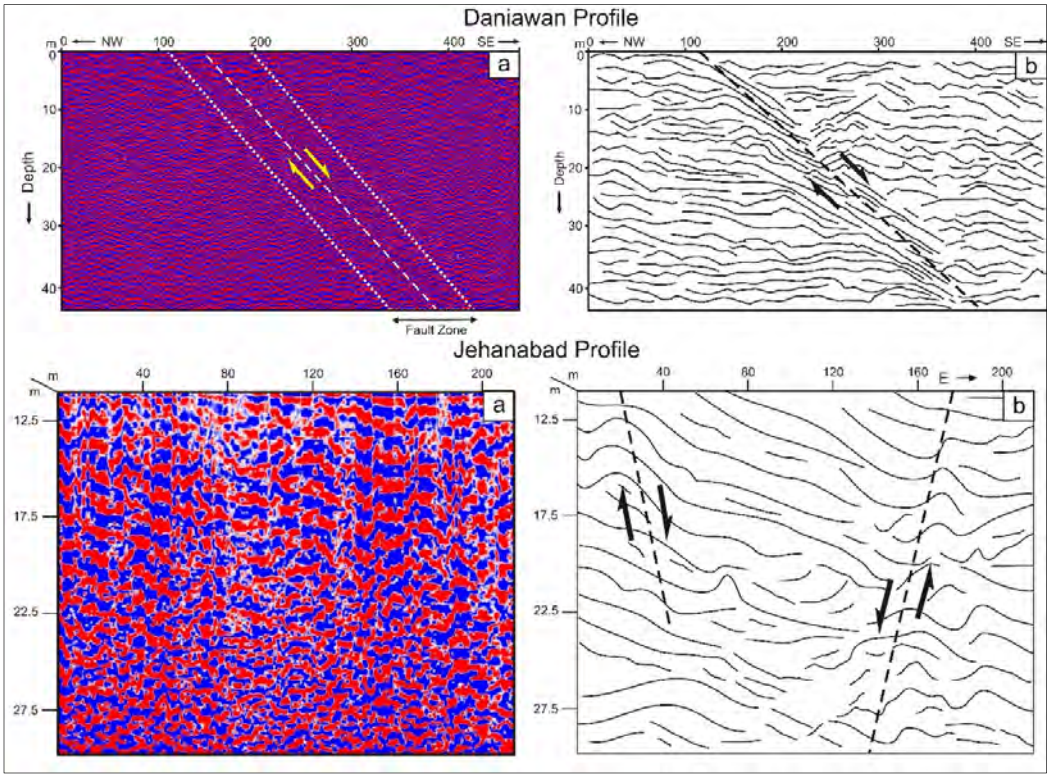

Figure 6.5 GPR profiles across the East Patna Fault show both antithetic and synthetic nature of secondary faults (a) Image of GPR profile obtained (b) Schematic diagram of the profile.

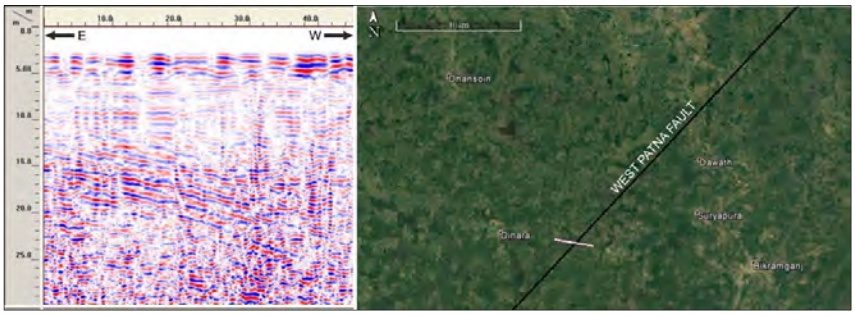

Figure 6.6 Ground Penetrating Radar (GPR) profile across West Patna Fault near Bikramganj. Figure on the left is a part of radargram showing the fault signatures. The right figure shows location of GPR survey path as white line (~3 km) across WPF (shown by black solid line). The base image is taken from Google Earth.

The Daniawan profile shows east dipping fault whereas the Jehanabad profile shows shallow faults dipping in both east as well as the west direction. The survey carried out across West Patna Fault near Dinara village in southern Bihar also shows soil layers dipping towards west. These subsurface deformations are related to the WPF and indicate its active nature. The model

by Gawthorpe and Leeder (2000) predicted this type of faults in such geological settings where the basement fault is overlain by thick sediment cover. The buried sediment layer deformations are highly susceptible to destruction in an active tectonic setting of unconsolidated sediment succession in short periods of geological time. Fluvial environment, or feeble tremors arising due to natural or artificial causes may provide enough force to remobilize the shallow subsurface sediments leading to attain uniformity in layers. Thus, the presence of shallow subsurface discontinuities in sediment layers indicates frequent reactivation of the fault.

Chapter 7

SUMMARY AND CONCLUSION

7.1 SUMMARY

The Sone megafan lies in the southern edge of the middle Ganga plain (MGP) in the Indo-Gangetic foreland basin. This oval shaped megafan covers an area of about 12000 km2 consisting of sediments derived from the Vindhyan highlands. Due to its proximity to the Indian craton, the sediment supply to the megafan is mainly controlled by tectonics and climate of the cratonic region, and subsequent modification by the tectonics and geomorphic processes of the Ganga plain. A major part of this megafan rests over the tectonic block bounded by two basement faults, i.e. the East Patna Fault (EPF) in the east and the West Patna Fault (WPF) in the west. Tectonic block tilting and sagging is a common process in the Ganga plain due to the influence of the Himalayan tectonics (Mohindra et al., 1992; Pati et al., 2011a). Block tilting causes rivers to migrate in the direction of tilt, leaving their paleo courses and flood plains. Thus, fluvio-geomorphic readjustment due to neotectonism and climatic fluctuations have modified the megafan in space and time.

Remote sensing images, field observations and OSL chronology record major three phases of fan-building process which left behind three generations of river plains and paleochannels progressively older towards the west (Fig. 7.1). This unidirectional channel migration over a large period of time is mainly triggered by block tilting due to the influence of the Himalayan tectonics. This caused major channel and flood plain abandonment on the megafan surface.

In the present study, the behaviour of the Sone River in the southern MGP has been studied together with the soil development, geophysical study and luminescence dating of the sediments to decipher the geomorphic and tectonic evolution of the Sone megafan during the Late Quaternary period. An integrated approach consisting of remote sensing and GIS study, fieldwork, sediment deformation, micromorphology study of soil, optically stimulated luminescence dating and ground penetrating radar study, was adopted to

understand recent geomorphic modifications that occurred in the southern MGP.

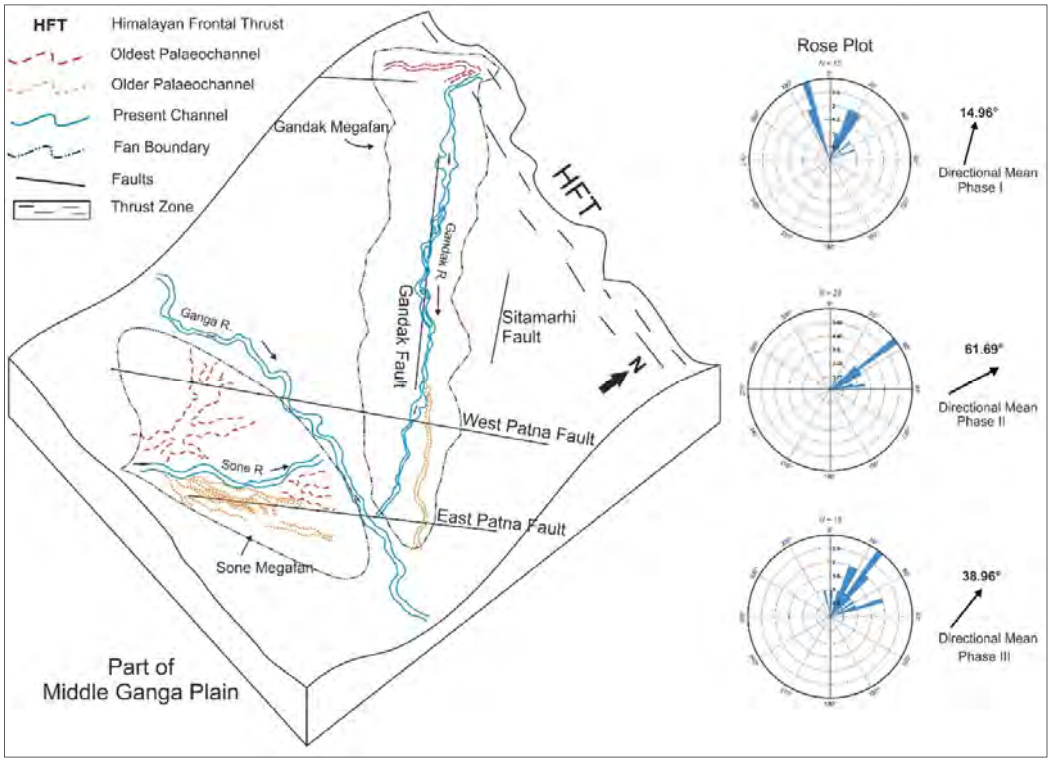

Figure 7.1 A 3-D representational model of middle Ganga plain showing major faults and three generations of Sone River channels in the study area. The rose plot of paleochannel direction shows NNE, ENE and NE direction of Sone during I, II and III phases, respectively. I-, II- and III-phase are oldest, older and present course of the river.

Distribution of paleochannels of the Sone River, recent drainage characteristics and natural ponds were examined in the abandoned plains of the Sone megafan with the help of remote sensing and GIS techniques. The results suggest an earlier inception of the megafan from the west towards east. Eastward shift of the Sone River implies subsidence of northeastern part of the tectonic block between WPF and EPF in relation to reactivation or movement along the EPF. This first phase of megafan development marks the Oldest Sone plain (OdSP) during (~22 to 14 Ka). However, other set of paleochannels and their chronological sequence of abandonment indicates an episode of westward migration of the river (~8 to 0.9 Ka). The river has stayed at its present course for at least last 400 years (Fig. 7.2). The fluvial environment is a dynamic river network system which constantly modifies the landscape and strives to balance the tectonic uplift by river erosion (Castelltort et al., 2012; Willett et al., 2014). The reverse shifting of river over a large time span could be attributed

to the uplift in the peripheral region causing an uplift of northeastern part of the block and as a result subsidence towards the southwest part. Thus, tilting and twisting of the tectonic block largely influenced the fluvial readjustment. Comparatively younger eastern plain is identified with two units, namely, Old Sone Plain (OSP) and Young Sone Plain (YSP). The YSP is distinguishable from OSP as a regime of most recent channel abandonment which appears as a roughly triangular zone of high moisture content in satellite images and possess several standing water bodies disconnected from the main channel.

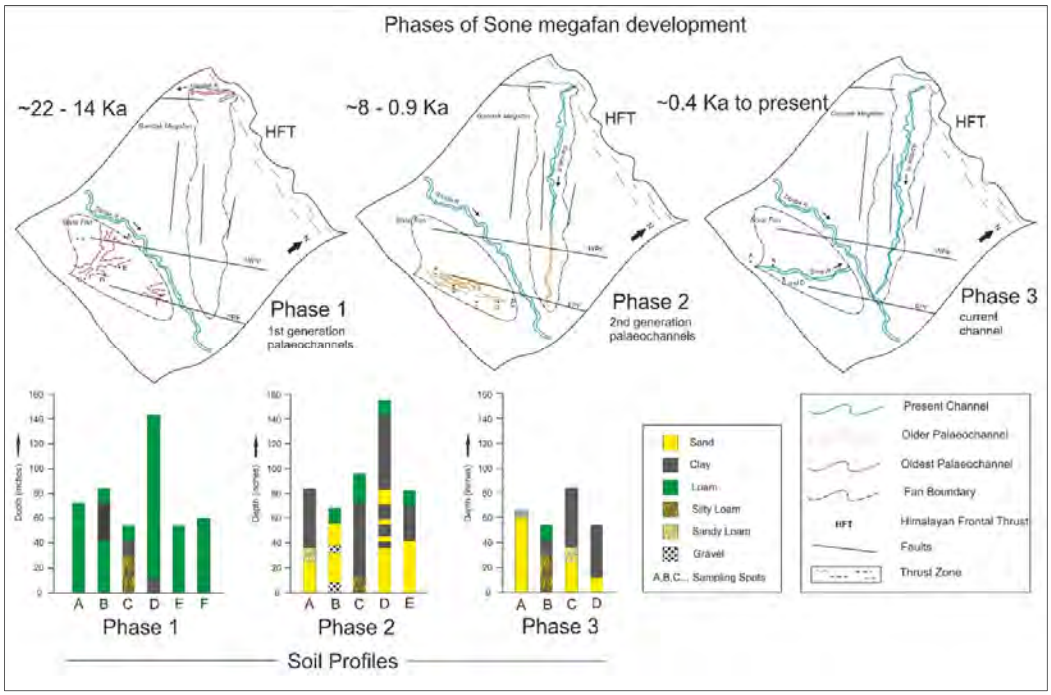

Figure 7.2 Different tilting direction causing distinct phases of Sone megafan evolution. Phase 1: development of oldest soils while eastward tilting. Phase 2: development of thick clay-sand alternating beds during westward tilting. Phase 3: deposition of coarse sand beds around current course of the Sone River during present stable period.

Soils of any area is an important indicator of degree of tectonic stability (Bhosle et al., 2008; Singh et al., 2006). The soil under constant exposure to moisture and organic matter tends to mature with time. Thus, the mature or well-developed soil and increased solum thickness (0.5 to 3 m) are associated with OdSP as compared to the eastern counterpart. Comparatively, areas with more recent sedimentation i.e. the younger plains (OSP and YSP) are observed with weakly developed pedo-features with solum thickness varying from 0.3 to 1.5 m. Due to gradual shift of the river, thick flood deposits are found capped on the active fluvial deposits. Similar features have been reported in the

Gandak megafan surface by Mohindra et al. (1992). The observations made in the field show a general thicker solum in OdSP as compared to that in OSP, whereas the YSP being closest to the present channel, is a domain of linear depressions i.e. most recent abandonment of Sone river, shows thick allogenic clay deposits. Thus, in relative chronological terms, the different geomorphic units of the Sone megafan are arranged as OdSP, OSP, YSP and AFP from oldest to youngest, respectively. Micromorphological study of soil samples from B-horizon of soil profiles in these plains show well to moderately developed pedo-features in OdSP and moderate to weak development of pedo-features in OSP.

Drainage anomaly on the megafan surface towards south of the Ganga River implies southward extension of EPF which was previously not reported. The reported anomaly is confined within a 20–30 km wide zone. Digital Elevation Models (DEMs) of the area also show high unevenness of the surface corresponding to the drainage anomaly zone. Surface elevation profiles extracted from the DEMs show relief break which is characteristic of buried faults in alluvial plains (Bhosle et al., 2009). Collectively, the results from remote sensing and GIS study helped to establish the augmentation of EPF towards south of the Ganga River and demarcate its fault zone. The topography in fluvial regimes is related to the tectonic uplift (Goren et al., 2014). The present study reveals 3 generations of paleochannels indicating at least 2 events of tectonic uplift in the adjacent craton area. This uplift has caused the movement along the basement faults and consequently the river responded to the change in surface gradient by shifting its channel laterally spreading the sediments in the plain to form the megafan.

Generally, in soft sediments such as in the Ganga plain, the basement faults grow towards the surface as deformation zones consisting of local structural discontinuities. These local discontinuities manifest into the sediment layers as secondary faults. The shallow subsurface faults, usually localized in a few kilometres wide zone, can be identified with the help of ground penetrating radar (GPR) survey across the fault zone. The present study has identified the near surface secondary faults of EPF and WPF in the radargrams.

The discontinuity recorded at a couple of locations show both synthetic and antithetic nature of the secondary faults of EPF. The Daniawan profile shows east dipping fault whereas the Jehanabad profile shows shallow faults dipping in both east as well as the west direction. The model by Gawthorpe and Leeder (2000) predicted this type of faults in such geological settings where the basement fault is overlain by thick sediment cover. These subsurface faults are created with the basement fault reactivation. At shallow depths, the sediment load is not enough to provide substantial strength to the soil, which is why such shallow structural discontinuities in alluvium are quite vulnerable to destruction in short period of time. Thus, the presence of shallow subsurface secondary faults in unconsolidated sediments of the study area suggests frequent activity along the faults.

The soft sediment deformation structures observed in riverine sediments from the study area were identified as seismites (Verma et al., 2017). These seismites formed due to liquefaction of sediments under stress of cyclic shear waves that originated from the strong earthquake and its close aftershocks. The seismites are in close proximity to EPF which is suggestive of either major earthquake from Himalayan Frontal Thrust (HFT) or moderate ($5 < M < 6.5$) earthquake on the EPF at least 0.6 Ka. It provides the evidence of recent fault reactivation and influence of Himalayan tectonics up to southernmost reaches of the MGP.

The inferences from remote sensing data, geomorphic and pedologic evidence and seismites have implications for a chronological model of the southern MGP. An older to younger temporal relationship between different geomorphic units of the Sone megafan has been established based on OSL chronology. The OSL ages obtained were found to be consistent with the relative chronological relationship established so far and fortified the speculations made regarding evolution of the megafan during Late Quaternary. OSL chronology reveals the megafan development begun ~22 Ka and eastward migration of Sone river consequently abandoned the OdSP ~14 Ka (end date). The second phase of river shifting is marked by eastern part of the Sone megafan i.e. OSP deposited at least ~8 Ka during westward channel

shifting. The YSP is the youngest unit which deposited between ~0.9 and 0.5 Ka while the river underwent frequent avulsions. The present course of the Sone River is possibly the most stable state where it is flowing since last 400 years. The sediments of active floodplain (AFP) of the Sone River were dated to be younger than 100 years and those from the floodplain of Ganga River show two events of recent southward encroachment into the megafan ~2.4 and 1.3 Ka.

The ground penetrating radar (GPR) can record only shallow subsurface discontinuity up to ~30–40 m depth at maximum. The discontinuity recorded at a couple of locations show both synthetic and antithetic nature of the secondary faults of EPF. The Daniawan profile shows east dipping fault whereas the Jehanabad profile shows shallow faults dipping in both east as well as the west direction. The model by Gawthorpe and Leeder (2000) predicted this type of faults in such geological settings where the basement fault is overlain by thick sediment cover. The area under survey consists of shallow cover of unconsolidated sediments that cannot preserve deformations in sediment strata for long periods of geological time. These subsurface faults are created with the basement fault reactivation. Thus, presence of seismites and secondary faults near EPF imply recent movement along the fault. The implication is also supported by the recent fluctuations in the Sone channel direction which are recorded as paleochannels in distal part of the Sone megafan (YSP).

The Gandak megafan lies towards north of the Ganga river in MGP. The sediment cover in northern plain is mostly derived from Himalayan erosion, which is significantly influenced by combined effect of climate and tectonic processes (Montgomery et al., 2001; Willett et al., 1993, 2006). It bears a close resemblance with the Sone megafan formed on its southern counterpart plain in terms of geomorphic, tectonic and pedological characteristics. The Gandak megafan developed by the migration of Gandak River in E–W direction in response to the active tectonic of the region. Fault controlled block tilting mechanism triggered by the adjacent Himalayan tectonics led to the evolution of the Gandak megafan. The western plain of the megafan revealing higher

solum thickness and well-developed soil is older as compared to the eastern Gandak plain which shows moderate to weakly developed soil (Pati et. al., 2008, 2011a, 2011b). The river migration towards the east and west direction occurred around 7 Ka and –Ka. The river migration has been correlated with the block tilting events. A similar tectonic configuration has also been observed in the Sone megafan. The tectonic block on which the Sone megafan rests, meets the Himalayan front at the Gandak depression, and the Himalayan system marks one of the highest rate of uplift in that region (Avouac et al., 2001; Bilham et al., 2001, 1997). Therefore, loading of thrust sheets at one end of the basement block promotes frequent uplift and subsidence of the tectonic blocks at the other end too. Therefore, the rivers on the tectonic block readjust themselves to accommodate this elevation and slope changes. Though the early inception of Sone megafan took place around Late Pleistocene, the Holocene framework of megafan evolution has largely been similar for both northern and southern plains of the middle Ganga plain. The involvement of same faults (WPF and EPF) in both megafans can be attributed to their comparable behaviour.

7.2 CONCLUSIONS

The following conclusions can be drawn from the present study:

1. Geomorphic domain, soil properties and OSL chronology demarcates four distinct geomorphic units on the Sone megafan surface.
2. The Late Quaternary witnessed at least two episodes of major block tilting events in the southern MGP.
3. The megafan building started at ~22 Ka leading to the development of the western part of the present megafan (OdSP) by eastward migration of Sone river – marks the first episode.
4. The second episode is marked by westward migration of the river which begun at least 8 Ka and the eastern plain (OSP) acquired the present form between ~8 to 0.9 Ka.
5. The downstream part of the river acquired different paleochannels during ~0.9 to 0.4 Ka in YSP where it has adjusted to the present stable course since 0.4 Ka.

6. This river shifting episodes have been correlated with basement fault reactivation and block tilting under the influence of the Himalayan tectonics and peripheral uplift.
7. Channel avulsion and flood plain abandonment is evidenced by gradually increasing degree of soil development and deposition of silt and clay (flood deposits) on the active channel deposits.
8. Basement fault activity has been mapped on the surface through drainage anomaly, seismites and GPR studies, which indicates the extension of the EPF to the south of the Ganga River.

BIBLIOGRAPHY

Agarwal, R.K., 1977. Structure and tectonics of Indo-Gangetic plains. Geophys. Case Hist. India. Assoc. Explor. Geophys. 1, 29–46.

Aitken, M.J., 1998. An Introduction to Optical Dating: The Dating of Quaternary Sediments by the Use of Photon-Stimulated Luminescence, 267 pp.

Alfaro, P., Gibert, L., Moretti, M., García-Tortosa, F.J., Sanz de Galdeano, C., Galindo-Zaldívar, J., López-Garrido, Á.C., 2010. The significance of giant seismites in the Plio-Pleistocene Baza palaeo-lake (S Spain). Terra Nov. 22, 172–179.

Allen, J.R.L., 1982. Sedimentary Structures: Their Character and Physical Basis Volume I, Developments in Sedimentology. Elsevier, Amsterdam.

Ambraseys, N.N., 1988. Engineering seismology: part II. Earthq. Eng. Struct. Dyn. 17, 51–105.

Ameen, S.M.M., Wilde, S.A., Kabir, M.Z., Akon, E., Chowdhury, K.R., Khan, M.S.H., 2007. Paleoproterozoic granitoids in the basement of Bangladesh: A piece of the Indian shield or an exotic fragment of the Gondwana jigsaw? Gondwana Res. 12, 380–387.

Amick, D., Gelinas, R., Maurath, G., Cannon, R., Moore, D., Billington, E., Kemppinen, H., 1990. Paleoliquefaction features along the Atlantic seaboard. Nuclear Regulatory Commission, Washington, DC (USA). Div. of Engineering; Ebasco Services, Inc., Greensboro, NC (USA).

Arrowsmith, J., Zielke, O., 2009. Tectonic geomorphology of the San Andreas Fault zone from high resolution topography: an example from the Cholame segment. Geomorphology 113, 70–81.

Atchley, S.C., Nordt, L.C., Dworkin, S.I., 2004. Eustatic control on alluvial sequence stratigraphy: a possible example from the Cretaceous-Tertiary transition of the Tornillo Basin, Big Bend National Park, West Texas, USA. J. Sediment. Res. 74, 391–404.

Audru, J.-C., Bano, M., Begg, J., Berryman, K., Henrys, S., Nivière, B., 2001. GPR investigations on active faults in urban areas: the Georisc-NZ project in Wellington, New Zealand. Comptes Rendus l'Académie des Sci. - Ser. IIA - Earth Planet. Sci. 333, 447–454.

Avouac, J.P., Bollinger, L., Lavé, J., Cattin, R., Flouzat, M., 2001. Le cycle sismique en Himalaya. Comptes Rendus l'Academie Sci. - Ser. IIa Sci. la Terre des Planetes 333, 513–529.

Azor, A., Keller, E.A., Yeats, R.S., 2002. Geomorphic indicators of active fold growth: South Mountain–Oak Ridge anticline, Ventura basin, southern California. Geol. Soc. Am. Bull. 114, 745–753.

Badura, J., Przybylski, B., 2005. Application of digital elevation models to geological and geomorphological studies–some examples. Prz. Geol. 53, 977–983.

Banghar, A., 1991. Mechanism Solution of Nepal-Bihar Eartbquake of August 20, 1988. Geol. Soc. India 37, 25–30.

Beck, R.A., Burbank, D.W., Sercombe, W.J., Riley, G.W., Barndt, J.K., Berry, J.R., Afzal, J., Khan, A.M., Jurgen, H., Metje, J., 1995. Stratigraphic evidence for an early collision between northwest India and Asia. Nature 373, 55.

Berra, F., Felletti, F., 2011. Syndepositional tectonics recorded by soft-sediment deformation and liquefaction structures (continental Lower Permian sediments, Southern Alps, Northern Italy): Stratigraphic significance. Sediment. Geol. 235, 249–263.

Bhatt, N., Bhonde, U.A., 2003. Quaternary fluvial sequences of south Saurashtra, western India. Curr. Sci. 1065–1071.

Bhatt, N., Patidar, A.K., Maurya, D.M., Chamyal, L.S., 2006. Delineation of three shallow subsurface faults using GPR in south Saurashtra, western India, in: 11th International Conference on GPR, Columbus, OH.

Bhosle, B., Parkash, B., Awasthi, a. K., Pati, P., 2009. Use of digital elevation models and drainage patterns for locating active faults in the Upper Gangetic Plain, India. Int. J. Remote Sens. 30, 673–691.

Bhosle, B., Parkash, B., Awasthi, A.K., Singh, S., Khan, M.S.H., 2008. Role of extensional tectonics and climatic changes in geomorphological, pedological and sedimentary evolution of the Western Gangetic Plain (Himalayan Foreland Basin), India. Himal. Geol. 29, 1–24.

Bilham, R., Gaur, V.K., Molnar, P., 2001. Himalayan Seismic Hazard. Science (80-.). 293, 1442–1444.

Bilham, R., Larson, K., Freymueller, J., 1997. GPS measurements of present-day convergence across the Nepal Himalaya. Nature.

Black, R.F., 1983. Pseudo-ice-wedge casts of Connecticut, northeastern United States. Quat. Res. 20, 74–89.

Bose, P.K., Mazumder, R., Sarkar, S., 1997. Tidal sandwaves and related storm deposits in the transgressive Protoproterozoic Chaibasa Formation, India. Precambrian Res. 84, 63–81.

Bristow, C., Jol, H. (Eds.), 2003. Ground penetrating radar in sediments, 211th ed, Geological Society of London (Special Publication). The Geolological Society, London.

Bullock, P., Fedoroff, N., Jongerius, A., Stoops, G., Tursina, T., 1985. Handbook for soil thin section description. Waine Research, U.K.

Burbank, D.W., Anderson, R.S. (Robert S., 2001. Tectonic geomorphology. Blackwell Science.

Burnett, A.W., Schumm, S.A., 1983. Alluvial-river response to neotectonic deformation in louisiana and Mississippi. Science (80-.). 222, 49–50.

Carter, D.P., Seed, H.B., 1988. Liquefaction potential of sand deposits under low levels of excitation. Univ. of California, Berkeley.

Castelltort, S., Goren, L., Willett, S.D., Champagnac, J.-D., Herman, F., Braun, J., 2012. River drainage patterns in the New Zealand Alps primarily controlled by plate tectonic strain. Nat. Geosci. 5, 744.

Chander, R., 1989. Southern limits of major earthquake ruptures along the Himalaya between longitudes 75 and 90 E. Tectonophysics 170, 115–123.

Cleveland, D.M., Atchley, S.C., Nordt, L.C., 2007. Continental sequence stratigraphy of the Upper Triassic (Norian–Rhaetian) Chinle strata, northern New Mexico, USA: allocyclic and autocyclic origins of paleosol-bearing alluvial successions. J. Sediment. Res. 77, 909–924.

Dasgupta, S., 1993. Tectono-geologic framework of the eastern Gangetic foredeep. Geol. Surv. India Spec. Publ. 31, 61–69.

Dasgupta, S., Mukhopadhyay, M., Nandy, D.R., 1987. Active transverse features in the central portion of the Himalaya. Tectonophysics 136, 255–264.

Davis, J.L., Annan, A.P., 1989. Ground-penetrating radar for high-resolution mapping of soil and rock stratigraphy. Geophys. Prospect. 37, 531–551.

Dewey, J.F., Bird, J.M., 1970. Mountain belts and the new global tectonics. J. Geophys. Res. 75, 2625–2647.

Dolphin, L.T., Beatty, W.B., Tanzi, J.D., 1978. Radar probing of Victorio Peak, New Mexico. Geophysics 43, 1441–1448.

Ékes, C., Friele, P., 2003. Sedimentary architecture and post-glacial evolution of Cheekye fan, southwestern British Columbia, Canada. Geol. Soc. London, Spec. Publ. 211, 87–98.

Fisher, S.C., Stewart, R.R., Jol, H.M., 1996. Ground Penetrating Radar (GPR) Data Enhancement Using Seismic Techniques. J. Environ. Eng. Geophys. 1, 89.

Frodella, W., Ciampalini, A., Gigli, G., Lombardi, L., Raspini, F., Nocentini, M., Scardigli, C., Casagli, N., 2016. Synergic use of satellite and ground based

remote sensing methods for monitoring the San Leo rock cliff (Northern Italy). Geomorphology 264, 80–94.

Galli, P., 2000. New empirical relationships between magnitude and distance for liquefaction. Tectonophysics 324, 169–187.

Galli, P., Bosi, V., 2003. Catastrophic 1638 earthquakes in Calabria (southern Italy): New insights from paleoseismological investigation. J. Geophys. Res. Solid Earth 108.

Gawthorpe, R.L., Collier, R.E.L., Alexander, J., Bridge, J.S., Leeder, M.R., 1993. Ground penetrating radar: application to sandbody geometry and heterogeneity studies. Geol. Soc. London, Spec. Publ. 73, 421–432.

Gawthorpe, R.L., Leeder, M.R., 2000. Tectono-sedimentary evolution of active extensional basins. Basin Res. 12, 195–218.

Geddes, A., 1960. The Alluvial Morphology of the Indo-Gangetic Plain : Its Mapping and Geographical Significance. Trans. Pap. (Institute Br. Geogr. 28, 253–276.

Gibling, M.., Tandon, S.K., Sinha, R., Jain, M., 2005. Discontinuity-Bounded Alluvial Sequences of the Southern Gangetic Plains, India: Aggradation and Degradation in Response to Monsoonal Strength. J. Sediment. Res. 75, 369–385.

Gibling, M.R., Sinha, R., Roy, N.G., Tandon, S.K., Jain, M., 2008. Quaternary fluvial and eolian deposits on the Belan river, India: paleoclimatic setting of Paleolithic to Neolithic archeological sites over the past 85,000 years. Quat. Sci. Rev. 27, 391–410.

Gilvear, D., Bryant, R., 2016. Analysis of remotely sensed data for fluvial geomorphology and river science. Tools Fluv. Geomorphol. 103–132.

Goren, L., Fox, M., Willett, S.D., 2014. Tectonics from fluvial topography using formal linear inversion: Theory and applications to the Inyo Mountains, California. J. Geophys. Res. Earth Surf. 119, 1651–1681.

GSI, 2000. Eastern Nepal Himalaya and Indo-Gangetic Plains of Bihar, in: Narula, P.L., Acharyya, S.K., Banerjee, J. (Ed.), Seismotectonics Atlas of India and Its Environs. Geological Survey of India, pp. 26–27.

Guiraud, M., Plaziat, J.-C., 1993. Seismites in the fluviatile Bima sandstones: identification of paleoseisms and discussion of their magnitudes in a Cretaceous synsedimentary strike-slip basin (Upper Benue, Nigeria). Tectonophysics 225, 493–522.

Hack, J., 1973. Stream-profile analysis and stream-gradient index. J. Res. US Geol. Surv. 1, 421–429.

Jackson, J., Leeder, M., 1994. Drainage systems and the development of normal faults: an example from Pleasant Valley, Nevada. J. Struct. Geol. 16, 1041–1059.

Jain, V., Sinha, R., 2005. Response of active tectonics on the alluvial Baghmati River, Himalayan foreland basin, eastern India. Geomorphology 70, 339–356.

Jaiswal, M., Chen, Y., Kale, V., Achyuthan, H., 2009. Residual luminescence in quartz from slack water deposits in Kaveri Basin, South India: a single aliquot approach. Geochronometria 33, 1–8.

Jaiswal, M., Srivastava, P., Tripathi, J., Islam, R., 2008. Feasibility of the SAR technique on Quartz sand of terraces of NW Himalaya: a case study from Devprayag. Geochronometria 31, 45–52.

Jaiswal, M.K., Bhat, M.I., Bali, B.S., Ahmad, S., Chen, Y.G., 2009. Luminescence characteristics of quartz and feldspar from tectonically uplifted terraces in Kashmir Basin, Jammu and Kashmir, India. Radiat. Meas. 44, 523–528.

Jana, A., Maiti, S., Biswas, A., 2017. Appraisal of long-term shoreline oscillations from a part of coastal zones of Sundarban delta, Eastern India: a study based on geospatial technology. Spat. Inf. Res. 25, 713–723.

Jana, A., Maiti, S., Biswas, A., 2016. Seasonal change monitoring and mapping of coastal vegetation types along Midnapur-Balasore Coast, Bay of Bengal using multi-temporal landsat data. Model. Earth Syst. Environ. 2, 7.

Jol, H.M., Smith, D.G., 1991. Ground penetrating radar of northern lacustrine deltas. Can. J. Earth Sci. 28, 1939–1947.

Jol, H.M., Smith, D.G., Meyers, R.A., 1996. Digital ground penetrating radar (GPR): A new geophysical tool for coastal barrier research (Examples from the Atlantic, Gulf and Pacific coasts, USA). J. Coast. Res. 960–968.

Jongerius, A., Heintzberger, G., 1975. Methods in soil micromorphology, a technique for the preparation of large thin sections, Soil Survey Papers. Netherlands Soil Survey Institute, Wageningen, Netherlands.

Kale, V.S., Singhvi, A.K., Mishra, P.K., Banerjee, D., 2000. Sedimentary records and luminescence chronology of Late Holocene palaeofloods in the Luni River, Thar Desert, northwest India. Catena 40, 337–358.

Kanoua, W., Merkel, B.J., 2016. Modification of a digital elevation model (DEM) in a flat topographic area with respect to manmade features. Geosci. J. 20, 101–115.

Karunakaran, C., Ranga Rao, A., 1979. Status of exploration for hydrocarbons in the Himalayan region–contribution to stratigraphy and structure. Geol. Surv. India Misc. Publ 41, 1–66.

Keller, E.A., Pinter, N., 1996. Active tectonics : earthquakes, uplift, and landscape. Prentice Hall.

Khan, M.S.H., Haque, M.M., Pati, P., Chowdhury, K.R., Biswas, S., 2015. OSL derived uplift rate of Dakhin Nhila anticline along the southeastern coast of the Bay of Bengal, Bangladesh. Himal. Geol. 36, 143–152.

Khan, M.S.H., Parkash, B., Kumar, S., 2005. Soil–landform development of a part of the fold belt along the eastern coast of Bangladesh. Geomorphology 71, 310–327.

Knight, R., Endres, A., 1990. A new concept in modeling the dielectric response of sandstones: Defining a wetted rock and bulk water system. Geophysics 55, 586–594.

Kraus, M.J., 1987. Integration of channel and floodplain suites, II. Vertical relations of alluvial paleosols. J. Sediment. Res. 57.

Kraus, M.J., Gwinn, B., 1997. Facies and facies architecture of paleogene floodplain deposits, Willwood formation, Bighorn Basin, Wyoming, USA. Sediment. Geol. 114, 33–54.

Kumar, P.S.J., Huan, T.L., Rossi, R.K., Yuan, Y., Li, X., 2018. Color fusion of remote sensing images for imparting fluvial geomorphological features of river Yamuna and Ganga over Doon valley. J. Geomatics 12, 270–286.

Kumar, S., Parkash, B., Manchanda, M.L., Singhvi, A.K., 1996. Holocene landform and soil evolution of the western Gangetic Plains: implications of neotectonics and climate. J. Geol 88, 100–108.

Kuribayashi, E., Tatsuoka, F., 1975. Brief review of liquefaction during earthquakes in Japan. Soils Found.

Lee, S., Pradhan, B., 2007. Landslide hazard mapping at Selangor, Malaysia using frequency ratio and logistic regression models. Landslides 4, 33–41.

Leeder, M.R., 1982. Soft sediment deformation structures, in: Sedimentology. Springer, pp. 111–116.

Lowe, D., LoPiccolo, R., 1974. The characteristics and origins of dish and pillar structures. J. Sediment. Res.

Lowe, D.R., 1975. Water escape structures in coarse-grained sediments. Sedimentology 22, 157–204.

Lyon-Caen, H., Molnar, P., 1985. Gravity anomalies, flexure of the Indian plate, and the structure, support and evolution of the Himalaya and Ganga Basin. Tectonics 4, 513–538.

Maiti, S., 2013. Interpretation of coastal morphodynamics of Subarnarekha estuary using integrated cartographic and field techniques. Curr. Sci. 1709–1714.

Maiti, S., Bhattacharya, A.K., 2011. A three-unit-based approach in coastal-change studies using Landsat images. Int. J. Remote Sens. 32, 209–229.

Maiti, S., Bhattacharya, A.K., 2009. Shoreline change analysis and its application to prediction: a remote sensing and statistics based approach. Mar. Geol. 257, 11–23.

Martinez, A., Byrnes, A.P., 2001. Modeling dielectric-constant values of geologic materials: An aid to ground-penetrating radar data collection and interpretation. Kansas Geological Survey, University of Kansas Lawrence, KS, USA.

Maurya, D.M., Patidar, A.K., Mulchandani, N., Goyal, B., Thakkar, M.G., Bhandari, S., Vaid, S.I., Bhatt, N.P., Chamyal, L.S., 2005. Need for initiating ground penetrating radar studies along active faults in India: An example from Kachchh. Curr. Sci. 88, 231–240.

McCarthy, P.J., Martini, I.P., Leckie, D.A., 1997. Anatomy and evolution of a Lower Cretaceous alluvial plain: sedimentology and palaeosols in the upper Blairmore Group, south-western Alberta, Canada. Sedimentology 44, 197–220.

Mccarthy, P.J., Plint, A.G., Mccarthy, P.J., Plint, A.G., 1998. Recognition of interfluve sequence boundaries : Integrating paleopedology and sequence stratigraphy 387–390.

Mellett, J.S., 1995. Ground penetrating radar applications in engineering, environmental management, and geology. J. Appl. Geophys. 33, 157–166.

Merritts, D., Vincent, K., 1989. Geomorphic response of coastal streams to low, intermediate, and high rates of uplift, Medocino triple junction region, northern California. Geol. Soc. Am.

Miall, A.D., 1991. Stratigraphic sequences and their chronostratigraphic correlation. J. Sediment. Res. 61.

Miall, A.D., 1981. Sedimentation and tectonics in alluvial basins. Geological Association of Canada, Department of Earth Sciences, University of Waterloo.

Miall, A.D., 1978. Fluvial sedimentology. Stacs Data Service Limited.

Miedema, R., Pape, T., Van der Waal, G.J., 1974. A method to impregnate wet soil samples, producing high-quality thin sections. Netherlands J. Agric. Sci. 22, 37–39.

Mohindra, R., Parkash, B., Prasad, J., 1992. Historical Geomorphology and Pedology of the Gandak Megafan, Middle Ganga Plains, India. Earth Surf. Process. Landforms 17, 643–662.

Montenat, C., Barrier, P., Ott dEstevou, P., Hibsch, C., 2007. Seismites: An attempt at critical analysis and classification. Sediment. Geol. 196, 5–30.

Montgomery, D.R., Balco, G., Willett, S.D., 2001. Climate, tectonics, and the morphology of the Andes. Geology 29, 579–582.

Moretti, M., Alfaro, P., Caselles, O., Canas, J.A., 1999. Modelling seismites with a digital shaking table. Tectonophysics 304, 369–383.

Moretti, M., Sabato, L., 2007. Recognition of trigger mechanisms for soft-sediment deformation in the Pleistocene lacustrine deposits of the Sant'Arcangelo Basin (Southern Italy): Seismic shock vs. overloading. Sediment. Geol. 196, 31–45.

Moro, M., Amicucci, L., Cinti, F.R., Doumaz, F., Montone, P., Pierdominici, S., Saroli, M., Stramondo, S., Di Fiore, B., 2007. Surface evidence of active tectonics along the Pergola-Melandro fault: A critical issue for the seismogenic potential of the southern Apennines, Italy. J. Geodyn. 44, 19–32.

Mukerji, A.B., 1963. Alluvial morphology of the upper Ganga-Yamuna doab.

Deccan Geogr. 2, 1–36.

Mukherjee, S., Joshi, P.K., Mukherjee, S., Ghosh, A., Garg, R.D., Mukhopadhyay, A., 2013. Evaluation of vertical accuracy of open source Digital Elevation Model (DEM). Int. J. Appl. Earth Obs. Geoinf. 21, 205–217.

Murray, A.S., Wintle, A.G., 2000. Luminescence dating of quartz using an improved single-aliquot regenerative-dose protocol. Radiat. Meas. 32, 57–73.

Neal, A., 2004. Ground-penetrating radar and its use in sedimentology: Principles, problems and progress. Earth-Science Rev. 66, 261–330.

Nikolakopoulos, K.G., Kamaratakis, E.K., Chrysoulakis, N., 2006. SRTM vs ASTER elevation products. Comparison for two regions in Crete, Greece. Int. J. Remote Sens. 27, 4819–4838.

Obermeier, S.F., 1996a. Using liquefaction-induced features for paleoseismic analysis. Int. Geophys. 62, 331–396.

Obermeier, S.F., 1996b. Use of liquefaction-induced features for paleoseismic analysis—an overview of how seismic liquefaction features can be distinguished from other features and how their regional distribution and properties of source sediment can be used to infer the locatio. Eng. Geol. 44, 1–76.

Ouchi, S., 1985. Response of alluvial rivers to slow active tectonic movement. Geol. Soc. Am. Bull.

Owen, G., 2003. Load structures: gravity-driven sediment mobilization in the shallow subsurface. Geol. Soc. London, Spec. Publ. 216, 21–34.

Owen, G., 1996. Experimental soft-sediment deformation: structures formed by the liquefaction of unconsolidated sands and some ancient examples. Sedimentology 43, 279–293.

Owen, G., 1995. Soft-sediment deformation in upper Proterozoic Torridonian

sandstones (Applecross Formation) at Torridon, northwest Scotland. J. Sediment. Res. 65.

Owen, G., 1987. Deformation processes in unconsolidated sands. Geol. Soc. London, Spec. Publ. 29, 11–24.

Owen, G., Moretti, M., 2011. Identifying triggers for liquefaction-induced soft-sediment deformation in sands. Sediment. Geol. 235, 141–147.

Pal, D.K., Bhattacharyya, T., Sinha, R., Srivastava, P., Dasgupta, A.S., Chandran, P., Ray, S.K., Nimje, A., 2012. Clay minerals record from Late Quaternary drill cores of the Ganga Plains and their implications for provenance and climate change in the Himalayan Foreland. Palaeogeogr. Palaeoclimatol. Palaeoecol. 356, 27–37.

Papadopoulos, G. a, Lefkopoulos, G., 1993. Magnitude-Distance Relations for Liquefaction in Soil from Earthquakes. Bull. Seismol. Soc. Am. 83, 925–938.

Parkash, B., Kumar, S., Rao, M.S., Giri, S.C., Kumar, C.S., Gupta, S., Srivastava, P., 2000. Holocene tectonic movements and stress field in the western Gangetic plains. Curr. Sci. 79, 438–449.

Parkash, B., Sharma, R.P., Roy, A.K., 1980. The Siwalik Group (molasse)—sediments shed by collision of continental plates. Sediment. Geol. 25, 127–159.

Pati, J.K., Lal, J., Prakash, K., Bhusan, R., 2008. Spatio-temporal shift of western bank of the Ganga river, Allahabad city and its implications. J. Indian Soc. Remote Sens. 36, 289–297.

Pati, J.K., Malviya, V.P., Prakash, K., 2006. Basement reactivation and its relation to Neotectonic activity in and around Allahabad, Ganga plain. J. Indian Soc. Remote Sens. 34, 47.

Pati, P., Parkash, B., Awasthi, A.K., Acharya, V., 2011a. Holocene tectono-geomorphic evolution of parts of the Upper and Middle Gangetic plains,

India. Geomorphology 128, 148–170.

Pati, P., Parkash, B., Awasthi, A.K., Acharya, V., Singh, S., 2011b. Concealed thrusts in the Middle Gangetic plain, India - A ground penetrating radar study proves the truth against the geomorphic features supporting normal faulting. J. Asian Earth Sci. 40, 315–325.

Pati, P., Parkash, B., Awasthi, A.K., Jakhmola, R.P., 2012. Spatial and temporal distribution of inland fans/terminal fans between the Ghaghara and Kosi rivers indicate eastward shift of neotectonic activities along the Himalayan front. A study from parts of the upper and middle Gangetic plains, India. Earth-Science Rev. 115, 201–216.

Pati, P., Pradhan, R.M., Dash, C., Parkash, B., Awasthi, A.K., 2015. Terminal fans and the Ganga plain tectonism: A study of neotectonism and segmentation episodes of the Indo-Gangetic foreland basin, India. Earth-Science Rev. 148, 134–149.

Pazzaglia, F.J., 2013. Fluvial Terraces, in: Treatise on Geomorphology. pp. 379–412.

Piégay, H., Kondolf, G.M., Minear, J.T., Vaudor, L., 2015. Trends in publications in fluvial geomorphology over two decades: A truly new era in the discipline owing to recent technological revolution? Geomorphology 248, 489–500.

Platt, N.H., Keller, B., 1992. Distal alluvial deposits in a foreland basin setting—the Lower Freshwater Miocene), Switzerland: sedimentology, architecture and palaeosols. Sedimentology 39, 545–565.

Pradhan, B., 2013. A comparative study on the predictive ability of the decision tree, support vector machine and neuro-fuzzy models in landslide susceptibility mapping using GIS. Comput. Geosci. 51, 350–365.

Pradhan, B., 2010. Remote sensing and GIS-based landslide hazard analysis and cross-validation using multivariate logistic regression model on three test areas in Malaysia. Adv. Sp. Res. 45, 1244–1256.

Pradhan, B., Lee, S., 2010. Regional landslide susceptibility analysis using back-propagation neural network model at Cameron Highland, Malaysia. Landslides 7, 13–30.

Prakash, K., Mohanty, T., Pati, J.K., Singh, S., Chaubey, K., 2017. Morphotectonics of the Jamini River basin, Bundelkhand Craton, Central India; using remote sensing and GIS technique. Appl. Water Sci. 7, 3767–3782.

Prakash, O., Sinha, A.P., Verma, N.P., Reddy, B.S.S., 1990. Quaternary geological and geomorphologival mapping of the Ganga–Sone alluvial belt in Aurangabad, Bhojpur, Jehanabad, Patna and Rohtas districts, Bihar. Rec. Geol. Surv. India 123, 8.

Prescott, J.R., Hutton, J.T., 1994. Cosmic ray contributions to dose rates for luminescence and ESR dating: large depths and long-term time variations. Radiat. Meas. 23, 497–500.

Prizomwala, S.P., Das, A., Chauhan, G., Solanki, T., Basavaiah, N., Bhatt, N., Thakkar, M.G., Rastogi, B.K., 2016. Late Pleistocene–Holocene uplift driven terrace formation and climate-tectonic interplay from a seismically active intraplate setting: An example from Kachchh, Western India. J. Asian Earth Sci. 124, 55–67.

Rajendran, C.P., John, B., Rajendran, K., Sanwal, J., 2016. Liquefaction record of the great 1934 earthquake predecessors from the north Bihar alluvial plains of India. J. Seismol. 1–13.

Rao, M.S., Bisaria, B.K., Singhvi, A.K., 1997. A feasibility study towards absolute dating of Indo-Gangetic alluvium. Curr. Sci. 72.

Rao, R.M.B., 1973. The Subsurface Geology of the Indo-Gangetic Plains. Geol. Soc. India; Vol. 14, Issue 3, Sept. 1973 14, 217–242.

Reynolds, J.M., 1997. An introduction to applied and environmental geophysics. John Wiley & Sons, New York.

Rodríguez-López, J.P., Liesa, C.L., Meléndez, N., Soria, A.R., 2007. Normal fault development in a sedimentary succession with multiple detachment levels: the Lower Cretaceous Oliete sub-basin, Eastern Spain. Basin Res. 19, 409–435.

Rodríguez-Pascua, M.A., Calvo, J.P., De Vicente, G., Gómez-Gras, D., 2000. Soft-sediment deformation structures interpreted as seismites in lacustrine sediments of the Prebetic Zone, SE Spain, and their potential use as indicators of earthquake magnitudes during the Late Miocene. Sediment. Geol. 135, 117–135.

Rossetti, D.D.F.D., 1999. Soft-sediment deformation structures in late Albian to Cenomanian deposits, São Luís Basin, northern Brazil: evidence for palaeoseismicity. Sedimentology 46, 1065–1081.

Russ, D., 1982. Style and significance of surface deformation in the vicinity of New Madrid, Missouri, in: Mckeown, F.A., Pakiser, L.C. (Ed.), Investigations of the New Madrid, Missouri, Earthquake Region. US Geological Surveys, pp. 95–114.

Sahu, S., Raju, N.J., Saha, D., 2010. Active tectonics and geomorphology in the Sone-Ganga alluvial tract in mid-Ganga Basin, India. Quat. Int. 227, 116–126.

Sahu, S., Saha, D., 2014. Geomorphologic, Stratigraphic and sedimentologic evidences of tectonic activity in sone–ganga alluvial tract in middle ganga plain, India. J. Earth Syst. Sci. 123, 1335–1347.

Sahu, S., Saha, D., Dayal, S., 2015. Sone megafan: A non-Himalayan megafan of craton origin on the southern margin of the middle Ganga Basin, India. Geomorphology 250, 349–369.

Sastri, V. V., Bhandari, L.L., Raju, T.R., Datta, A.K., Raju, A.T.R., Datta, A.K., 1971. Tectonic framework and subsurface stratigraphy of the Ganga Basin. J. Geol. Soc. India 12, 222–233.

Saucier, R.T., 1989. Evidence for episodic sand-blow activity during the 1811-

1812 New Madrid (Missouri) earthquake series. Geology 17, 103–106.

Sauret, B., Bousquet, J.C., 1984. ‘Manifestations d’instabilite du sol dans la zone epicentrale du seisme de Messine de 1908 le role de la liquefaction,’’. Mouvements de terrains 83, 63–74.

Schumm, S.A., Khan, H.R., 1972. Experimental Study of Channel Patterns. GSA Bull. 83, 1755–1770.

Seeber, L., Armbruster, J.G., 1981. Great detachment earthquakes along the Himalayan Arc and long-term forecasting. Earthq. Predict. 259–277.

Seeber, L., Gornitz, V., 1983. River profiles along the Himalayan arc as indicators of active tectonics. Tectonophysics 92, 335–337, 341–367.

Seed, H., 1979. Soil liquefaction and cyclic mobility evaluation for level ground during earthquakes. J. Geotech. Eng. Div. 105, 201–255.

Seilacher, A., 1984. Sedimentary structures tentatively attributed to seismic events. Mar. Geol. 55, 1–12.

Seilacher, A., 1969. Fault-graded beds interpreted as seismites. Sedimentology 13, 155–159.

Sengupta, S.N., 1996. The Vindhyan under the north Indian plains. Mem. Soc. India 257–266.

Shanley, K.W., McCabe, P.J., 1994. Perspectives on the sequence stratigraphy of continental strata. Am. Assoc. Pet. Geol. Bull. 78, 544–568.

Sharma, K., Bhatt, N., Shukla, A.D., Cheong, D.-K., Singhvi, A.K., 2017. Optical dating of late Quaternary carbonate sequences of Saurashtra, western India. Quat. Res. 87, 133–150.

Shukla, S.B., Chowksey, V.M., Prizomwala, S.P., Ukey, V.M., Bhatt, N.P., Maurya, D.M., 2013. Internal sedimentary architecture and coastal dynamics as revealed by ground penetrating radar, Kachchh coast, western India. Acta Geophys. 61, 1196–1210.

Singh, A.K., Jaiswal, M.K., Pattanaik, J.K., Dev, M., 2016. Luminescence chronology of alluvial fan in North Bengal, India: Implications to tectonics and climate. Geochronometria 43, 102–112.

Singh, A.K., Pattanaik, J.K., Jaiswal, M.K., 2017. Late Quaternary evolution of Tista River terraces in Darjeeling-Sikkim-Tibet wedge: Implications to climate and tectonics. Quat. Int. 443, 132–142.

Singh, D.S., Awasthi, A., 2011a. Implication of Drainage Basin Parameters of Chhoti Gandak River, Ganga Plain, India. J. Geol. Soc. India 78, 370.

Singh, D.S., Awasthi, A., 2011b. Natural hazards in the Ghaghara River area, Ganga Plain, India. Nat. Hazards 57, 213–225.

Singh, D.S., Awasthi, A., Bhardwaj, V., 2009. Control of tectonics and climate on Chhoti Gandak river basin, East Ganga Plain, India. Himalyan Geol. 30, 147–154.

Singh, D.S., Gupta, A.K., Sangode, S.J., Clemens, S.C., Prakasam, M., Srivastava, P., Prajapati, S.K., 2015. Multiproxy record of monsoon variability from the Ganga Plain during 400–1200 AD. Quat. Int. 371, 157–163.

Singh, D.S., Singh, I.B., 2005. Facies architecture of the Gandak megafan, Ganga plain, India. Spec. Publ. Palaeontol. Soc. India 2, 125–140.

Singh, H., Parkash, B., Gohain, K., 1993. Facies analysis of the Kosi megafan deposits. Sediment. Geol. 85, 87–113.

Singh, I.B., 1996. Geological Evolution of Ganga Plain - An Overview. J. Palaeontol. Soc. India 41, 99–137.

Singh, I.B., Rajagopalan, G., Agarwal, K.K., Srivastava, P., Sharma, M., Sharma, S., 1997. Evidence of Middle to Late Holocene neotectonic activity in the Ganga Plain. Curr. Sci. 73, 1114–1117.

Singh, S., Jain, A.K., 2007. Liquefaction and fluidization of lacustrine deposits from Lahaul-Spiti and Ladakh Himalaya: Geological evidences of

paleoseismicity along active fault zone. Sediment. Geol. 196, 47–57.

Singh, S., Parkash, B., Rao, M.S., Arora, M., Bhosle, B., 2006. Geomorphology, pedology and sedimentology of the Deoha/Ganga-Ghaghara Interfluve, Upper Gangetic Plains (Himalayan Foreland Basin) - Extensional tectonic implications. Catena 67, 183–203.

Sinha, R., Ahmad, J., Gaurav, K., Morin, G., 2014. Shallow subsurface stratigraphy and alluvial architecture of the Kosi and Gandak megafans in the Himalayan foreland basin, India. Sediment. Geol. 301, 133–149.

Sinha, R., Friend, P.F., 1994. River systems and their sediment flux , Indo-Gangetic plains , Northern Bihar , India. Sedimentology 825–845.

Sinha, R., Ghosh, S., 2012. Understanding dynamics of large rivers aided by satellite remote sensing: a case study from Lower Ganga plains, India. Geocarto Int. 27, 207–219.

Sinha, R., Gibling, M., Jain, V., Tandon, S., 2005a. Sedimentology and avulsion patterns of the anabranching Baghmati River in the Himalayan foreland basin, India. Spec. Publs int. Ass. Sediment. 35, 181–196.

Sinha, R., Kettanah, Y., Gibling, M.R., Tandon, S.K., Jain, M., Bhattacharjee, P.S., Dasgupta, A.S., Ghazanfari, P., 2009. Craton-derived alluvium as a major sediment source in the Himalayan Foreland Basin of India. Geol. Soc. Am. Bull. 121, 1596–1610.

Sinha, R., Tandon, S.K., Gibling, M.R., 2010. Shallow sub-surface stratigraphy of the Ganga basin, Himalayan foreland: Present status and future perspectives. Quat. Int. 227, 81–86.

Sinha, R., Tandon, S.K.K., Gibling, M.. R., Bhattacharjee, P.. S., Dasgupta, A.. S., 2005b. Late Quaternary geology and alluvial stratigraphy of the Ganga basin. Himal. Geol. 26, 223–240.

Smith, B., Sandwell, D., 2003. Accuracy and resolution of shuttle radar topography mission data. Geophys. Res. Lett. 30.

Srivastava, P., 2001. Paleoclimatic implications of pedogenic carbonates in Holocene soils of the Gangetic Plains, India. Palaeogeogr. Palaeoclimatol. Palaeoecol. 172, 207–222.

Srivastava, P., Parkash, B., Sehgal, J.L., Kumar, S., 1994. Role of neotectonics and climate in development of the Holocene geomorphology and soils of the Gangetic Plains between the Ramganga and Rapti rivers. Sediment. Geol. 94, 129–151.

Srivastava, P., Rajak, M.K., Sinha, R., Pal, D.K., Bhattacharyya, T., 2017. A high-resolution micromorphological record of the Late Quaternary paleosols from Ganga – Yamuna interfluve ... Quat. Int. 227, 127–142.

Srivastava, P., Rajak, M.K., Sinha, R., Pal, D.K., Bhattacharyya, T., 2010. A high-resolution micromorphological record of the Late Quaternary paleosols from Ganga–Yamuna interfluve: Stratigraphic and paleoclimatic implications. Quat. Int. 227, 127–142.

Srivastava, P., Sharma, M., Singhvi, A.K., 2003. Luminescence chronology of incision and channel pattern changes in the River Ganga, India. Geomorphology 51, 259–268.

Srivastava, P., Shukla, U.K., Mishra, P., Sharma, M., Sharma, S., Singh, I.B., Singhvi, A.K., 2000. Luminescence chronology and facies development of Bhur sands in the interfluve region of Central Ganga Plain, India. Curr. Sci. 498–503.

Thomas, J. V, Parkash, B., Mohindra, R., 2002. Lithofacies and palaeosol analysis of the Middle and Upper Siwalik Groups (Plio – Pleistocene), Haripur-Kolar section , Himachal Pradesh , India 150, 343–366.

Thompson, C., McMechan, G., Szerbiak, R., Gaynor, N., 1995. Three-dimensional GPR imaging of complex stratigraphy within the Ferron sandstone, Castle Valley, Utah, in: Symposium on the Application Og Geophysics to Engineering and Environmental Problems. pp. 435–443.

Thorson, R.M., Clayton, W.S., Seeber, L., 1986. Geologic evidence for a large

prehistoric earthquake in eastern Connecticut (USA). Geology 14, 463–467.

Tinsley, J.C., Youd, T.L., Perkins, D.M., Chen, A.T.F., 1985. Evaluating liquefaction potential. Eval. Earthq. Hazards Los Angeles Reg. Earth-Science Perspect. ed. JI Ziony. US Geol. Surv. Prof. Pap. 1360.

Valdiya, K.S., 1976. Himalayan transverse faults and folds and their parallelism with subsurface structures of North Indian plains. Tectonophysics 32, 353–386.

Valdiya, K.S., Sanwal, J., 2017. Ganga–Brahmaputra Plains, in: Developments in Earth Surface Processes. Elsevier, pp. 151–184.

Verma, A.K., Pati, P., Sharma, V., 2017. Soft sediment deformation associated with the East Patna Fault south of the Ganga River, northern India: Influence of the Himalayan tectonics on the southern Ganga plain. J. Asian Earth Sci. 143, 109–121.

Wang, C.-Y., 2007. Liquefaction beyond the Near Field. Seismol. Res. Lett. 78, 512–517.

Wheeler, R.L., 2002. Distinguishing seismic from nonseismic soft-sediment structures: Criteria from seismic-hazard analysis. Spec. Pap. Soc. Am. 1–12.

Whittaker, A.C., Cowie, P.A., Attal, M., Tucker, G.E., Roberts, G.P., 2007. Bedrock channel adjustment to tectonic forcing: Implications for predicting river incision rates. Geology 35, 103–106.

Willett, S., Beaumont, C., Fullsack, P., 1993. Mechanical model for the tectonics of doubly vergent compressional orogens. Geology 21, 371–374.

Willett, S.D., McCoy, S.W., Perron, J.T., Goren, L., Chen, C.-Y., 2014. Dynamic Reorganization of River Basins. Science (80-.). 343.

Willett, S.D., Schlunegger, F., Picotti, V., 2006. Messinian climate change and erosional destruction of the central European Alps. Geology 34, 613–616.

Williams, M. a J; Clarke, M.F., 1984. Late Quaternary Environments in north-central India. Nature 633–635.

Williams, M.A.J., Clarke, M.F., 1995. Quaternary Geology and Prehistoric Environments in the Son and Belan Valleys, North Central India. Mem. Geol. Soc. India 32, 282–308.

Wu, T.-S., Jaiswal, M.K., Lin, Y.N., Chen, Y.-W., Chen, Y.-G., 2010. Residual luminescence in modern debris flow deposits from western Taiwan: A single grain approach. J. Asian Earth Sci. 38, 274–282.

Youd, T.L., 1977. Discussion of “Brief review of liquefaction during earthquakes in Japan.” Japanese Geotech. Soc. 15, 82–85.